

Implications of functional diversity for the pandemic risk of highly pathogenic coronaviruses

Inaugural-Dissertation

to obtain the academic degree
Doctor rerum naturalium (Dr. rer. nat.)

submitted to the Department of Biology, Chemistry, Pharmacy
of Freie Universität Berlin

by

Simon Schroeder

Institute of Virology

Charité Universitätsmedizin Berlin

August 2020

The experiments for this thesis were performed at the Institute of Virology, Universitätsklinikum Bonn, between April 2016 and August 2017, and at the Institute of Virology, Charité Universitätsmedizin Berlin, both directed by Professor Dr. Christian Drosten, between September 2017 and June 2020.

I declare that this thesis was composed by myself, that the work contained herein is my own except where explicitly stated otherwise in the text, and that this work has not been submitted for any other degree or professional qualification.

1st Reviewer: PD. Dr. Marcel Alexander Müller
Institute of Virology
Charité Universitätsmedizin Berlin
Charitéplatz 1
10117 Berlin

2nd Reviewer: Prof. Dr. Katja Nowick
Institute of Biology - Zoology
Freie Universität Berlin
Königin-Luise-Straße 1-3
14195 Berlin

Date of defense: 09.12.2020

Acknowledgments

I would like to thank Dr. habil. Marcel A. Müller and Prof. Dr. Christian Drosten for giving me the opportunity to work in this fascinating field of virology and for their guidance, inspirations and supervision throughout the project.

I would like to thank Prof. Dr. Katja Nowick for agreeing to be part of my thesis committee and for reviewing my thesis.

I would like to thank all my collaborators, especially Hannah Kleine-Weber, Dr. Markus Hoffmann, Prof. Dr. Stefan Pöhlmann, Christine Mache, Dr. Steeve Boulant, Dr. Megan Stannifer, Thao Tran, Prof. Dr. Volker Thiel and Prof. Dr. Ronald Dijkman for their contributions to my projects and publications.

Thanks to all former and present members of the institute, particularly the ones from the coronavirus lab. I would also like to thank Jackson Emanuel for spellchecking this thesis.

At last and foremost, thanks to everyone involved in my life outside the institute, in particular to my friends and family, for your mental support and inspiration over all these years.

Abstract	1
Zusammenfassung	2
1 – General Introduction	3
1.1 – CoV genome complexity	4
1.2 – CoV diversity and bat ancestry	5
1.3 – Highly pathogenic CoVs: MERS-, SARS- and SARS-CoV-2	7
1.4 – CoV genome organization and protein expression strategy	8
1.5 – CoV life cycle and replication strategy	10
1.6 – Interaction of CoVs with the innate immune system	12
1.7 – Drivers of CoV evolution and population dynamics	15
2.1 – Comprehensive phenotypic analysis of MERS-CoV lineages	17
2.1.1 – Introduction	17
2.1.2 – Results	20
2.1.2.1 Generation of MERS-CoV isolates from clinical samples obtained from Saudi Arabian patients	20
2.1.2.2 Deep sequencing of generated MERS-CoV isolates	21
2.1.2.3 Genome analysis of generated MERS-CoV isolates	21
2.1.2.4 Phylogeny and recombination analysis of generated MERS-CoV isolates	22
2.1.2.5 Enhanced Replication of MERS-CoV lineage 5 in cell culture	25
2.1.2.6 MERS-CoV lineage 5 has enhanced competitive replicative fitness	26
Analysis of stages of viral replication cycle	28
2.1.2.7 MERS-CoV EMC and lineages 3, 4 and 5 show similar host cell entry	28
2.1.2.8 MERS-CoV EMC and lineages 3, 4 and 5 show similar host cell entry capacity and DPP4-binding	28
2.1.2.9 All MERS-CoV lineages are comparably neutralized by anti-MERS-CoV-positive human and camel sera	31
2.1.2.10 MERS-CoV lineage 5 shows an earlier commencement of replication	32
2.1.2.11 MERS-CoV lineage 5 shows reduced cytokine induction	33
2.1.2.12 MERS-CoV lineage 5 is less sensitive to IFN treatment	34
2.1.2.13 Increased replication of MERS-CoV lineage 5 is not exclusively correlated to antagonism of JAK/STAT signaling	35
2.1.2.14 MERS-CoV lineage 5 shows increased replication in models of the human respiratory tract	36
2.1.3 – Discussion	37
2.2 – Phenotypic comparison of SARS-CoV- and SARS-CoV-2-specific IFN antagonism	41
2.2.1 – Introduction	41
2.2.2 – Results	43

2.2.2.1 Replication kinetics of SARS-CoV-2 and SARS-CoV in IFN competent and incompetent cell lines.....	43
2.2.2.2 SARS-CoV-2 is more sensitive towards IFN treatment than SARS-CoV	45
2.2.2.3 SARS-CoV-2 is less efficient in antagonizing cytokine and IFN-stimulated gene induction than SARS-CoV	47
2.2.2.4 Availability of the host protease TMPRSS2 is a major driver for SARS-CoV-2, but not SARS-CoV replication	49
2.2.2.4 SARS-CoV-2 protein 6 has reduced function in antagonizing IFN signaling	50
2.2.3 – Discussion	52
3 – Methods	55
3.1 - General cell culture procedures	55
3.2 - MERS-CoV isolate stock production	55
3.3 - IFN, Ruxolitinib and Camostat mesylate treatment.....	56
3.4 - MERS-, SARS- and SARS-CoV-2 infections	56
3.5 - Synchronized MERS-CoV infections.....	57
3.6 - Plaque titration assay.....	57
3.7 - Primary human airway epithelium infection and culture procedures.....	58
3.8 - Lung explants infection and culture procedures	58
3.9 - Plaque Reduction Neutralization Test (PRNT)	59
3.10 - Virus competition assay.....	59
3.11 - Deep sequencing of MERS-CoV virus stocks.....	59
3.12 - Sequence assembly of NGS reads	60
3.13 - Phylogenetic analysis of MERS-CoV genome sequences	60
3.14 - In-depth recombination analysis	60
3.15 - Cloning of MERS-CoV lineage-specific spike gene expression vector by mutagenesis PCR.....	61
3.16 - Isolation of plasmid DNA.....	62
3.17 - Generation of MERS-CoV spike protein-pseudotyped VSV particles (VSVpp) and virus transduction studies.....	62
3.18 - Quantification of MERS-S binding to DPP4 by flow cytometry	63
3.19 - IRF3 translocation assays.....	64
3.20 - Western blot analysis.....	64
3.21 - Manual isolation of viral RNA	64
3.20 - Manual isolation of total cellular RNA	65
3.21 - Automated isolation of viral RNA	65
3.22 - Purification of PCR products.....	65
3.23 - Photometric quantification of nucleic acid concentration	65
3.24 - Bacterial transformation, colony PCR and glycerol stock production.....	66

3.25 - Sanger Sequencing.....	66
3.26 - Quantitative real-time PCR (q-RT-PCR).....	66
3.27 - Cloning of recombinant rSARS-CoV _{ORF6-SARS-CoV-2} and rSARS-CoV _{ΔORF6} cDNA constructs by red-mediated recombination.....	67
3.28 - Linearization and phenol-chloroform extraction of rSARS-CoV cDNA	68
3.29 - Generation of infectious rSARS-CoV <i>in vitro</i> transcripts.....	69
3.30 - Generation of recombinant virus from <i>in vitro</i> transcripts.....	69
4 – Materials	70
4.1 - Cell Lines	70
4.2 - MERS-CoV viruses isolates.....	71
4.3 - SARS- and SARS-CoV-2 isolates.....	72
4.4 - Bacteria strains	72
4.5 - Bacteria medium and supplements	72
4.6 - Enzymes	72
4.7 - DNA markers for agarose gel electrophoresis	73
4.8 - Oligonucleotides (Primers).....	73
4.8.1 - Forward primers for MERS-CoV Sanger sequencing.....	73
4.8.2 - Reverse primers for MERS-CoV Sanger sequencing	74
4.8.3 - MERS-CoV Spike mutagenesis primer.....	75
4.8.4 - Quantitative real-time PCR primers and probes.....	75
4.9 - Plasmids.....	77
4.10 - Commercial Kits.....	77
4.11 - Antibodies	78
4.12 - Software.....	78
4.13 - Technical Equipment	79
5 - Abbreviations	81
6 - Supplements.....	83
7 - References.....	90
Publications	101

Abstract

The last two decades have seen the zoonotic emergence of three highly pathogenic coronaviruses (CoVs): MERS-, SARS- and SARS-CoV-2. Their epidemic and pandemic spread, respectively, underlines the importance of monitoring emerging CoVs and of developing a deeper understanding of the molecular mechanisms that contribute to their emergence and pathogenicity. CoV are highly diverse in their animal reservoirs, yet how this diversity translates to phenotypical traits that may account for the zoonotic and pandemic potential of these viruses remains elusive.

In the first part, several generated clinical Middle East respiratory syndrome coronavirus (MERS-CoV) isolates pertaining to different phylogenetic clades were analyzed for their *in-vitro* and *ex-vivo* infection phenotypes. Importantly, the isolate diversity used here reflects phylogenetic lineages sampled before and after the year 2015, when a novel phylogenetic lineage emerged by a recombination event (MERS-CoV lineage 5) and superseded other, hitherto co-circulating viral lineages from circulation, as well as causing large nosocomial outbreaks in Saudi Arabia and South Korea. The present studies demonstrate that MERS-CoV recombinant lineage 5 isolates have increased replicative capacity in the human lung, in correlation with increased interferon resilience and signaling antagonism. These phenotypic differences might explain the dominance of lineage 5 on the Arabian Peninsula and suggests an increased pandemic potential of the currently circulating MERS-CoV lineage 5.

The second part comprises a phenotypical comparison of severe acute respiratory syndrome coronavirus (SARS-CoV) and SARS-CoV-2, focusing on potential differences in their capacity to antagonize the innate immune response. Both viruses share a completely homologous repertoire of open reading frames (ORFs) and pertain to the same phylogenetic clade of SARS-related CoV, yet display differences in their transmission efficiencies and pathogenic traits. The data presented here show that SARS-CoV-2 is more sensitive to the antiviral activity of interferons and that SARS-CoV-2 is less efficient in antagonizing cytokine induction and interferon signaling. SARS-CoV-2 protein 6 expressed in the context of a fully replicating SARS-CoV backbone had reduced functionality in suppressing interferon signaling induction, suggesting that the overall reduced antagonism of SARS-CoV-2 might therefore be a function of reduced antagonistic capacity of protein 6.

Zusammenfassung

Drei hochpathogene Coronaviren (CoV) sind in den letzten zwei Jahrzehnten auf den Menschen übergegangen: MERS-, SARS- und SARS-CoV-2. Insbesondere die Ausbreitung des SARS-CoV-2 zeigt auf, wie wichtig die Überwachung neu auftretender CoV ist. Die aktuelle Pandemie demonstriert auch welche Relevanz es für unser Gesundheitswesen hat ein tiefergehendes Verständnis für jene Faktoren zu entwickeln, die das Infektionsrisiko und die Pathogenität solcher Viren beeinflussen. Die Diversität von CoV ist in ihren tierischen Reservoiren groß, doch wie sich diese Vielfalt auf phänotypische Merkmale auswirkt, besonders auf solche, die das zoonotische und pandemische Potenzial dieser Viren beeinflussen könnten, ist nach wie vor unklar.

Im ersten Teil der Dissertation wurden in verschiedenen *in-vitro*- und *ex-vivo*- Modellen mehrere klinische MERS-CoV-Isolate phänotypisch analysiert. Es konnte gezeigt werden, dass die hierfür isolierten Viren repräsentativ für drei unterschiedliche phylogenetischen Kladen sind, und mit MERS-CoV Linie 5 jene Klade beinhalten, die in oder vor 2014 durch ein Rekombinationsereignis entstanden ist, und nachträglich alle bis dato zirkulierenden Viruslinien verdrängt hat. Die vorliegende Studie zeigt, dass Virusisolate der rekombinanten MERS-CoV-Linie 5 eine erhöhte Replikationskapazität in der menschlichen Lunge haben, die mit einer erhöhten Interferon-Resilienz und einer effektiveren Unterdrückung der Interferon-spezifischen Signaltransduktionskaskade korrelierend. Diese phänotypischen Unterschiede könnten die mögliche Dominanz der Linie 5 auf der Arabischen Halbinsel erklären und implizieren, dass die aktuell zirkulierende MERS-CoV Linie 5 ein erhöhtes zoonotisches und pandemisches Risiko für den Menschen darstellt.

Der zweite Teil der Dissertation umfasst einen phänotypischen Vergleich von SARS- und SARS-CoV-2 mit besonderem Fokus auf die virale Interaktion mit der angeborenen Immunität in Wirtszellen. Beide Viren zeigen ein vollständig homologes Repertoire von offenen Leserahmen (open reading frames, ORFs) und gehören der gleichen phylogenetischen Art, den SARS-verwandten CoV an. Die Viren unterscheiden sich jedoch deutlich in ihrer Übertragungseffizienz und in ihrer Pathogenese im Menschen. In dieser Arbeit konnte gezeigt werden, dass SARS-CoV-2 weniger resilient gegenüber der antiviralen Wirkung von Interferon ist. Im Vergleich zu SARS-CoV kann SARS-CoV-2 die Zytokininduktion und Interferon-Signalübertragung weniger effizient unterdrücken. Mittels reverser Genetik konnte gezeigt werden, dass das SARS-CoV-2 Protein 6 im Kontext eines vollständig replizierenden SARS-CoV eine geringere Effizienz als SARS-CoV Protein 6 hat, die Interferon-Signaltransduktionskaskade zu blockieren.

1 – General Introduction

Coronaviruses (CoV; order *Nidovirales*, family *Coronaviridae*) are positive sense, single stranded RNA viruses of exceptional genomic complexity and the capacity to infect a broad range of invertebrate and vertebrate hosts [1-3]. Human pathogenic CoVs (HCoVs) have first been notified in the late 1960s and have since then been observed as a frequent, yet mild cause of “common cold”-like, acute respiratory syndromes in humans [4, 5].

The global spread of three highly pathogenic CoVs within the last two centuries (SARS-CoV in 2002, MERS-CoV in 2012 and SARS-CoV-2 in 2019 [6-8]) has shifted that perception and demonstrated the importance of monitoring newly emerging CoVs and to develop a deeper mechanistic understanding of their biology and evolution (**Figure 1**).

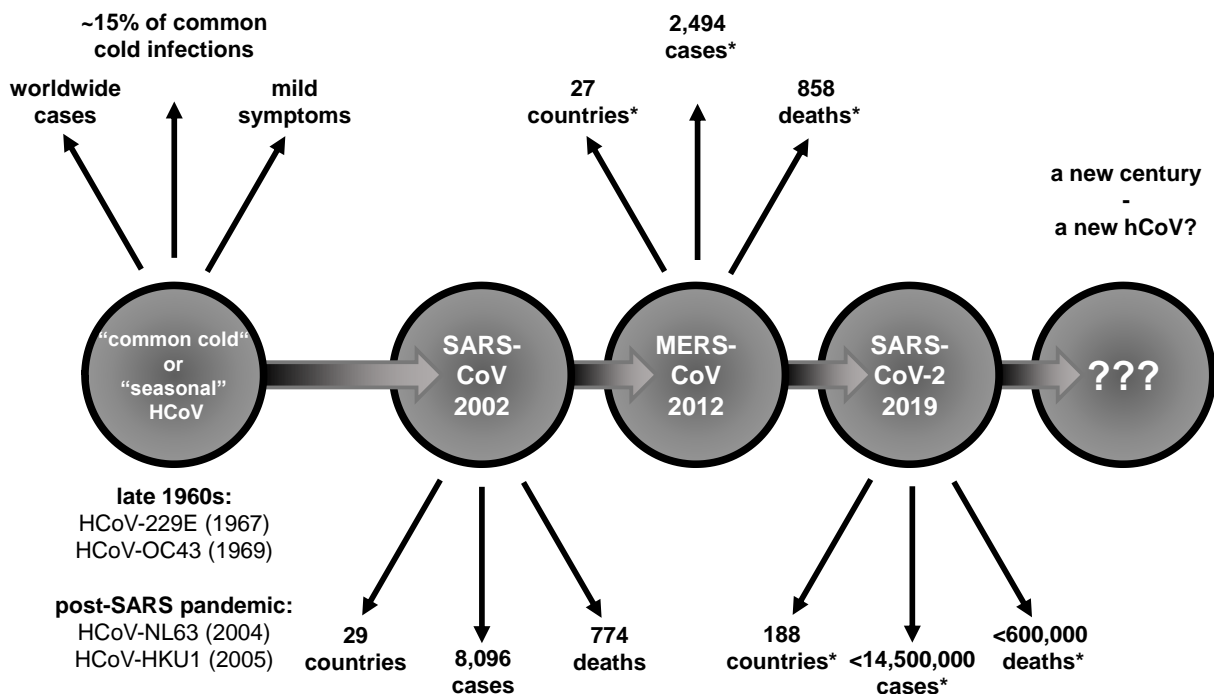


Figure 1: CoVs known to infect humans (HCoV) and their time point of emergence. CoVs were initially discovered in poultry (Infectious Bronchitis Virus, IBV) in 1937 [9]. IBV and other animal CoVs are important livestock pathogens, but not focused on here. The low pathogenic HCoV-229E and OC43 have been known to cause seasonal “common cold” respiratory syndromes in humans for over 50 years [4, 5]. The SARS pandemic in 2003 intensified CoV surveillance and led to the discovery of two more HCoVs, HCoV-NL63 and HKU1 [10, 11]. Seasonal HCoV are estimated to cause around 15% of acute respiratory tract infections in humans [12-14]. References for SARS-, MERS- and SARS-CoV-2 emergence are displayed in the main text. * refers to the date of writing, i.e. 20.07.2020.; case and country numbers are provided by the WHO (2020).

1.1 – CoV genome complexity

With genomes sizes of 12 to 41 kb (averaging 26 to 31 kb) *Nidovirales* constitute the largest known RNA based lifeforms on earth [15]. A prevailing dogma, proposed by Manfred Eigen (†2019) in his famous 1971 paper, states a positive correlation between genome complexity and replication fidelity [16]. The large *Nidovirales* RNA genomes appear to be a remarkable exception to that rule, since other RNA virus families (averaging 2 to 12 kb genomes) show average replication error rates 10,000 to 100,000 times higher than DNA replication error rates [17-20], trapping RNA viruses at the lower end of genome complexity. Fundamentally, RNA polymerases lack the ability to correct for errors during replication (proofreading) and have evolved a replication fidelity low enough to allow for the generation of a maximally diverse “cloud” of variants in the population (referred to as the viral quasispecies) [21-23]. The quasispecies provides the basis for natural selection to work upon and contributes a major explanation for the huge adaptability observed in RNA virus species [24, 25]. However, artificial increases in the mutation rate of RNA viruses pushes species into a state of intolerable accumulation of mutations, often referred to as “error catastrophe” [26-29].

Nidovirales evolution has uniquely overcome this trap by acquisition of a complex replication machinery of which one protein subunit (non-structural protein 14, nsp14) encodes for a domain with exonuclease activity (ExoN), similar in function to proofreading domains of DNA polymerases [30-34]. The emergence of RNA proofreading activity is believed to have facilitated genome expansion in *Nidovirales* and is in line with Eigen’s theory that predicts inverse correlation of mutation rate and genome complexity (reviewed in [2]). In a Darwinian sense, increased genomic complexity provides a broader basis for natural selection to work upon and may have facilitated the diversity and broad host tropism of the *Nidovirales* order (chapter 1.2).

1.2 – CoV diversity and bat ancestry

Nidovirales are considered the second most diverse order of positive-sense RNA viruses, after the *Picornaviridae*, comprising 109 formally recognized species, 46 of which pertain to the family *Coronaviridae* [35]. The remaining species of *Nidovirales* belong to the family of *Arteriviridae* and *Roniviridae* [35]. Phylogenetic inferences suggest a further division of *Coronaviridae* into four genera, the *Alpha-*, *Beta-*, *Gamma-*, and *Deltacoronavirus* (**Figure 2B**), each of which contains several sub-clades. Interestingly, the split of alpha-/betacoronaviruses and gamma-/deltacoroanviruses coincides with a split in host tropism, with members of the former group infecting primarily mammals, and the latter infecting primarily (but not exclusively) birds [36]. Five of the seven CoVs known to infect humans (including the three highly pathogenic strains, SARS-CoV, SARS-CoV-2, MERS-CoV; as well as HCoV-OC43 and HCoV-HKU1; **Figure 1**), pertain to the genus *Betacoronavirus* and two belong to the alphacoronaviruses (HCoV-229E and HCoV-NL63) (**Figure 2A**).

There is strong evidence for a zoonotic origin of all human CoVs, i.e. that they originated in animal reservoirs (reviewed in [37]). Phylogenies constructed from the increasingly complex data of metagenomics strongly suggest that ancestral CoVs might have emerged in bat species (reviewed in [38]). In fact, all of the CoVs known to infect humans have bat ancestors, but frequently involve intermediate hosts [39-49], with the exception of HCoV-OC43 and HKU1 for which rodent ancestry has been proposed [50, 51] (**Figure 2C**).

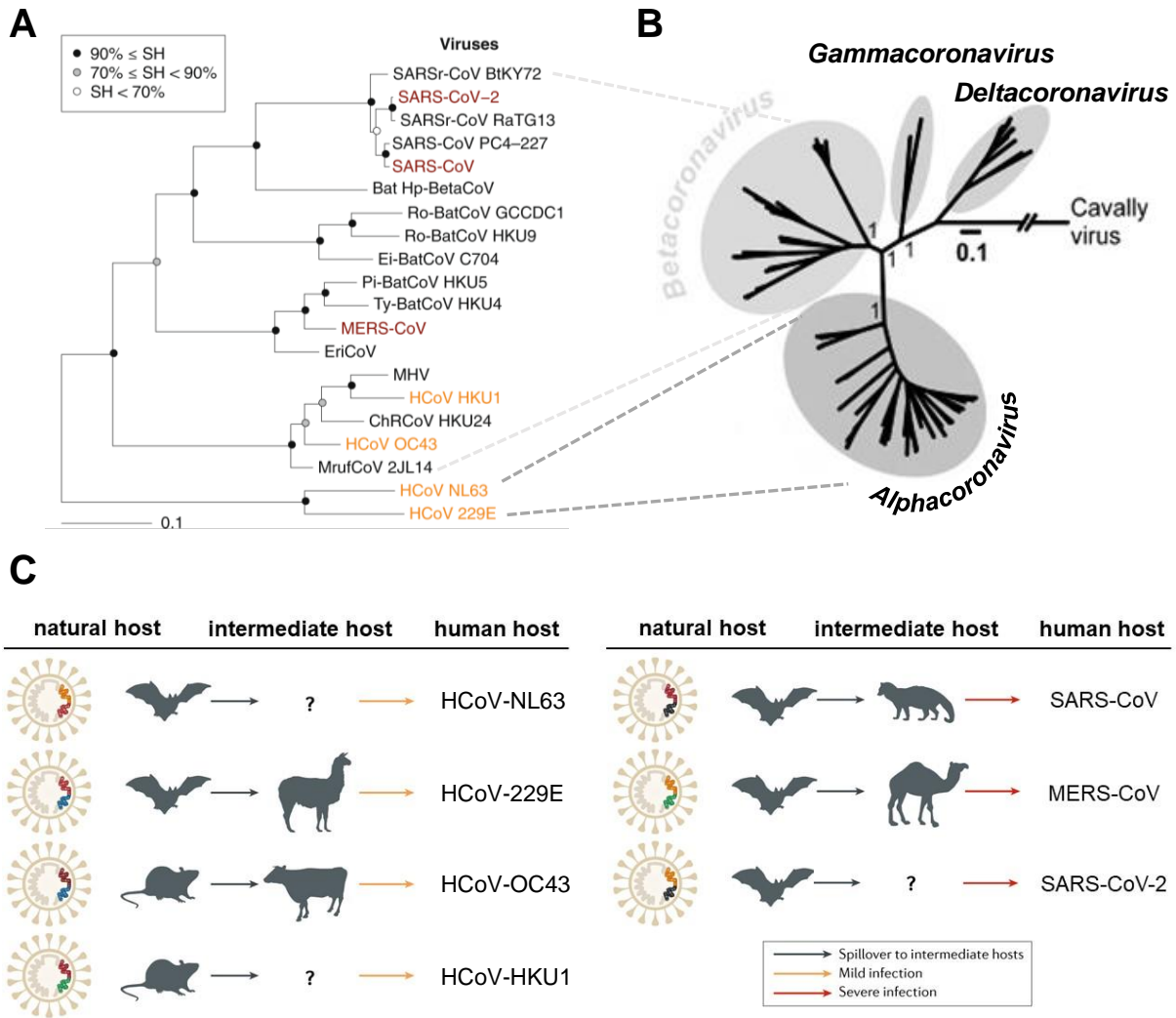


Figure 2: CoV phylogeny and animal origin, with focus on HCoV. **A)** Displayed is a maximum-likelihood phylogeny of selected *Alpha*- (HCoV-229E and -NL63) and *Betacoronavirus* (all other names) species. CoVs known to infect humans (red names, severe infection in humans; orange names, mild infection), cluster within clades of species identified in bats (black names), arguing for close evolutionary distance between them (not shown for alphacoronaviruses). The tree was calculated with the Shimodaira–Hasegawa (SH) method and 1,000 replicates (the higher the %-value (SH-ratio), the higher the support of a node; top left panel) and was adapted from [52] **B)** Bayesian inference phylogeny of selected members of the *Coronaviridae* family, with Cavally virus as an outlier species. The tree displays the split into the four genera *Alpha*-, *Beta*-, *Gamma*-, and *Deltacoronavirus* and was adapted from [38]. More details on the construction of phylogenies in A) and B) are provided in the respective references. **C)** Schematic display of emergence of HCoVs, with color code as above. Left panel shows HCoVs that cause mild disease in humans, right panel the highly pathogenic CoVs. Adapted from [37].

1.3 – Highly pathogenic CoVs: MERS-, SARS- and SARS-CoV-2

Middle East respiratory syndrome coronavirus (MERS-CoV), a 2c betacoronavirus, is the causative agent of a novel form of severe viral pneumonia in humans [7]. MERS-CoV emerged in 2012 and the majority of currently more than 2,494 notified cases, including 858 deaths, occurred on the Arabian Peninsula. Travel-associated cases were diagnosed in 27 countries and sparked secondary case clusters in some. The largest MERS-CoV outbreak outside the Arabian Peninsula occurred in South Korea in 2015, involving 186 cases and 36 deaths (WHO, June 2020). MERS-CoV is acquired as a zoonotic infection from dromedary camels [53-56] and likely originated in bats [42, 57]. Spillover from dromedaries to humans can lead to local outbreaks with limited human-to-human transmission [58, 59]. Healthcare facilities can experience protracted outbreaks with severe infections in co-morbid patients [60]. Behavioral factors like family patient care may accelerate outbreaks [61-63].

SARS-CoV is a group 2b betacoronavirus that emerged in 2002 in the Guangdong Province of China and was identified as the causative agent of the Severe Acute Respiratory Syndrome (SARS) [6]. The transmission dynamics of SARS-CoV are relatively low and despite having spread to 29 countries and infecting more than 8000 patients with 774 deaths the SARS pandemic was halted by public health interventions in 2003 [64]. As described in chapter 1.2, SARS-related CoVs originate in bats, but in the case of the 2002 SARS-CoV, palm civets and raccoon dogs have been implicated to act as intermediate hosts [65].

SARS-CoV-2 was identified as the etiological agent of a novel viral pneumonia, called COVID-19 in late 2019 [8]. Since then, it has rapidly shifted from initial local case clusters in the Hubei province in China to a pandemic with over 12,000,000 cases and over 600,000 deaths (WHO, July 2020). The novel virus pertains to the same species as the etiological agent of the SARS pandemic in 2002/3 [52]. Therefore, SARS-CoV-2 and SARS-CoV share striking similarities in their genome architecture [66], in receptor and host protease usage [67] and in emergence from an initial zoonotic acquisition with bat ancestry [46]. However, SARS-CoV-2 seems to be distinct from SARS-CoV in its clinical and epidemiological presentation, with lower pathogenicity and case fatality rate but higher human-to-human transmission rate and incidence [68].

1.4 – CoV genome organization and protein expression strategy

CoV genomes contain several higher order RNA structures. The 5' and 3' ends of the viral genome comprise untranslated regions (UTR) required for genome replication and transcription. UTRs may vary in sequence length between different CoV species, but share a conserved core area in the 5'UTR, which comprises the leader TRS (transcription regulatory sequence, TRS) that interacts with body TRS located upstream of structural and accessory genes during their transcription (see below) [69, 70] (**Figure 3**).

Two thirds of the genome comprises ORF1 that is translated directly from the capped and polyadenylated genomic RNA as two large polyproteins (pp1a and pp1ab) by means of an RNA pseudoknot-mediated -1 ribosomal frameshift [71]. The polyproteins are proteolytically processed by the viral proteases PLpro (Papain-like protease, in nsp3) and 3CLpro (chymotrypsin-like protease 3, in nsp5) to yield 16 (in some species only 15) nsps [72, 73]. While mutagenesis studies could demonstrate an essential function of the nsps for replication, their precise individual function is still under debate, particularly because most exhibit multifunctionality. Yet in principle, the nsps encode for the components of the multi-structural replication transcription complex (RTC) that governs the production of viral RNAs, for proteins that rearrange cellular membranes to create a double-membrane vesicle environment proposed to host CoV replication, or for proteins that interfere with the antiviral host response (see below) [74-80].

The last third of the CoV genome encodes for structural and accessory proteins that are translated from subgenomic mRNAs (sgmRNAs; chapter 1.5). Structural proteins form the virus particle and are common to all CoVs. These comprise the spike protein, which mediates entry into and attachment to host cells by binding to host cell proteins (called receptors), the envelope (E) and membrane (M) protein, as well as the genome-encapsidating nucleocapsid (N) protein [67, 81, 82]. Accessory proteins comprise a range of proteins that may vary in number between different CoV species. These are non-essential for virus replication (therefore called accessory), but implicated in *in vivo* pathogenesis and/or suppression of the antiviral host reaction (chapter 1.6) [83-86] (**Figure 3**).

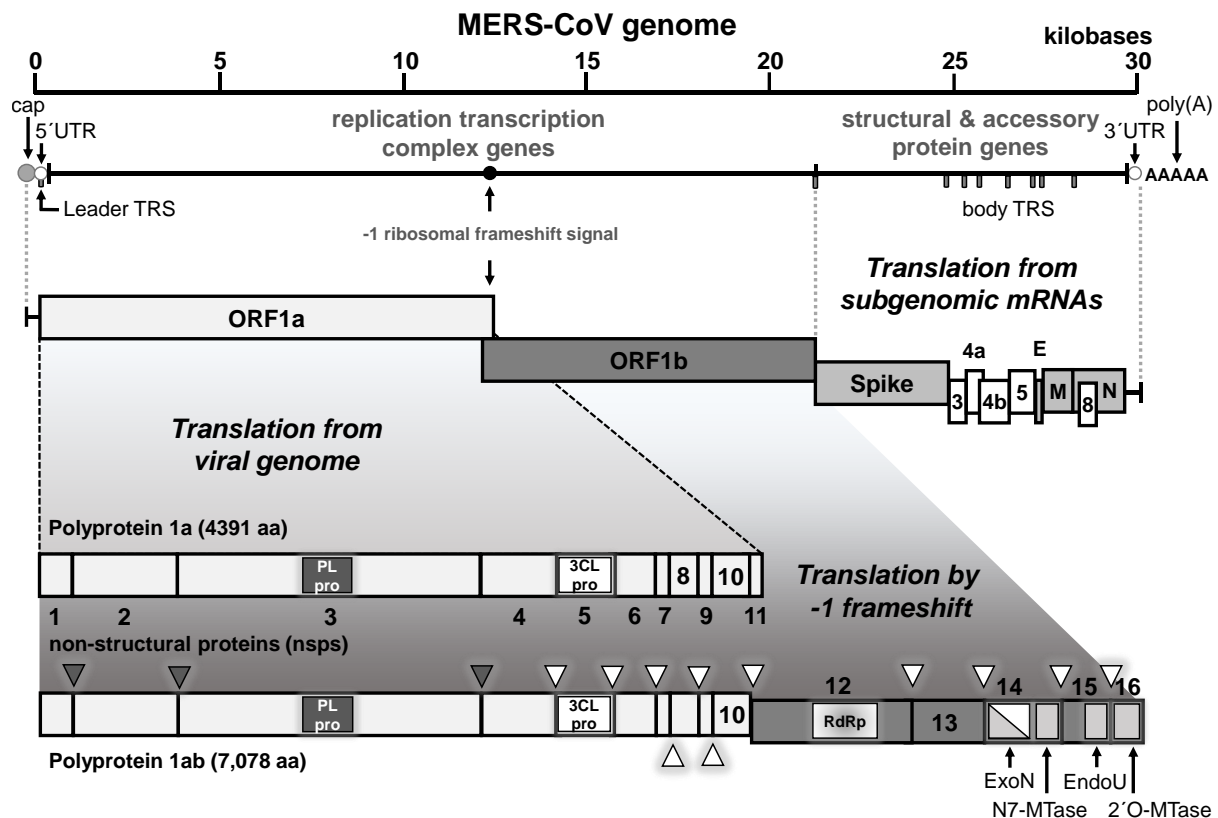


Figure 3: CoV genome organization and protein expression strategy. Exemplified for MERS-CoV. *Upper panel:* MERS-CoV genome and its 11 open reading frames (ORFs): ORF1 (split into ORF1a and ORF1b, which express proteins required for replication and transcription), the structural ORFs (expressing spike-, envelope- (E), membrane- (M), nucleocapsid- (N) protein), and accessory ORFs (expressing p4a, p4b, p5 and p8). *Replicase and structural ORFs are present in all CoVs; the number of accessory ORFs varies between species. SARS- and SARS-CoV-2 encode for nine accessory ORFs (not shown here).* Important regulatory RNA elements are shown in the top panel (left to right): cap structure, 5' UTR (for ntranslated region), Leader TRS (for Transcription Regulatory Sequence; see chapter below), RNA stem-loop causing a -1 ribosomal frameshift to govern ORF1b expression, nine body TRS, 3' UTR and the poly(A) tail. *Bottom panel:* viral polyprotein expression and maturation. Both polyproteins are translated from the viral genome, 1ab via a -1 ribosomal frameshift. The numbers indicate respective non-structural proteins (nsps). Triangles indicate cleavage sites in the viral polyprotein, with matching color code (PLpro sites in dark; 3CLpro sites in white). Functional protein domains that are mentioned in this or following sections of the main text are highlighted. PLpro, Papain-like protease (nsp3); 3CLpro, chymotrypsin-like protease 3 (nsp5); RdRp, RNA-dependent RNA polymerase (nsp12); ExoN, 3'-to-5' exoribonuclease (nsp14); N7-MTase, N7-guanine methyl transferase (nsp14); endoU, uridylate-specific endoribonuclease (nsp15); 2'-O-MTase, 2'-O-methyl transferase (nsp16). Structural and accessory proteins expression follows translation from sgmRNAs, produced by discontinuous transcription (see chapter 1.5).

1.5 – CoV life cycle and replication strategy

CoV follow a unique replication and transcription strategy, summarized in **Figure 4** and reviewed in [87].

Attachment to host cells is mediated by protein-protein interactions between viral spike and cellular receptor proteins, dipeptidylpeptidase 4 (DPP4) in MERS- [81] and angiotensin-converting enzyme 2 (ACE2) in SARS- and SARS-CoV-2 infection [67, 88]. Attachment may be augmented by additional binding to cellular sugar residues, sialic acids in the case of MERS-CoV [89] or additional cellular proteins, DC-SIGN in SARS-CoV infection, respectively [90]. Receptor recognition triggers conformational changes in the spike protein that drive the fusion of viral envelope and cellular membranes [91]. In the classical pathway, fusion occurs inside cellular endosomes following receptor-mediated endocytosis of receptor bound viral particles [91]. An alternative pathway that allows for fusion directly at the plasma membrane in dependence of additional proteolytic spike protein procession by cellular proteases could be demonstrated for all three highly pathogenic CoVs (MERS-, SARS- and SARS-CoV-2) [92-100]. Following receptor-mediated entry, the viral genome is uncoated and released into the host cytoplasm. As detailed above, viral nsps are translated directly from the viral genome. Following their expression and proteolytic procession, the nsps rearrange host membranes to form double-membrane vesicles, the putative platform of virus replication and transcription [74, 101, 102]. Here, the replication-transcription complex replicates the viral genome and transcribes structural and accessory protein encoding sgRNAs, detailed below. Nascent virus particles are formed by interaction of expressed structural proteins and nucleocapsid-mediated interaction of replicated genomes at ER-Golgi intermediate compartments (ERGIC) and follow export and maturation over the trans-Golgi route [82, 103-106] (**Figure 4A**).

Genome replication requires the transcription of full-length (genomic) negative-strand (minus-strand) RNA, which serves as the template for the production of full-length (genomic) positive-strand (plus-strand) RNA (**Figure 4B**). The production of sgRNAs is governed by a process called discontinuous transcription and is fundamentally different to genome replication (reviewed in [72, 107]). In essence, the viral replication-transcription complex uses genomic positive-strand RNA as template and starts the transcription of negative-strand RNA from the 3' end of the viral genome. When a body TRS, located 5' of each structural or accessory gene, is encountered, negative-strand transcription either continues to the next TRS, or the replication-transcription complex dissociates to transfer the nascent RNA to the leader TRS at the 5' end of the genome, guided by sequence complementarity of body TRS and leader TRS. Transcription of negative-strand RNA continues over the leader until the 5' end of the genome

is reached. Fused leader-body negative-strand RNAs are transcribed to yield positive-strand sgmRNAs, the template for viral protein translation (**Figure 4B**). Discontinuous transcription is a hallmark of the *Nidovirales* family and the resulting production of a set of 3' coterminal, or "nested" sgmRNAs has coined their name ("nido" is the Latin word for "nest"). Of note, the process also allows for a passive control over the abundance of transcripts, as the ORFs towards the 3' end of the genome will be transcribed more frequently.

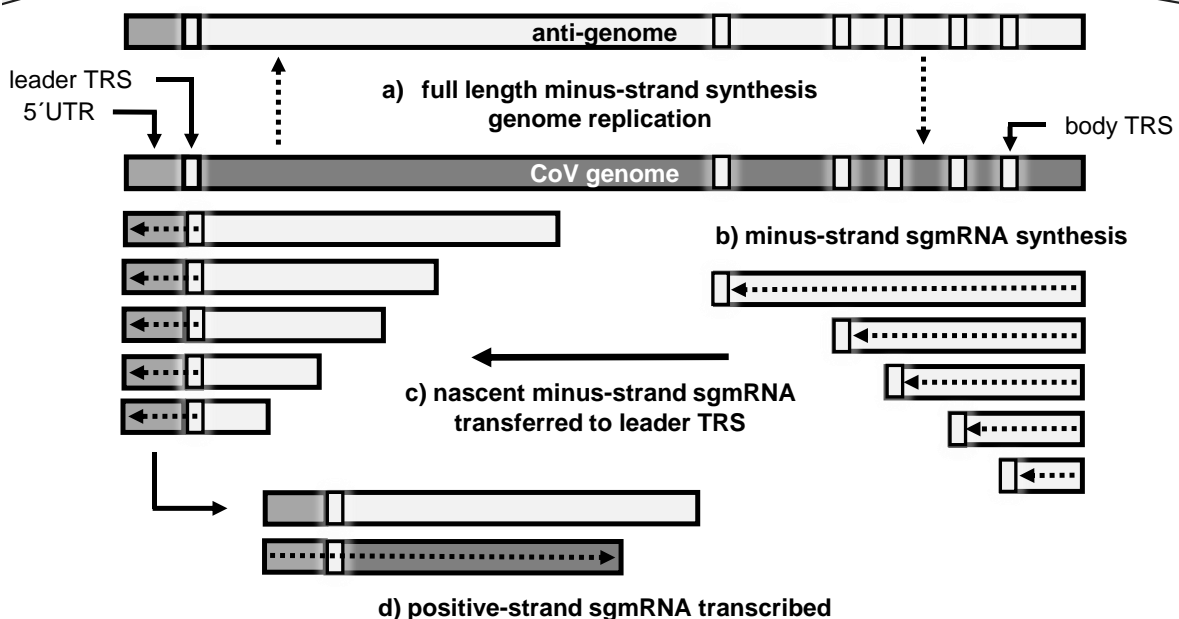
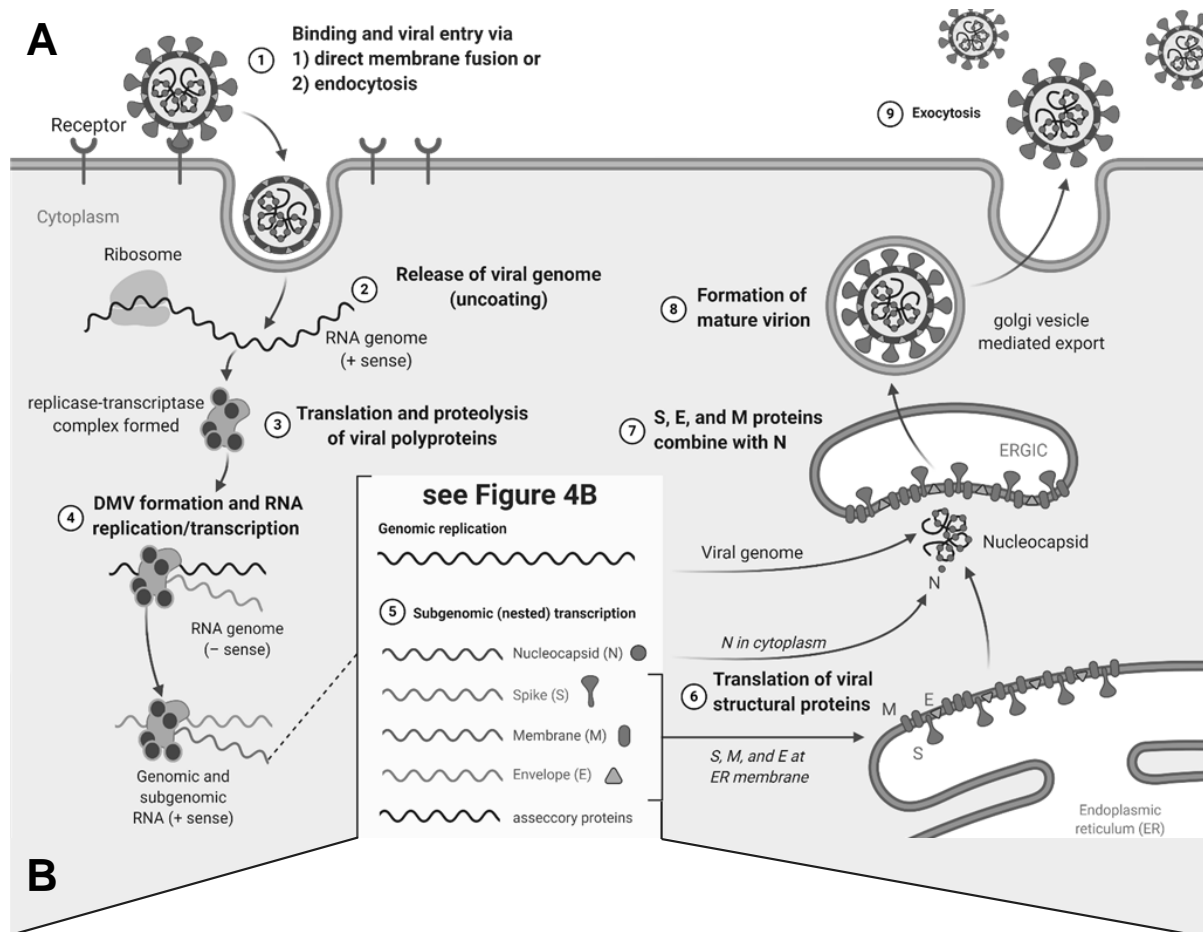


Figure 4: CoV life cycle and replication strategy. A) CoV life cycle. After receptor-mediated entry (1), the viral RNA is uncoated in the cytoplasm (2). Viral nsps are translated and proteolytically processed directly from the viral genome (3). The nsps rearrange cellular membranes to form double-membrane vesicles (DMV) (4) which host the viral replication and sgRNA transcription (5) and detailed in B). sgRNAs are translated to structural proteins (6) that are assembled into the nucleocapsid and viral envelope at the ER–Golgi intermediate compartment (ERGIC) (7), followed by Golgi-mediated release (8) of the nascent virion from the infected cell (9) **B)** CoV Replication strategy. a) genome replication, full-length negative-strand (- sense) RNA copies of the genome are produced that serve as templates for full-length positive-strand (+ sense) RNA genomes. b-d) discontinuous transcription of structural and accessory proteins sgRNAs. b) sg minus-strand RNAs are transcribed starting from the 3' end of the genome until a body TRS is encountered. Transcription either continues to the next TRS or c) the nascent strand is transferred to the leader TRS. Transcription continues over the leader TRS sequence. d) The produced leader-fused negative-strand sgRNAs are transcribed into positive strand sgRNAs, the template for translation.

1.6 – Interaction of CoVs with the innate immune system

The complex interactions between viruses and their hosts has driven metazoan evolution to develop sophisticated immune systems to fight virus infections. In turn, in an “evolutionary arms race,” viruses have evolved innumerable strategies to overcome these systems [108-111].

Vertebrate immune systems comprises two subtypes that are acting and interacting in complementing ways to fight infections: adaptive (or antigen-specific) immunity and innate (or antigen-non-specific) immunity, reviewed in [112]. In essence, adaptive immunity comprises “tailor-made,” specific responses to a specific antigen and primarily acts via subsets of cells, the leukocytes, including antibody producing B-cells and cytotoxic (cell killing) T-cells. The adaptive immune response is launched in a time-delayed fashion, as the activation and maturation of these cells requires previous antigen recognition and processing [113].

In contrast, components of innate immunity are present in all cell types and can immediately engage in a rather unspecific response by a mechanism called “pattern recognition”. Fundamentally, distinct “non-self” structural motives, called pathogen associated molecular patterns (PAMPs), are detected by a number of sentinel proteins, or pattern recognition receptors (PRRs) [114]. The detection of PAMPs activates a signaling cascade leading to downstream activation and nuclear translocation of transcription factors, in the case of viral infections most notably interferon (IFN) regulator factors (IRF3 and IRF7) and nuclear factor kB (NF-kB) [114]. In CoV infection, the innate immune response is primarily launched by the cellular helicase melanoma-differentiation antigen 5 (MDA5) that binds to double-stranded

RNA replication intermediates, produced during negative-strand synthesis [115]. The activation of NF- κ B and IRFs exemplifies two complementary antiviral strategies: NF- κ B induces the transcription of chemokines that primarily act in the recruitment and activation of leukocytes, while IRFs induce the transcription of type I and type III IFNs (IFN-I, comprising IFN α and IFN β subtypes and IFN-III, respectively, comprising IFN λ subtypes). In a paracrine manner, secreted IFNs induce IFN-stimulated genes (ISGs) by binding to cellular IFN receptors and activating the Janus kinase/ signal transducers and activators of transcription (JAK/STAT) signaling cascade (also called IFN signaling cascade) [116]. ISGs encode for over 300 proteins with antiviral properties that can be broadly categorized as proteins immediately impeding virus replication (e.g. Mx1, ISG56, proteins of the IFIT and IFITM family), sentinel proteins (e.g. TLRs, the RIG-I-like receptor family, including MDA5), transcription factors (e.g. the STAT family or IRFs) and proteins functioning in immune regulatory signaling [117, 118].

CoVs are highly sensitive to the antiviral action of IFN signaling, *in vitro* and in non-human primate models [119-125]. IFN treatment can abolish CoV infections and mouse-adapted SARS-CoV-infected STAT1-knockout mice show higher viral loads and pathology than wild-type mice [126]. In the course of the evolutionary arms race, CoVs have therefore evolved multiple strategies to evade and antagonize the induction of IFNs and IFN signaling.

Multiple viral nsps are implicated in evading pattern recognition. 2' O methyltransferase activity of nsp16 together with N7-methyltransferase activity of the nsp10/14 complex produces a 5' cap structure that mimics host mRNAs and significantly reduces recognition of viral RNAs by MDA5 [78, 80, 127-130]. Nsp15 encodes for a domain with EndoU (uridylyate-specific endoribonuclease) activity that cleaves viral polyuridine sequences (produced in negative-strand poly(A) tail transcription) to avoid recognition by MDA5 [131, 132]. Analogously, nsp14 contributes a second mechanism to recognition evasion, by ExoN-mediated degradation of RNA PAMPs [75, 133]. The formation of double-membrane vesicles, a hallmark of CoV replication, likely contributes to evasion of pattern recognition by shielding viral replication from cytosolic sensor proteins, as particularly the interior of these compartments stains positive for dsRNA [101, 102]. In accumulation, these multidimensional strategies of pattern recognition evasion probably contribute to the phenotype of very low IFN induction in CoV-infected *ex vivo* lung cells [121, 134].

In addition to the above-mentioned strategies of evading pattern recognition, CoV have evolved strategies to directly antagonize the activation of antiviral signaling cascades. Nsp1 of SARS- and MERS-CoV has been demonstrated to induce the degradation of host mRNA synthesis, including that of IFN-I mRNAs [135-138]. Two different motives contribute to nsp3-mediated immune antagonism: For SARS-CoV, the removal of the macrodomain in nsp3 that has a ADP-ribose-1'-phosphatase domain results in an increased IFN and ISG induction

in infected cells by a yet unknown mechanism [139]. MERS- and SARS-CoV nsp3 further encode for a deubiquitinating domain, which seems to counteract the antiviral function of a major ISG, ISG15, and the transcriptional activity of IRF3 [140-143]. ISG and IFN promoter activation assays suggest an antagonistic function of SARS-CoV protein 3b, protein 6, protein 9 and the nucleocapsid protein [144, 145]. Recently, promoter activation assays implicated SARS-CoV-2 nsp13, nsp14, nsp15 and protein 6 to have similar antagonistic capacity as their SARS-CoV homologues [146]. Promoter activation assays need to be interpreted with care, as artificial overexpression of single viral proteins does not reflect endogenous protein expression during infection. However, for SARS-CoV protein 9 additional evidence demonstrated protein 9-induced degradation of an important PRR signaling molecule, called MAVS [145]. SARS-CoV protein 6 function in IFN signaling antagonism has been clarified by immunoprecipitation assays that demonstrated binding and sequestration of importin alpha 1 and beta 1, required for nuclear translocation of the ISG-inducing transcription factor STAT1 [147]. An analogous function has evolved for MERS-CoV protein 4b, which contains a nuclear localization signal that competes with the transcription factor NF- κ B for binding to importins and nuclear import [85]. MERS-CoV accessory protein 4a antagonizes IFN induction by binding to dsRNA and inhibiting MDA5 activation, possibly by binding to its activator PACT [86, 148]. While initial evidence was gathered from promoter activation assays, the antagonistic properties of endogenous protein 4a and 4b have been clarified in the context of virus infection [149, 150].

1.7 – Drivers of CoV evolution and population dynamics

In principle, virus populations are subject to the same evolutionary drivers that shape all kingdoms of life: natural selection, random genetic drift and recombination. The force of natural selection, genetic drift and recombination correlates with the subjected population's mutation rate, population size and fluctuation therein. As all of these determinants are extremely high in RNA viruses, RNA viruses exhibit overall evolutionary rates much higher than other organisms [151].

Natural selection acts on the viral quasispecies and will select for mutations that confer the greatest increase in fitness, i.e. replicative success. It is therefore non-random and deterministic. Particularly when selection pressure is high, e.g. upon adapting to a new host, or upon exposure to antiviral treatment, beneficial mutations will increase in frequency and eventually become fixed in the virus population (positive selection or adaption), while deleterious mutations will decrease in frequency (negative or purifying selection). Importantly and frequently misunderstood, mutations themselves are stochastically more likely to exhibit neutral or even deleterious than beneficial effects to virus fitness [152-154].

Genetic drift describes the random, non-deterministic process that can lead to fixation of random mutations by a sampling error in transmission. In viruses, genetic drift is particularly conceivable, since only a random minority (possibly not the representing the consensus of the quasispecies, therefore constituting a sample error) will infect a new cell or host to produce progeny and fix the transmitted genotypes [24, 151].

Both the effect of natural selection and genetic drift are dependent on population size, which stringently fluctuates in virus life cycles [155]. Particularly inter-host, but also cell-to-cell transmission events exhibit severe bottlenecks through which only a random minority of the viral quasispecies will pass, followed by phases of massive population expansion in a naïve host. These frequent fluctuations in population size significantly expedite the effects of genetic drift [151, 155]. Virus population dynamics in an environment with unchanged selection pressure (e.g. in the same host species or not exposed to antiviral treatment) therefore tend to be more strongly determined by random genetic drift than by positive selection. Because of the stochastically increased likelihood of neutral or deleterious mutations over beneficial mutations, virus populations face the dilemma of a “genetic meltdown”, i.e. the continuous random fixation of neutral or deleterious mutations. This idea of advancing loss in fitness by genetic drift was particularly emanated by the geneticist H. J. Muller (†1967) in his famous 1964 paper, in which he coined the term Muller's ratchet as a metaphor for the unidirectional, stepwise loss of fitness [156-158].

Unsegmented RNA viruses overcome Muller's ratchet by the process of genomic recombination [159, 160]. Analogously to meiotic crossing-over events in sexual reproduction, recombination provides asexual organisms with a tool to purge deleterious mutations from debilitated genomes. Mechanistically, recombination occurs upon co-infection with a related virus, but also within the viral quasispecies, upon random template switches of the viral polymerase during replication (template switch, or copy choice mechanism) [161-163]. In CoV evolution, the process of discontinuous transcription in sgRNA production that involves template switches from the body TRS to the leader TRS, may have selected for a replication complex particularly prone to template switching. An additional substantial evolutionary advantage of recombination events, other than avoidance of Muller's ratchet, is the possibility to combine unlinked beneficial mutations, in consequence creating a genome with higher overall replicative fitness. Linkage of beneficial mutation is of particular relevance for quasispecies dynamics, as individual beneficial mutations would otherwise compete with each other for fixation, in a process referred to as "clonal inference" [159, 161, 162, 164].

Recombination appears to be a central aspect of RNA virus biology that has shaped the genomes of many RNA viruses [45, 50, 165-175]. Its importance on CoV evolution has recently been visualized by demonstrating that the 2002 SARS-CoV genome could have been formed by sequential recombination events within SARS-related CoV lineages circulating in a single bat colony [45].

2.1 – Comprehensive phenotypic analysis of MERS-CoV lineages

2.1.1 – Introduction

MERS-CoV phylogeny currently comprises three major clades, provisionally named clades A, B and C [173, 176, 177]. Whereas clades A and C contain extinct strains and strains not circulating in the Arabian Peninsula, clade B strains currently infect humans and camels in this area. Clade B is subdivided into five phylogenetic lineages. A presumed recombination between lineage 3 and 4 resulted in the formation of a recombinant lineage (lineage 5, also termed NRC for *novel recombinant clade*) during or before the year 2014 [172-174, 178]. As detailed above, recombination is a hallmark of CoV evolution and has been described for different CoVs infecting humans and animals [42, 44, 165, 166, 168, 169, 175]. Given that the current human-to-human transmission rate for MERS-CoV is close to the critical threshold for sustained transmission ($R_0 \approx 0.6-1$) [58], the emergence of a recombinant MERS-CoV lineage deserves critical attention. As described in chapter 1.7, recombination events may have beneficial effects on the recipient genome that may increase transmissibility, particularly by contribution of epistatic effects in linking beneficial mutations [179, 180].

From a public health perspective, the enzootic distribution of MERS-CoV in camels across the Middle East is a complex and difficult subject. Because seroprevalence studies show that MERS-CoV was prevalent before its incidental discovery in 2012 [53, 54], the sudden increase of notified cases after 2013 must be ascribed to the introduction of diagnostic tools. Reduced availability of diagnostics and reduced commitment of affected countries to surveillance and hospital infection control may have caused an apparent decline of notified cases after 2015 [181]. Whereas the availability of notification data over a timespan of seven years (2013-2020) now enables a better assessment of health security risks, functional knowledge about MERS-CoV, particularly concerning phenotypical differences between circulating lineages, is limited. Virological studies have been largely restricted to the reference strain EMC (for Erasmus Medical Centre), which pertains to a genetic lineage that was never again isolated after 2012. Sequencing activities and data sharing have surged since some time into 2015. Based on more recent studies it now emerges that since 2015 the recombinant lineage 5 has essentially replaced all other endemic strains [182] (**Figure 5**).

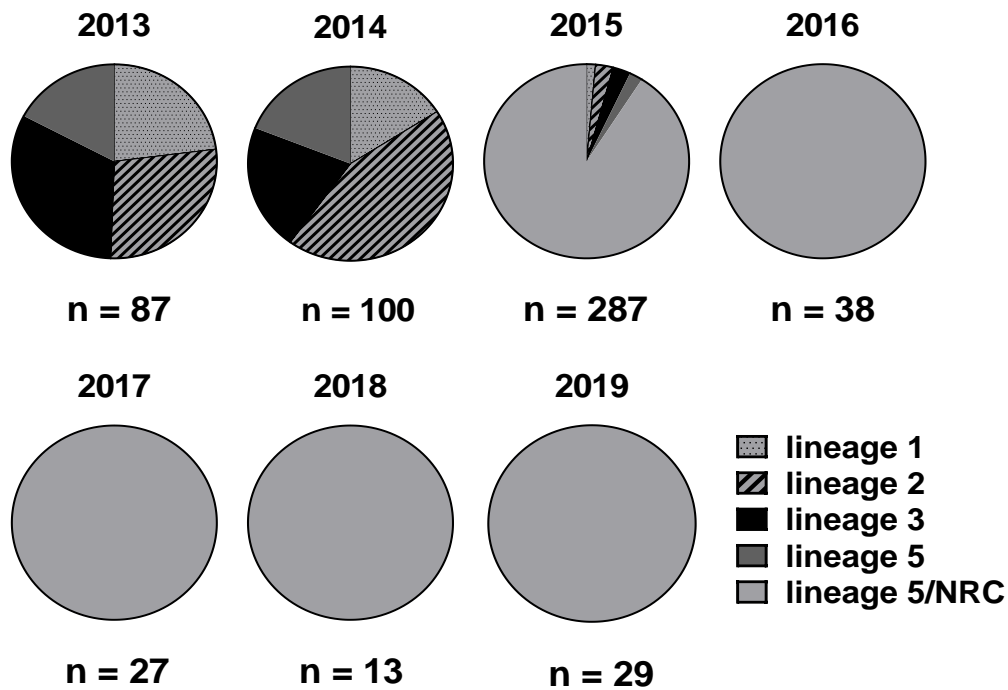


Figure 5: MERS-CoV sequences uploaded to NCBI GenBank between 2013 and 2020. All available GenBank entries for MERS-CoV with a sequence length $\geq 5,000$ nucleotides were included ($n = 561$). The collection date provided in GenBank was used for assigning a year to each sequence.

This continuous circulation of a single virus clade over several years is unusual, as prior to the emergence of lineage 5, frequent exchange and co-circulation of clades with co-detection of different virus lineages even in single hospital outbreaks was the norm. The novel dominance of a single viral lineage therefore deserves clarification, particularly because any change of phenotype might indicate alterations in the already existing potential for human-to-human transmission. Changes of phenotype in association with lineage 5 emergence have been suspected, but phenotypic studies of MERS-CoV strains are generally limited. Mutations in the spike protein positions I529T and D510G observed during the outbreak in South Korea were suggested to have contributed to antibody evasion [183]. However, these polymorphisms evolved during and not prior to the Korean MERS-CoV outbreak and hence cannot explain the dominance of lineage 5 since 2015 [184]. Earlier studies looking into functional differences between MERS-CoV clades other than lineage 5 found little evidence for phenotypic differences [176, 185-187]. One complicating feature of MERS-CoV is that the infection phenotype as seen in humans is difficult to reflect in small animal models [188].

In this first part of the thesis, I aimed to understand phenotypic traits of lineage 5 virus isolates, in using different cell-, epithelial-, and *ex-vivo* human lung models to compare patient virus isolates belonging to lineage 5 as well as the parental lineages 3 and 4. As MERS-CoV is known to act against the induction of cytokines and overcome the effects of antiviral genes

(see chapter 1.6) [85, 86, 121, 132, 189], differences in immune gene activation and suppression of viral replication in response to IFN signaling were studied.

The presented studies demonstrated that lineage 5 MERS-CoV isolates replicate more efficiently, show decreased antiviral IRF3- and NF-kB-dependent signaling, and are less susceptible to the IFN response.

2.1.2 – Results

2.1.2.1 Generation of MERS-CoV isolates from clinical samples obtained from Saudi Arabian patients

Between March 2014 and November 2015 over 3,000 clinical samples were obtained from Saudi Arabian MERS patients. Virus isolations were attempted on 99 samples with a high virus load (CT-value > 25), as determined by quantitative real-time PCR (chapter 3.26) [190]. These 99 samples were used to inoculate Vero B4 and Caco-2 cells in parallel. In 31/99 samples virus replication could be detected, evident by cytopathic effects (CPE) of the inoculated cells after 3-4 days. Virus replication was confirmed by real-time PCR, and the culture supernatant of these 31 samples was used to produce passage 2 working stocks (chapter 3.2). Virus stocks were purified using vivaspin columns 72 hours post infection (hpi) and virus titers were quantified by plaque titration (chapter 3.6). No plaque purification was performed to avoid the introduction of virus selection bottlenecks. The complete workflow for MERS-CoV isolate generation as applied here, including subsequent genomic analyses (chapter 2.1.2.2-2.1.2.3), phylogenetic analyses (chapter 2.1.2.4) and phenotypical characterizations (chapter 2.1.2.5-2.1.2.14) is illustrated in **Figure 6**.

1	> 3,000 putative MERS patient samples	03/2014-11/2015
2	Quantification of virus load by real-time PCR (N = 99/> 3,000 samples with CT-value > 25 identified)	Chapter 2.1.2.1
3	Primary MERS-CoV isolation (N = 99) (inoculation of Vero B4 and Caco-2 cells)	
4	Monitoring of virus replication (CPE and real-time PCR) (N = 31/99)	
5	Working stock production, purification and titration (N = 31)	
6	Next generation sequencing (N = 31)	
7	Full genome assembly and analyses (N = 26/31 full genomes assembled)	Chapter 2.1.2.2-2.1.2.3
8	Phylogenetic and recombination analyses (N = 26)	Chapter 2.1.2.4
9	Phenotypical characterization of MERS-CoV lineages	Chapter 2.1.2.5-2.1.2.14

Figure 6: Overview of the workflow to isolate and characterize MERS-CoV isolates, as applied in this thesis.

2.1.2.2 Deep sequencing of generated MERS-CoV isolates

Viral RNA was isolated from the 31 purified virus stocks and subjected to ultra-deep sequencing on a MiSeq platform (chapter 3.11). Using the Geneious software, all obtained NGS reads were mapped to the EMC reference genome. For 5/31 virus stocks, the NGS read count was insufficient to cover the full genome sequence. These samples showed an average of 80,000 reads, of which only 300-6,000 mapped to the EMC reference genome. Of note, these five virus stocks also showed the lowest viral load, which suggests that sequencing failed due to insufficient viral template. For 26/31 virus stocks, NGS read coverage was sufficiently high to assemble full genome sequences, with read counts between 1,000,000 and 1,500,000 reads of which 600,000 to 1,200,000 reads mapped to the EMC genome.

2.1.2.3 Genome analysis of generated MERS-CoV isolates

No deletions/insertions or changes in ORFs were observed in any of the sequenced genomes. Genetic nucleotide identity was 99.8% between the assembled sequences and EMC. The position of single nucleotide polymorphisms (SNPs) in comparison to the reference strain EMC is illustrated in **supplementary Figure 1**. Nucleotide alignments with MERS-CoV full-genome sequences available in the NCBI GenBank in August 2017 were used to scan for non-silent SNPs in the assembled genomes, with monthly updates of sequences published later than August 2017. The majority of SNPs present in the generated MERS-CoV sequences mapped to previously published sequences. All differences in amino acid expression that are shared by all isolates within their respective phylogenetic lineages (see chapter 2.1.2.4) are listed in **supplementary table 1**. Five non-silent SNPs in three MERS-CoV isolates did not map to published sequences. One unique SNP in Riyadh-1732 2015 encodes for an amino acid substitution from aspartic acid to histidine at position 510 in the spike protein. D510 is located in the receptor-binding domain and is predicted to directly interact with the MERS-CoV receptor, DPP4 [191]. Changes other than histidine in that position (D510A and D510G) have been described to reduce receptor-binding affinity in a proposed tradeoff for reduced antibody recognition [183]. A second unique spike protein mutation, from glutamine to histidine at position 522, was identified in isolate Jeddah-9313 2014. Q522H is also located inside the receptor-binding domain, however it is not predicted to interact with DPP4 [191]. Two unique mutations mapped to nsp3 (E1050D in isolate Riyadh-1764 2015 and R859V in Riyadh-1147 2014). In isolate Riyadh-1764 2015, a S64L substitution was identified in the envelope protein.

2.1.2.4 Phylogeny and recombination analysis of generated MERS-CoV isolates

For taxonomic classification phylogenetic trees based on whole-genome sequences were inferred (**Figure 7**). All virus isolates clustered with either lineage 3, lineage 4 or the recombinant lineage 5. As expected, lineage 5 sequences branched from lineage 3 in a tree based on a whole-genome alignment [172, 173, 178]. Seven isolates, originating from a MERS-CoV outbreak in Riyadh in 2014 [192], pertained to lineage 3. In whole-genome alignments, these isolates showed 98.6% average nucleotide identity with published lineage 3 strains. Eight isolates pertain to lineage 4 and originate from a 2014 outbreak in Jeddah [186] with 99.1% average nucleotide identity to published lineage 4 sequences. Another eight isolates belong to lineage 5 and stem from patients treated in Riyadh between September and November 2015. These lineage 5 isolates are 98.9% identical to published lineage 5

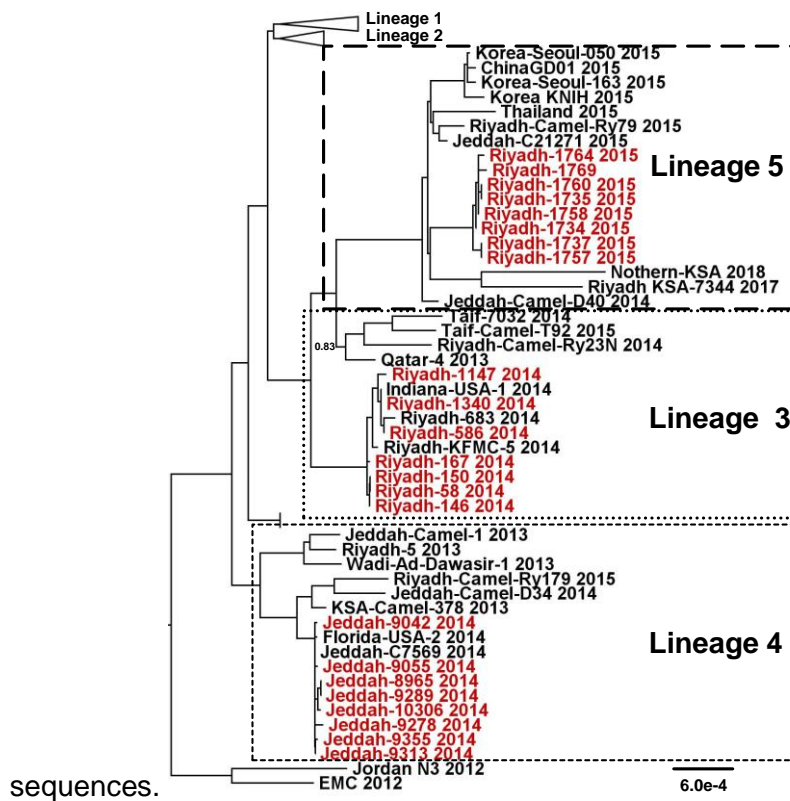


Figure 7. MERS-CoV isolates from Saudi Arabian patients cluster with three distinct phylogenetic lineages. RaxML phylogenetic trees including reference sequences and coding-complete genomes of newly generated virus isolates (red). Phylogenetic lineages 1 and 2 are collapsed only to focus the figure.

As detailed in chapter 2.1.1, MERS-CoV lineage 5 originates from a recombination event between lineage 3 and lineage 4 [172-174, 178]. Methodologically, detection of recombination between genomes is based on observation of conflicting topologies in phylogenetic trees. Because phylogenies give an account of similarity between sequences, recombinant genomes will cluster incongruently with related sequences, relative to their recombination breakpoint. Two different methods were used to confirm the recombination event for the MERS-CoV lineage 5 isolates. First, BootScan (implemented in SimPlot) was applied to construct several maximum likelihood phylogenetic trees for several frames of a nucleotide alignment. For each frame in the alignment the program indicates the percentage of congruency in each of the calculated trees (reported as percent of permuted trees), for each frame in the alignment. In an alignment with MERS-CoV EMC, lineage 3, lineage 4 and lineage 5 sequences, the BootScan analysis detected a clear signature of recombination for lineage 5. Lineage 5 genomes clustered with lineage 3 sequences at genome sites 1 to 16,174 and 23,953 to 29,714 bp, and with lineage 4 sequences from 16,175 to 23,952 bp (**Figure 8A**), in accordance with previous recombination analyses of the recombinant lineage 5 [172, 173]. As a second method of recombination detection, phylogenetic trees were inferred with the previously proposed outer and inner non-recombinant segments [173]. Both phylogenies show the typical pattern of topological incongruence when inferring trees from alignments that cover different genome portions relative to the two recombination breakpoints (**Figure 8B**). As expected, lineage 5 sequences cluster with lineage 3 sequences in trees inferred from the outer recombinant region, whilst they cluster with lineage 4 sequences in the inner recombinant region.

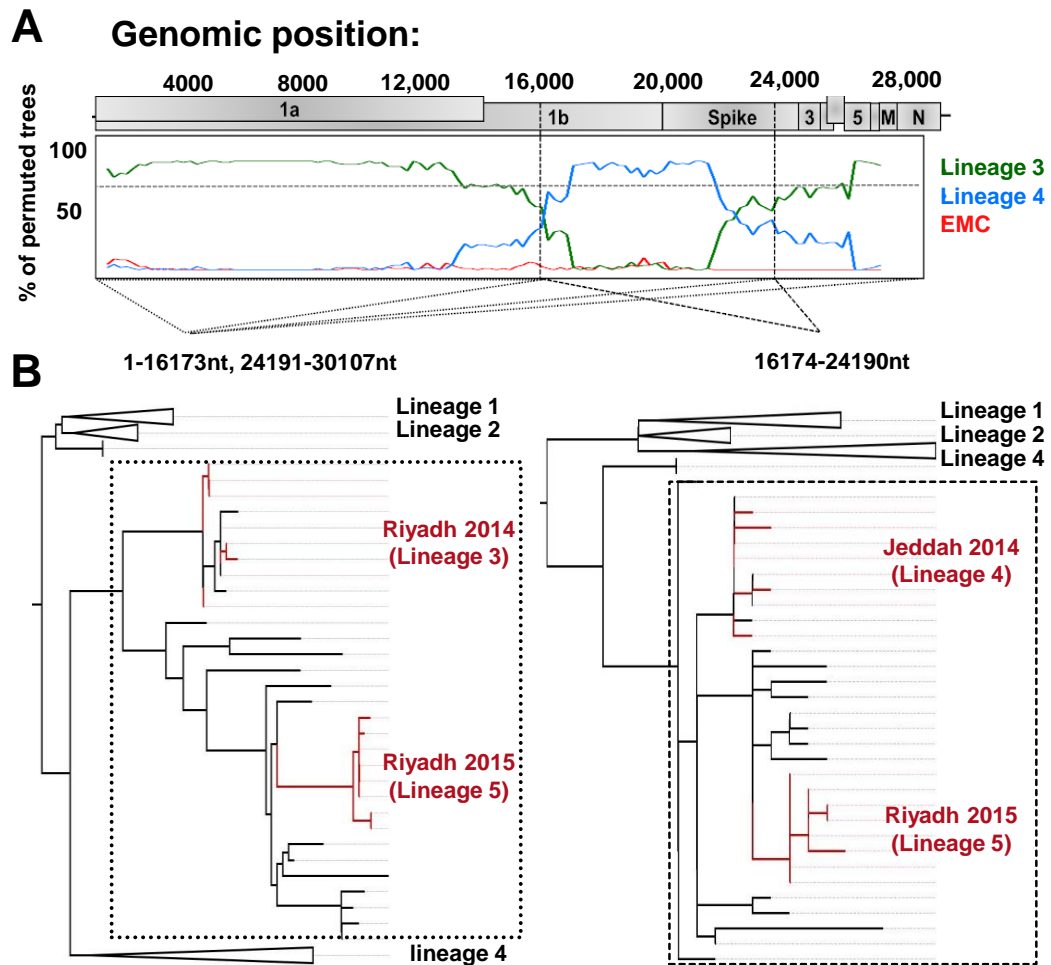


Figure 8. In depth analysis of the recombination event in MERS-CoV isolates confirm recombination in lineage 5 **A)** BootScan recombination analysis based on a whole-genome alignment. Riyadh-1764 (lineage 5) was set as query and compared to Riyadh-146 (lineage 3), Jeddah-10306 (lineage 4) and EMC/2012 (outlier) sequences (GenBank accession number JX869059). **B)** Bayesian phylogenetic tree based on alignments comprising concatenated 5'-proximal and 3'-distal sequences as indicated in the figure (left), as well as the central fragment situated between recombination breakpoints (right). Posterior support values are only shown if below 0.85. Viruses isolated in the present study are highlighted in red.

2.1.2.5 Enhanced Replication of MERS-CoV lineage 5 in cell culture

To avoid cell culture-derived selection biases, all quantitative experiments were done on different representative isolates per viral clade with subsequent pooling of results.

To compare viral replication of the different MERS-CoV lineages, multi-cycle growth curves in Vero B4 monkey kidney cells that are widely used for diagnostic isolation of MERS-CoV were performed. No significant growth differences between isolates were found (**Figure 9A**). Because of the known deficiency of Vero cells in type I IFN induction, multi-cycle growth curve experiments were additionally performed in human lung- and colon carcinoma cell lines Calu-3 and Caco-2, respectively. These experiments yielded up to 10-fold increased replication levels for all tested isolates pertaining to lineage 5. Growth was enhanced over that of the EMC reference strain, but also over that of all tested isolates pertaining to parental lineage 3 and 4 (**Figure 9B-C**).

Two representative isolates per lineage were tested in these experiments initially. In order to minimize any influence of possible inter-isolate phenotypic variability an extended range of virus isolates was used for the experiment in Calu-3 cells (**Figure 9C**). In each of four independent experiments summarized in the figure, infections were performed with different sets of two viral isolates for each lineage, resulting in each lineage to be represented by eight different viral isolates in the experiment (refer to **supplementary Table 2** for virus isolates used in each experimental repetition). Overall, the tested MERS-CoV isolates pertaining to lineage 5 produced viral titers at least 5-fold higher than lineage 3 and lineage 4 isolates at 24 hpi (**Figure 9B and 9C**). Within individual experiments, representatives of lineage 5 reached up to 10-fold higher infectious titers than those of lineage 3 and 4. The highly replicated experiment in **Figure 9B** yielded an average concentration of 1.23×10^5 plaque forming units/ml (PFU/ml) for lineage 5 isolates compared to 2.2×10^4 PFU/ml for lineage 3 and 2.4×10^4 PFU/ml for lineage 4. All of these differences were highly significant. In addition the difference against MERS-CoV EMC was highly significant ($p < 0.0006$). To better represent the conditions of viral replication at respiratory epithelia, polarized Calu-3 cells grown under air-liquid interface conditions were infected, resulting in the same viral phenotypes (**Figure 9D**).

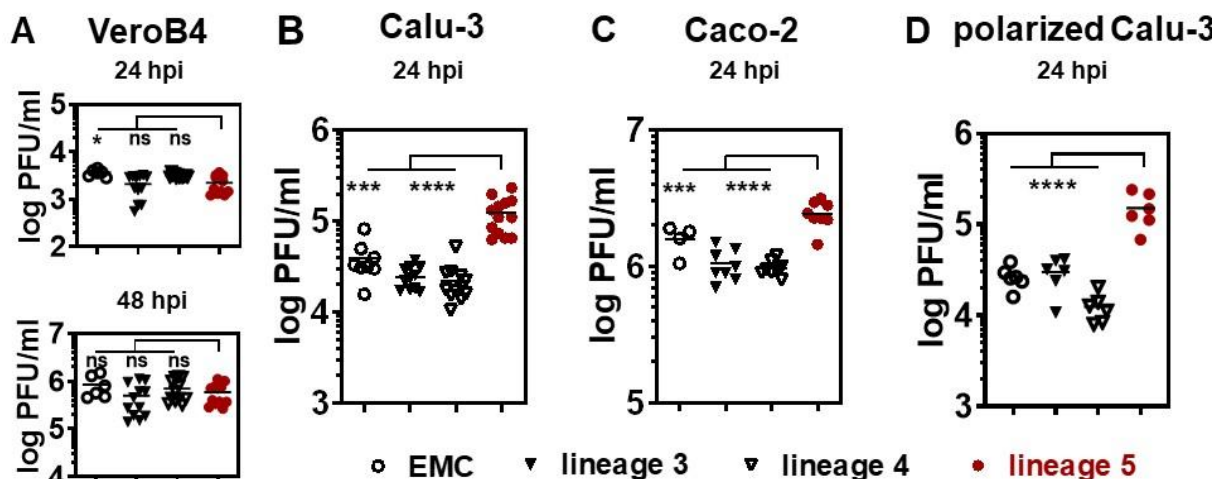


Figure 9. Enhanced replication of lineage 5 virus isolates on permanent and primary cells. Cells were infected at MOI = 0.002 and virus progeny in supernatant quantified by plaque assay in cell culture supernatants. **A)** Vero B4 cells, 24 and 48 hpi; **B),** Caco-2 colon cells, 24 hpi; **C)** Calu-3 lung cells, 24 hpi; **D)** polarized Calu-3 lung cells grown as air-liquid interface culture, 24 hpi. Every dot constitutes the average of triplicate infections, performed in four (Calu-3) or two (Caco-2, Vero B4 and polarized Calu-3 cells) independent experiments on different days. Statistical significance in difference of PFU/ml between MERS-CoV lineage 5 and other lineages was determined by Krustall-Wallis test in A) (* $P > 0.0332$, ns $P < 0.05$), and by two-tailed t-test in B), C) and D) (** $P < 0.0021$; *** $P < 0.0002$; **** $P < 0.0001$).

2.1.2.6 MERS-CoV lineage 5 has enhanced competitive replicative fitness

Cell culture growth kinetics can be limited by systematic and random errors, which can be partially controlled for by competitive replication studies in which viral isolates compete in a single culture dish [193, 194]. A given virus is likely to have superior relative fitness if it can become dominant in a virus population in spite of starting as a minority population in the initial virus seed dose [24]. To test this, Calu-3 cells were infected with a mixture of representative virus of lineage 5 and lineage 3, serving as the competitor, in two different ratios (1:1 and 9:1; lineage 3 : lineage 5). The total infectious dose in these cultures was 10,000 PFU, corresponding to an intermediate MOI = 0.04 which enables a short multi-cycle growth experiment while avoiding stochastic errors in the seed dose. As the total virus amplification may be too limited to detect shifts in lineage ratios when starting from this seed dose, four additional amplification cycles were done. In preliminary experiments, such as multi-cycle infection experiment detailed in chapter 2.1.2.5, the yield of infectious virus progeny when infecting Calu-3 cells at MOI = 0.04 was determined to be in the range of $10e4$ - $10e5$ PFU/ml at 24 hpi. Therefore, 24 hpi supernatants were diluted to a new seed dose of approximately

1,000-10,000 PFU and used as an inoculum for a second passage. This process was repeated until a completion of five passages. Viral RNA was isolated from the initial inoculum (p0) and from the supernatant after five passages (p5) and directly sequenced with two different single nucleotide polymorphisms (SNP) sites that were each amplified from the virus population in three separate RT-PCR reactions to control for PCR-based artifacts.

Based on Sanger sequencing, peak heights of the sequencing reaction was analyzed with the web-based Chromat Quantitator (Mullins lab, University of Washington; chapter 4.12) to quantify how much of each virus lineage was present at p0 and p5 (**Figure 10A**). The ratio of virus progeny at p5 was found to shift in favor of lineage 5 (**Figure 10B**) in all cases, which strongly argues for an increased replicative fitness of lineage 5 MERS-CoV isolates.

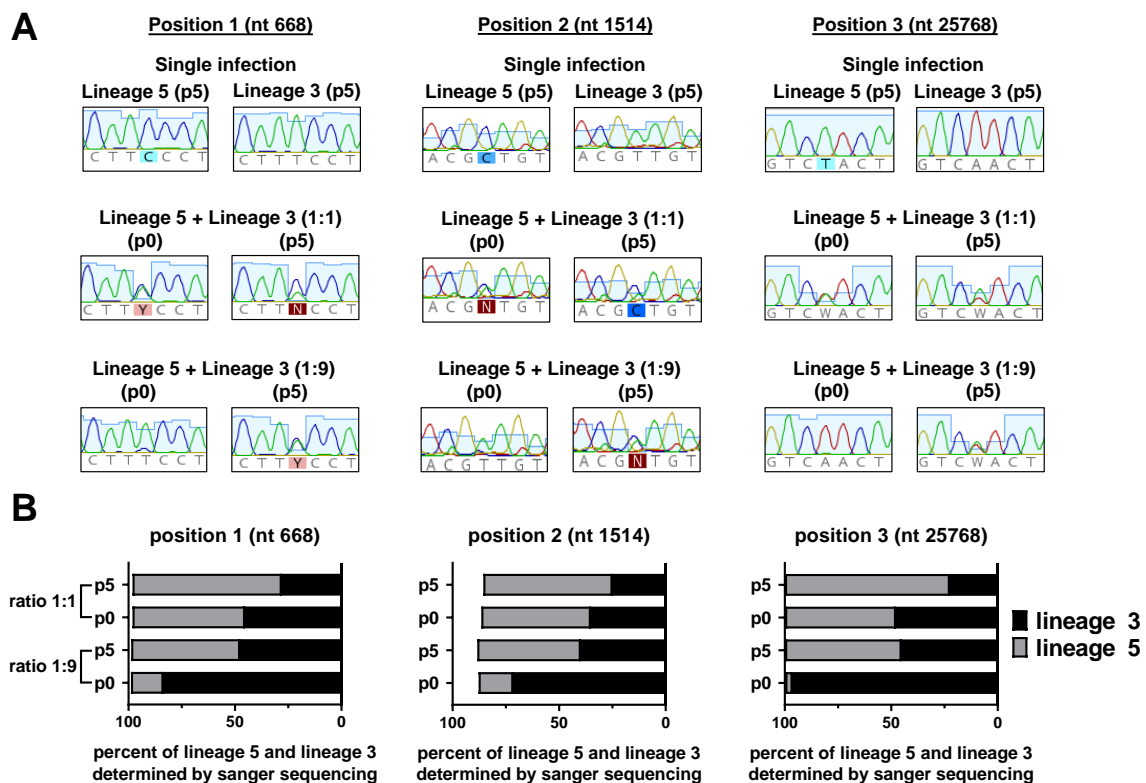


Figure 10: Lineage 5 outcompetes a parental virus strain of lineage 3 in an *in-vitro* fitness competition assay. Calu-3 cells were infected in duplicates with 10,000 PFU containing the indicated ratios of a lineage 3 : lineage 5 virus isolate at the time of initial infection (p0). 1,000-10,000 PFU were transferred in 5 subsequent passages. **A)** At p0 and p5, viral RNA was isolated from the inoculum/supernatant and two RT-PCRs over two SNP that discriminate lineage 3 and lineage 5 were performed. RT-PCR amplicons were subjected to Sanger sequencing over the respective SNPs to investigate changes in sequencing chromatograms. **B)** average peak heights in sequencing chromatograms at each SNP were analyzed using the Chromat Quantitator server and compared between p0 and p5 populations

Analysis of stages of viral replication cycle

Multiple factors could be responsible for enhanced MERS-CoV growth in cell cultures, including improved virus attachment, entry, transcription, replication, infectious particle production, or innate immune counteraction.

In the following sections, it was delineated which parts of the virus life cycle contributes to the increased replication observed in the lineage 5 isolates.

2.1.2.7 MERS-CoV EMC and lineages 3, 4 and 5 show similar host cell entry

The spike protein mediates attachment and entry into host cells via the host receptor DPP-4 [81]. Its N-terminus additionally mediates virus attachment via sialic acid domains [89]. Comparison of viral sequences provide no indications for the involved spike proteins to differ in their sialic acid-binding and receptor-binding properties. All spike sequences are identical to each other with the following exceptions (**Supplementary Figure 2**): lineage 3 genomes uniquely encode for a L411F substitution, situated in the receptor-binding domain (RBD). The RBD domain is responsible for binding to the entry receptor, consequently mutations in the RBD may influence receptor binding. However, previous studies of the L411F polymorphism demonstrated unaltered binding affinity and entry efficiency for this polymorphism [183]. Lineage 4 genomes uniquely encode for a Q833R substitution. Position 833 lies outside of the RBD and is therefore unlikely to have phenotypic consequences. All three lineages are distinct from the EMC reference strain by the Q1020R mutation that is shared among all MERS-CoV sequences pertaining to phylogenetic clade B. The spike protein N-terminus is identical in all four lineages and no differences in glycosylation that could influence sialic acid binding affinity were predicted *in silico*, using the NetNGlyc and NetOGlyc server (see chapter 4.12). All three lineages are predicted to have three O-glycosylations in total, two at the N-terminal domain and one at the C-terminal domain. Nine significant hits were detected for N-glycosylation in all three lineages, with the majority being present in the N-terminal domain, as expected [89].

2.1.2.8 MERS-CoV EMC and lineages 3, 4 and 5 show similar host cell entry capacity and DPP4-binding

In order to verify the sequence-informed hypothesis that the spike proteins of lineage 3, 4 and 5 do not differ in their capacity to mediate host cell entry and receptor-binding, expression vectors carrying the spike proteins of lineage 3, lineage 4 and lineage 5 were cloned and incorporated into a rhabdoviral vesicular stomatitis virus (VSV)-based pseudotyping system [183]. The VSV system enables a quantitative assessment of entry capacity, as each pseudotyped particle transduces target cells with a firefly luciferase (fLuc) gene upon cell entry.

Fluc activity in transduced cells therefore serves as a direct correlation of how efficiently the transfected spike protein gene facilitates host cell entry.

No significant differences in host cell entry capacity was observed between the pseudotyped VSV particles (**Figure 11A-C**). Entry capacity was tested in cell lines expressing high and low amounts of TMRPSS2 (high: Calu-3 and Caco-2, **Figure 11A** and **11B**; low: Huh7, **Figure 11C**) to account for entry capacity with protease primed and non-primed spike protein [195]. In order to determine differences in DPP4-binding capacity of each spike, lineage-specific spike genes were expressed in 293T cells and incubated with varying concentrations of soluble human DPP4. Subsequently, bound DPP4 was incubated with a Fluorophore-conjugated anti-human antibody, which was quantified by flow cytometry. No significant differences in DPP4-binding capacity between the spike proteins of each lineage were found (**Figure 10D**).

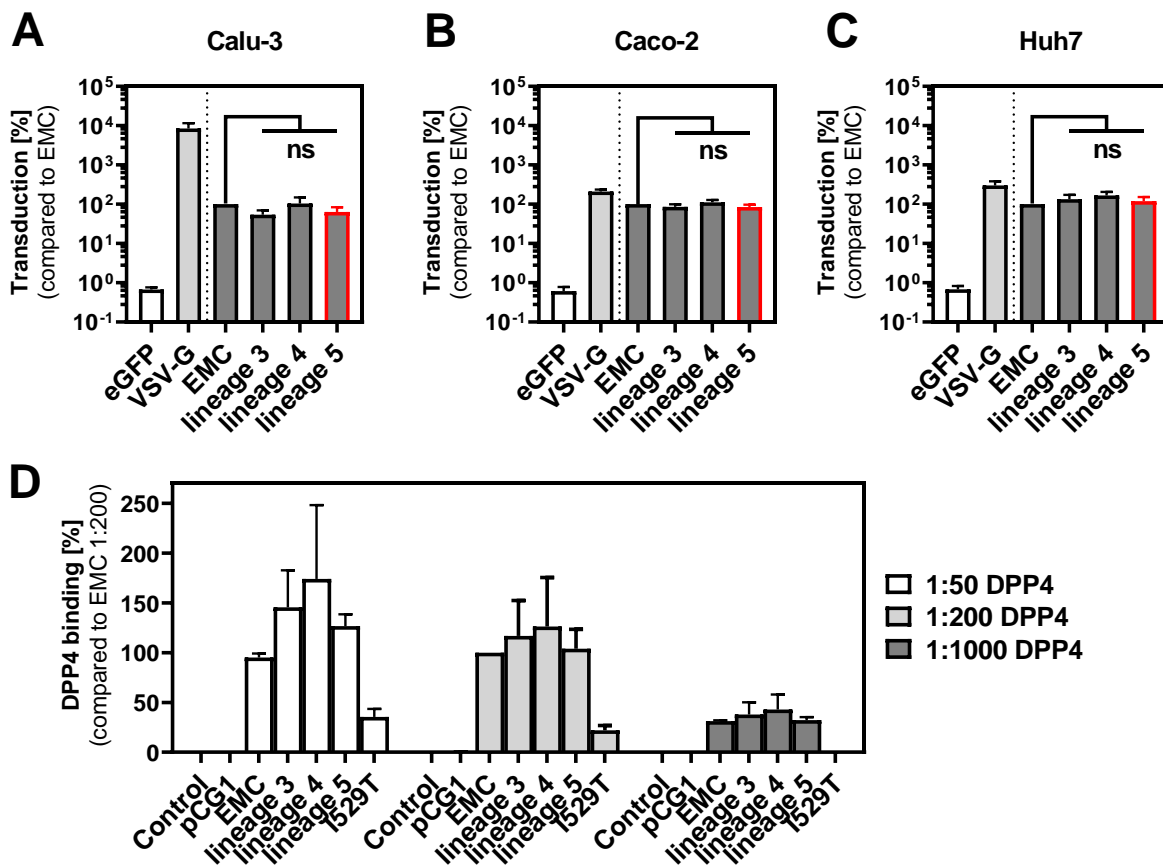


Figure 11: lineage specific MERS-CoV spike proteins show no difference in host cell entry and DPP4-binding capacity. **A-C)** rhabdoviral particles harboring MERS-CoV spike proteins of the EMC isolate, lineage 3, lineage 4 and lineage 5, VSV-G (positive control), or eGFP (negative control) were inoculated onto TMRPSS2 expressing Calu-3, Caco-2 and TMRPSS2 negative Huh7 cells. Transduction efficiency was quantified at 18 hours post transduction by measuring the activity of virus-encoded luciferase in cell lysates. Transduction mediated by EMC spike protein was set as 100%. The averages from three individual experiments performed with quadruplicate samples are shown; error bars

indicate SEMs. Statistical significance was analyzed by paired two-tailed Student's t-tests. **D)** 293T cells transfected to express MERS-CoV lineage-specific spike proteins or empty expression vector (pCG1) were detached and incubated with human Fc-tagged, soluble DPP4 (solDPP4-Fc), diluted 1:50, 1:200 and 1:1,000 and an Alexa Fluor 488-conjugated anti-human antibody before DPP4-binding was quantified by flow cytometry. For normalization, binding of 1:200 solDPP4-Fc to EMC spike was set as 100%. For background subtraction of samples incubated with just Alexa Fluor 488-conjugated antibodies (control) was performed for each sample. EMC spike carrying the I529T SNP was included as an internal control, since this SNP has been previously shown to reduce DPP4-binding [183]. The results of a single representative experiment carried out with triplicate samples are shown and were confirmed in a separate experiment. Error bars indicate SDs.

As viral proteins other than the spike protein may influence the entry process, infection assays in Calu-3 cells using virus isolates were performed, in a single-cycle infection (MOI = 1). Intracellular genomic RNA uptake 1 hour and 4 hours after virus adsorption was quantified by real-time PCR. All cell cultures were infected at 4°C to ensure that cell entry initiation is simultaneously achieved by a temperature shift to 37°C. Genomic RNA as well as sgRNA N were quantified as an early and sensitive indicator of the onset of transcription after the conclusion of the entry process. As a control, several stages of MERS-CoV entry were simultaneously blocked using inhibitors of clathrin-mediated endocytosis (classical entry pathway), host membrane serine proteases (alternative entry pathway via direct fusion with the plasma membrane), as well as endosomal proteases (downstream endosomal fusion).

No significant differences in genomic and sgRNA quantities among all virus lineages were detected 1 and 4 hours post binding (**Figure 12**). Chemical blocking of virus entry revealed that all four lineages had entered into the stage of sgRNA transcription by 4 hours post adsorption, without discernible difference in transcription levels.

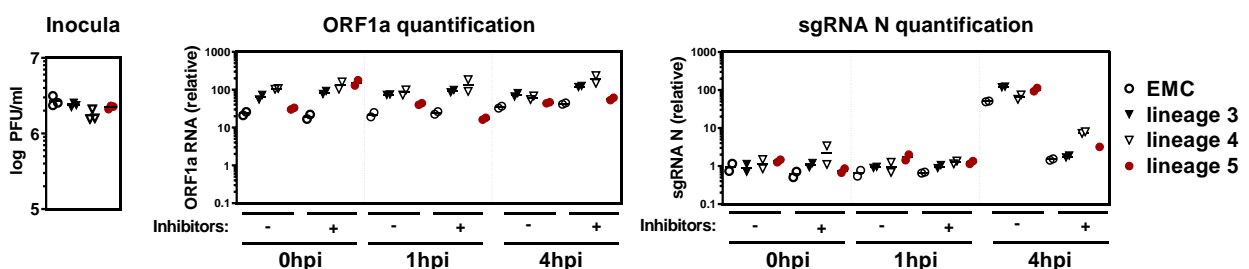


Figure 12. All tested MERS-CoV strains show similar host cell entry. Calu-3 cells were infected in duplicates with one virus isolate of all each phylogenetic lineage (EMC, lineage 3, lineage 4 and lineage 5) at MOI = 1 in the presence or absence of CoV entry inhibitors. Entry inhibited samples were pre-incubated for 1 hour with a cocktail of 25 μ M Cathepsin L inhibitor, 25 μ M Pitstop II, and 100 μ M Camostat mesylate. The inhibitor cocktail remained on the cells during the whole course of infection. To allow for a synchronized virus entry, virus attachment was performed at 4°C for 1 hour, followed by four

washing steps with PBS. After virus attachment, infected Calu-3 cells were either immediately lysed (0 hpi), or incubated at 37°C for 1 hour or 4 hours, respectively (1 hpi and 4 hpi, respectively). Total RNA was isolated from lysed cells and viral genomic RNA (ORF1a) and sgmRNA N was quantified by real-time qPCR and plotted relative to the amount of the housekeeping gene TBP. The inocula of each phylogenetic lineage were back-titrated by plaque assay to confirm that highly similar amounts of infectious particles were used to infect the cells.

2.1.2.9 All MERS-CoV lineages are comparably neutralized by anti-MERS-CoV-positive human and camel sera

Because neutralizing antibodies may act via proteins or domains other than the spike N-terminus and RBD, serum neutralization based on a highly sensitive plaque reduction neutralization assay (PRNT) on live viruses was tested. If antibody-mediated virus neutralization was different between the lineages, this would imply that different dilutions of sera are required for a 50% reduction in plaques. However, all virus isolates were neutralized with equal efficiency, i.e. the same serum dilution factor, by human (N=2) and camel (N=3) sera as summarized in **Table 1** [11].

Table 1. Plaque reduction neutralization assays (PRNT50 dilutions) with five sera for four MERS-CoV isolates.

Reference serum designation	Virus strain*			
	EMC/2012 (clade A)	Riyadh- 1147 (lineage 3)	Jeddah- 9313 (lineage 4)	Riyadh- 1732 (lineage 5)
Munich-1 (MERS patient, Germany 2014) [196]	1:1,280	1:1,280	1:1,280	1:1,280
SA278 (MERS patient, KSA 2014) [187]	1:2,560	1:2,560	1:2,560	1:2,560
Dubai-S1 (camel, UAE 2014) [197]	1:10,240	1:10,240	1:10,240	1:10,240
Kenia-ILRI (camel, Kenya 2017) [54]	1:5,120	1:5,120	1:5,120	1:5,120
Pakistan-493 (camel, Pakistan 2015) [198]	> 1:10,240	> 1:10,240	> 1:10,240	> 1:10,240

*indicated viruses were neutralized with two human sera and three camel sera as indicated. The data indicate serum dilutions at which 50% of plaque forming units are neutralized as compared to control.

2.1.2.10 MERS-CoV lineage 5 shows an earlier commencement of replication

The above-mentioned experiments used synchronized infections at high MOI. Next, multi-cycle, low MOI replication experiments were performed in Calu-3 and Vero B4 cells, to ensure that the early phase of replication is less masked by input viral RNA. Virus inoculation of cells was done at 4°C to allow virus particle attachment to the cellular receptors before simultaneous cell entry was induced by shifting the temperature to 37°C. sgRNA transcripts of the nucleocapsid gene (sgRNA N) were quantified as an indicator for early virus transcription whereas genomic ORF1a-specific RNA was detected to monitor the onset of full virus genome replication. Additionally, PFU/ml were quantified in the supernatant to analyze differences in virus particle formation and egress (**Figure 13**).

Overall, there was little difference between sgRNA N and genomic ORF1a transcript quantification, which is plausible considering that both are copied from the same template and replicative intermediates accumulate in parallel [121]. Virus infections in Calu-3 cells showed an earlier onset of replication than in Vero B4 cells, which may be attributable to the availability of TMPRSS2 providing an additional entry pathway in Calu-3 cells [199]. Already from the beginning of detectable replication, lineage 5 viruses showed a higher level of RNA transcription than the parental lineages 3 and 4. Enhanced infectious virus production of lineage 5 was only seen in Calu-3- but not in type I IFN-deficient Vero B4 cells, which corresponds to the previous observations in multi-cycle infection experiments (**Figure 9**).

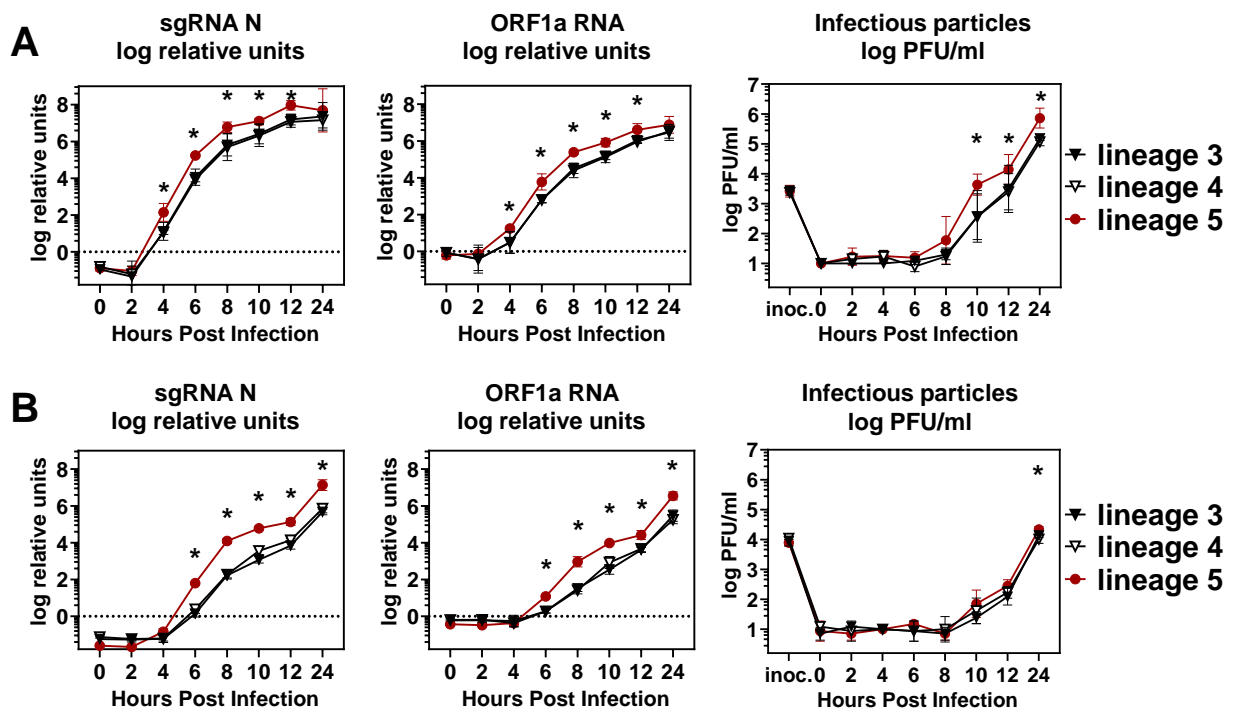


Figure 13. sgRNA N, ORF1a and PFU quantification at early stages of infection. A) Calu-3 and **B)** Vero B4 cells were infected at an MOI of 0.002 with one virus isolate of each phylogenetic lineage in

duplicates for each indicated time point. At the indicated time points, cell culture supernatant was collected and subjected to virus quantification by plaque assay. Infected cells were lysed and total RNA was isolated to be subjected to quantification by real-time PCR of sgRNA N and ORF1a RNA. Cycle thresholds were normalized to the housekeeping gene TBP and the amount of RNA at 0 hpi. Statistical significance of differences in virus replication was analyzed by Mann-Whitney test (p -value <0.0332 ;*).

2.1.2.11 MERS-CoV lineage 5 shows reduced cytokine induction

Results up to this point suggested that lineage 5 has a higher intrinsic replication level than viruses belonging to parental lineages. To explore if higher replication triggers a higher cytokine induction, Calu-3 cells were infected with two viruses of each phylogenetic lineage in a single-cycle, high MOI infection. mRNA expression levels were analyzed for a set of immune-related genes at 12 hpi. IRF3-regulated genes *IFNB1* and *IFNL1*, NF κ B-regulated genes *CCL5* and *TNFA*, as well as IFN-stimulated gene *Mx1* were included to reflect various common pathways in antiviral innate immunity. To enable single-cycle virus infection, cells were infected at MOI = 2 (**Figure 14A**). Under these conditions, the two lineage 5 isolates used in the experiment replicated to a higher 4.4- and 7.7-fold level than the MERS-CoV isolates of lineage 3 and 4, respectively (two strains each). Intriguingly, lineage 5 induced significantly lower levels of *IFNs* and *CCL5* mRNA compared to isolates pertaining to lineage 3 and 4 (**Figure 14B**). Immune gene mRNA induction in general seemed to be highest with lineage 3 strains. Average *IFNB1* levels were reduced 12.4 and 3.1-fold and average *IFNL1* mRNA expression was reduced 3.7- and 1.4-fold in Calu-3 cells infected with lineage 5, over Calu-3 cells infected with lineage 3 and 4 virus isolates, respectively. Average *CCL5* transcripts were induced 2.9- and 2.1-fold in cells infected with lineage 5, over cells infected with lineage 3 and 4 virus isolates, respectively.

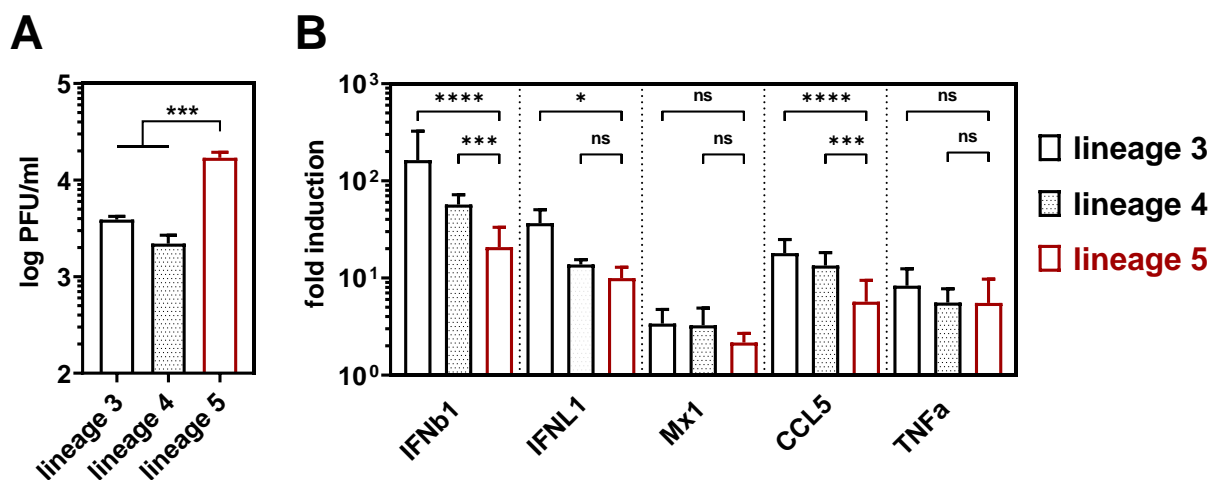


Figure 14. Lineage 5 MERS-CoV strains show reduced immune gene induction. Calu-3 cells were infected with two isolates of each phylogenetic lineage with a high multiplicity of infection (MOI = 2) for subsequent quantitative real-time PCR (q-RT-PCR) analysis of key immune genes. **A)** infectious virus

production as quantified by plaque assay 12 hpi. **B)** immune gene induction as quantified by real-time RT-PCR on lysed Calu-3 cells 12 hpi, expressed as fold induction over the non-infected control cells, normalized to the housekeeping gene TBP. Statistical significance of differences in virus replication was analyzed by Mann-Whitney test ($p > 0.05$, ns; $p \leq 0.05$, *; $p \leq 0.01$, **; $p \leq 0.001$, ***).

2.1.2.12 MERS-CoV lineage 5 is less sensitive to IFN treatment

Previous studies have shown that MERS-CoV EMC is highly sensitive towards type I IFN pretreatment [52]. To analyze IFN sensitivity among the different MERS-CoV lineages, virus replication was monitored in Calu-3 cells pre-treated with type I IFN for 16 hours. IFN concentrations were chosen to induce mainly an upregulation of cellular helicases (2.5 units IFN), as well as IFN concentrations high enough to induce a complete antiviral state (25 units) in treated Calu-3 cells.

Replication of the reference strain EMC was already suppressed by low level IFN pretreatment, in accordance to published results [120]. Lineage 3 strains showed similarly high IFN sensitivity, while lineage 4 and lineage 5 strains were not suppressed by 2.5 units of IFN (**Figure 15**). 25 units of IFN markedly reduced virus replication of all lineages. The reduction of replication caused by this dose was 6.5-fold for lineage 5 and 23- and 18-fold for virus isolates pertaining to lineage 3 and 4, respectively.

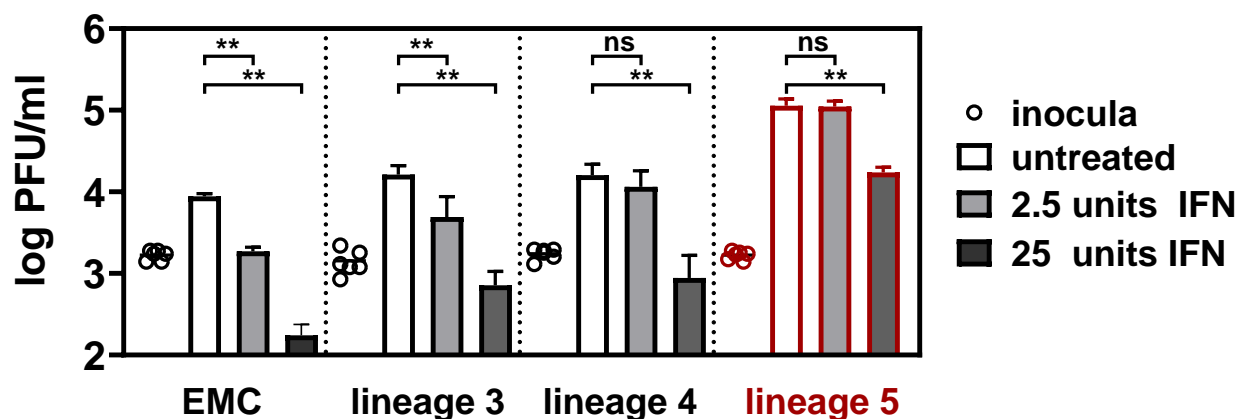


Figure 15. Lineage 5 MERS-CoV isolates show decreased IFN sensitivity. Calu-3 cells were incubated for 16 hours with 2.5 or 25 units type-I IFN prior to infection at MOI = 0.002 with two MERS-CoV isolates of each indicated lineage in triplicates. Inocula, as well as virus progeny in supernatant 24 hpi were quantified by plaque assay. Shown are the combined data of two independent experiments with error bars indicating the SD. Statistical significance of differences in virus replication was analyzed by Mann-Whitney test (ns, $P > 0.1234$; ** $P \leq 0.0021$).

2.1.2.13 Increased replication of MERS-CoV lineage 5 is not exclusively correlated to antagonism of JAK/STAT signaling

To investigate if lineage 5 viruses show a lower IFN sensitivity due to increased antagonism of IFN signaling alone, Calu-3 cells were infected with lineage 3, 4 and 5 virus isolates in the presence of the JAK/STAT inhibitor Ruxolitinib (**Figure 16A**). Additionally, virus replication was compared in MERS-CoV-susceptible T84 cells carrying an IFN-alpha and -lambda receptor double knock-out (**Figure 16B**). Whereas control experiments confirmed the higher replication levels of lineage 5, both approaches to IFN receptor inactivation caused lineage 5 strains to lose a minor part of their replicative prominence. Overall, lineage 5 strains retained a significantly higher replication level than strains pertaining to lineage 3 and 4, suggesting that IFN signaling alone does not explain the observed differences.

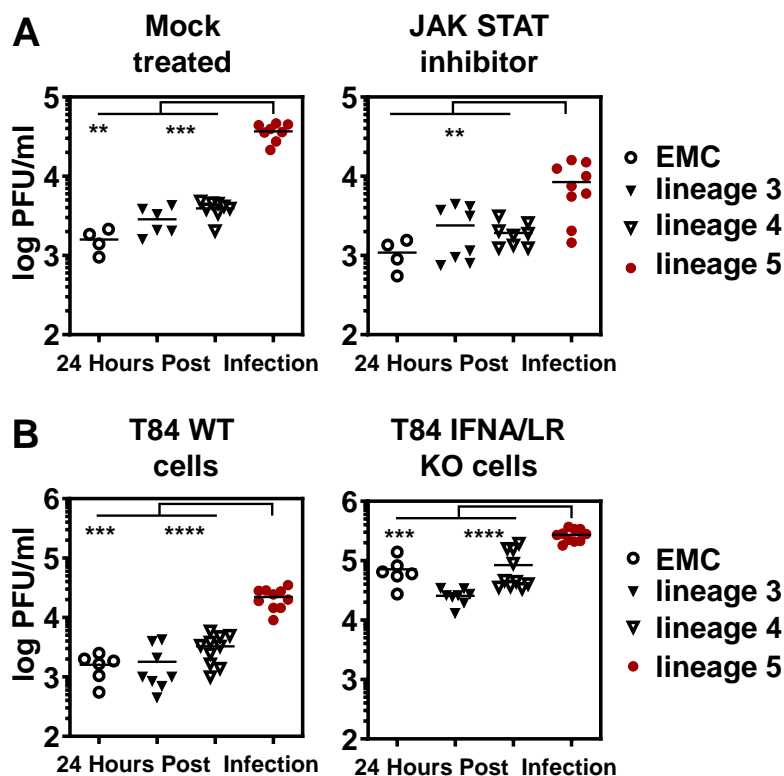


Figure 16: Replication of MERS-CoV isolates in JAK/STAT signaling inhibited and IFN receptor knock-out cells. Higher replication of lineage 5 MERS-CoV is additionally linked to IFN action via the JAK/STAT signaling pathway. **A)** Calu-3 cells were treated with 50 nM of the JAK/STAT inhibitor Ruxolitinib 1 hour prior and during the infection with two viruses per phylogenetic lineage (lineage 3, lineage 4 and lineage 5) in duplicates. Virus progeny in the supernatant was quantified by plaque assay at 24 hpi. Statistical significance of differences in virus replication was analyzed by Mann-Whitney test (** $P \leq 0.0021$, *** $P \leq 0.0002$). **B)** T84 wt and type I and III IFN receptor knock-out cells (IFNAR/IFNLR KO cells) were infected in triplicates. Virus progeny in the supernatant was quantified by plaque assay at 24 hpi. Statistical significance of differences in virus replication was analyzed by Mann-Whitney test (*** $P \leq 0.0002$; **** $P \leq 0.0001$).

2.1.2.14 MERS-CoV lineage 5 shows increased replication in models of the human respiratory tract

To more closely reflect virus replication in the respiratory tract [41], fully differentiated human airway epithelia (HAEs) were infected with two representative isolates from each phylogenetic lineage. According to previous observations supernatants were samples exclusively from the apical site of differentiated HAE were sampled and virus progeny was quantified every 24 hours for four subsequent days [45]. Lineage 5 isolates reached average titers up to 15-fold higher compared to lineage 3, lineage 4 and the EMC reference strain, with significant differences at 24 and 48 hpi (**Figure 17A**). To provide a model of infection that most closely resembles infection of the human lung, *ex-vivo* infections were performed in human lung explants, derived from patients that have undergone lung resection. One representative virus isolate per phylogenetic lineage was included to infect lung explants derived from three different donors (**Figure 17B**). Supernatants of infected lung explants were harvested at 16, 24, 48 and 72 hpi. Similar to HAEs, lineage 5 reached titers up to 5-fold higher compared to lineage 3, lineage 4 and the EMC reference strain, with significant differences at 24 and 48 hpi (**Figure 17B**).

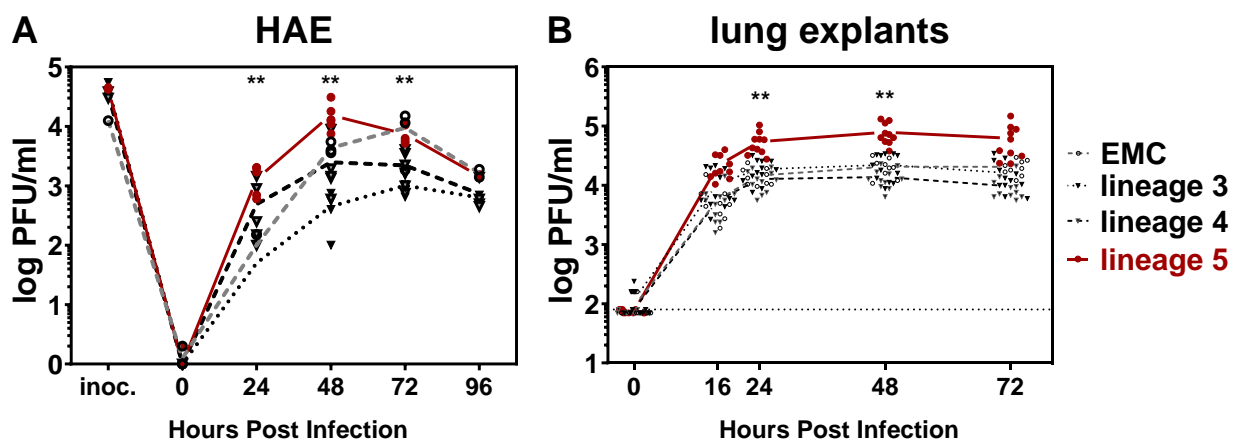


Figure 17. Growth kinetics of MERS-CoV isolates in models of the human respiratory tract. A) Replication on primary human airway epithelium (HAE) of a single donor. Two isolates of each phylogenetic lineage were used for infection in triplicates. Virus progeny in apical washes was quantified by plaque assay every 24 hours by plaque assay. Statistical significance in difference of PFU/ml between lineage and other lineages was determined by two-tailed Mann-Whitney test (** $P < 0.0021$). Statistical significant differences in PFU/ml were found at 24 hpi for lineage 5 between lineage 3 (**) and EMC (*); at 48 hpi between lineage 5 and lineage 3 (**), lineage 4 (**) and EMC (*); at 72 hpi between lineage 5 and lineage 3 (*) and lineage 4 (**). **B)** Growth kinetics of MERS-CoV isolates on lung explants, derived from three different patients that have undergone lung resection. One isolate of each phylogenetic lineage was used for infection in triplicate for each explant and virus progeny in the supernatant was quantified by plaque assay. Differences in PFU/ml between lineage 5 and other lineages was tested for significance using Krustall-Wallis test (** $P < 0.0021$).

2.1.3 – Discussion

The present comprehensive *in vitro* and *ex vivo* studies with clinical MERS-CoV isolates reflecting virus lineages prior to and past the shift towards the recombinant lineage 5, demonstrate a higher replicative fitness of MERS-CoV lineage 5 isolates over previously circulating lineages, as a function of lower level of cytokine induction and IFN resilience.

Since 2015, lineage 5 was highly prevalent in sampled dromedary camels and humans in Saudi Arabia, and caused a major outbreak in South Korea [172-174, 200]. This upsurge triggered speculations as to the transmissibility of the novel virus variant. Nevertheless, the phenotype of these viruses, as opposed to viruses circulating earlier, has not been studied to date. The data presented in this part of the thesis provide the first comprehensive phenotypical assessment of lineage 5 isolates, and reveal changes that likely correlate with transmissibility and pandemic potential. Primarily, higher relative fitness and increased replication levels may translate into higher excreted virus doses during infection. Transmission of higher average doses will inevitably increase the viral capability to adapt to humans [24, 201]. As detailed in chapter 1.7, virus transmission from one host to another constitutes a bottleneck through which only the excreted minority of the virus population will pass [202]. If a higher average virus dose is excreted, the chances that a more adaptive variant will pass through the bottleneck are increased. Secondly, reduced cytokine induction as observed here is considered an indicator of increased virulence and major determinant in overcoming species barriers (reviewed in [203]).

One can conclude from the performed experiments that the increased fitness of members of lineage 5 does not result from changes affecting viral entry and is unlikely to be based on an altered interference with IFN receptor-dependent signaling. Most likely, the differences in this part are caused secondarily due to clear differences in either infection sensing or downstream elements of cytokine induction cascades. Any functional diversity of circulating MERS-CoVs on the Arabian Peninsula is somewhat surprising given that earlier studies found little indication for phenotypic differences between viral lineages [176, 178, 186, 204]. A study of African viruses found functional diversity [176] that could be attributed to deletions in ORF4b encoding a suppressor of RNase L that acts via an active phosphodiesterase function [85, 150, 189]. However, the present viruses have a full gene repertoire and thus provide little angle to link changes of phenotype to any defined gene target. Viral proteins that have previously been associated with innate immune antagonism in MERS- and related CoVs, including nsp1, nsp3, nsp14, nsp15, nsp10/16, p4a and p4b are fully conserved in the present lineages or show amino acid substitutions unlikely to affect protein function (i.e. no addition/loss of charge or polarity or bulkiness, **supplementary Table 1** [85, 86, 132, 135, 141, 150, 189].

The further search for mechanisms to explain the viral phenotype and host response will therefore have to involve comprehensive studies such as shuffling of gene portions based on reverse genetics. Identifying causal mutations will help to understand whether and how cooperating mutations may have been assembled into one genome following recombination, and how the recombinant virus phenotype was selected for. Mapping those causal mutations to functional domains within the viral genome might even be used to assess the pathogenicity of future emerging MERS-CoV. Novel reverse genetic systems, such as *in yeast* cloning by transformation associated recombination (TAR cloning) may help to overcome the technical hurdles of shuffling large genome sections and have been already been initiated [205].

It should be clearly understood that the observed phenotype of lineage 5 does not constitute evidence for selection in humans. Analyses of viral populations have led to the conclusion that human-to-human transmission does not currently play a relevant role in MERS-CoV evolutionary dynamics, and selection therefore will have taken place in the animal reservoir [180]. However, the reduced induction of cytokine expression is compatible with selection in dromedary camels as immune sensors and appending signal transduction cascades triggering cytokine induction are conserved among mammals [206, 207]. Selection for virulence in dromedary camels may involve a collateral benefit for the virus once transmitted to humans. Importantly, increased virus dose in the camel population increases the likelihood of spillover events and hence heightens the zoonotic potential of the recombinant MERS-CoV lineage 5 over previously circulating lineages.

In the light of virus population dynamics, the emergence of a recombinant virus lineage with increased fitness is an intriguing piece of evidence that recombination events may have functional relevance on virus populations, other than purging deleterious mutations from the genome (chapter 1.7) [151]. An example of recombination between CoV lineages giving rise to a more pathogenic strain has been provided by the cases of feline CoVs and IBV [34, 35]. To the best of my knowledge, the present study is the first report of a recombinant CoV lineage with a change of phenotype in humans. Its occurrence in MERS-CoV is particularly relevant from a public health perspective, as the current human-to-human transmission rate for MERS-CoV is close to the critical threshold for sustained transmission ($R_0 \approx 0.6-1$) [58, 59]. As detailed in the chapter 1.7, recombination events may introduce shifts in a population's fitness landscape that are of larger scale than genetic drift alone, and may therefore increase the stochastic potential for a more transmissible stain to emerge. Future studies should address which viral factors are responsible for the increased fitness of lineage 5. The recombination event may itself be causal if individually neutral or beneficial mutations from donor lineages were shuffled together to increase fitness though epistasis. Virus population dynamics are driven by clonal inference, i.e. the within a quasispecies occurring competition of beneficial

mutations for the fixation in the population, rendering changes in fitness sequential [208]. Conceivably, beneficial variants were already competing for fixation in lineage 3 and 4 and the recombination event alleviated these variants from clonal inference in fusing beneficial mutations, resulting in overall increased fitness. In that line, there is some evidence from the data presented here that members of the parental lineage 4 show an attenuated cytokine-based immune response, but these viruses do not show increased overall fitness (chapter 2.1.2.11 and 2.1.2.12). Alternatively, fitness-increasing mutations might have occurred after the recombination event. It is conceivable that the recombination event caused drastic alteration in fitness landscape that enabled the exploration of secondary mutations, which may have diversified the viral quasispecies and therefore may have increased the probability for a fitter variant to be selected for (survival of the flattest theory) [209]. However, for most RNA virus species an upsurge of mutations is deleterious to fitness [26-29]. Yet, there is some evidence that natural selection works on viral quasispecies as a whole, opposed to single mutant variants of the “cloud”, and that a diversified quasispecies itself may grant fitness advantages [210]. For all lineage 5 genomes that were sequenced here, I obtained a sequencing read coverage deep enough to detect minority variants (chapter 2.1.2.2). However, in highly stringent NGS read consensus, there was no evidence for a diversified quasispecies that may have been detectable as an increase of nucleotide ambiguities in lineage 5 sequencing data over other lineages. To exclude quasispecies diversity as the driver for increased fitness in lineage 5, in depth analysis of existing sequencing data should be performed and complemented with sequencing techniques that enable discrimination between false reads and real minorities [211-213].

It is a limitation of the present study that a deeper mechanistic investigation cannot be provided. It should be noted that the observed differences in virus-host interaction may originate outside the direct infection sensing and cytokine induction mechanisms, so that changes in cytokine induction as well as the partial differences in IFN sensitivity might be collateral effects. Particularly a functionally increased replication complex that changes the expression pattern of viral immune antagonists is conceivable. Early or increased expression of viral antagonists could promote overall fitness by increased reduction of the antiviral host responses. Comprehensive studies of the replication complexes of each MERS-CoV lineages could delineate a possible correlation of increased replication and reduced antiviral signaling induction. Such studies would require the establishment of complex reporter-coupled replicon systems for each MERS-CoV lineage by reverse genetics.

Under the impressions of an ongoing SARS-CoV-2 pandemic, the emergence and epidemiological dominance of a more replicative strain of MERS-CoV should be acknowledged by public health authorities and warrants an increased surveillance of circulating MERS-CoV

species. Comprehensive studies on the biology and evolution of pre-pandemic CoV species as provided in this thesis can contribute to our understanding of the dynamics of emergence and epidemiology of this important RNA virus family.

2.2 – Phenotypic comparison of SARS-CoV- and SARS-CoV-2-specific IFN antagonism

2.2.1 – Introduction

SARS- and SARS-CoV-2 pertain to the same virus species, the SARS-related CoVs, within the genus *Betacoronavirus* [52]. However, SARS-CoV-2 shows features distinct to SARS-CoV in its clinical and epidemiological presentation, with lower pathogenicity and case fatality rate but substantially higher human-to-human transmission rate and incidence [68]. Both viruses show an identical genomic architecture with a homologous set of ORFs, however the amino acids encoded in the ORFs are not identical in sequence [66]. Consequently, putative determinants of differential pathogenicity and transmission capacity might be linked to the amino acid divergence of these ORFs.

There is good evidence that the increased human-to-human transmission rate of SARS-CoV-2 is a function of tissue tropism [67, 93, 214]. Clinical observations suggest that SARS-CoV-2 is replicating in –and importantly is shed from– the upper and lower respiratory tract, while SARS-CoV mainly replicates in the lower respiratory tract, despite identical receptor usage [214]. Recent studies imply that the differential tissue tropism correlates with spike protein divergence. As detailed in chapter 1.5, the SARS-CoV spike protein might interact with the host protease TMPRSS2 to employ the preferred and more efficient cell entry route of particle fusion at the plasma membrane [67, 92, 95]. A striking feature of the SARS-CoV-2 spike protein is a polybasic amino acid stretch (RRAR) at position 813 to 816, upstream of the S2 domain that mediates membrane fusion. Nascent SARS-CoV-2 spike proteins probably undergo furin-mediated pre-cleavage at this polybasic amino acid stretch, which primes the SARS-CoV-2 spike proteins for preferential TMPRSS2-mediated entry at the plasma membrane [93]. Further, an overall higher binding affinity of SARS-CoV-2 spike protein to the cellular receptor ACE2 was demonstrated, yet the contribution of divergent amino acids in the RBD remains to be clarified [215]. In synopsis, the altered tropism and increased transmissibility of SARS-CoV-2 might be a function of spike protein divergence and cellular co-factor distribution, particularly of TMPRSS2, which is highly abundant in the upper respiratory tract [67, 93, 216]. Of note, a similar mechanism of pre-egression furin-mediated spike cleavage is also employed by the MERS-CoV spike protein [99], yet DDP4 expression, in contrast to ACE2 expression, is limited to the lower respiratory tract [217].

If and how broader host tropism of SARS-CoV-2 contributes to pathogenicity remains elusive. A major driver of virus pathogenicity other than cell entry capacity is the evasion of innate

immunity. As detailed in chapter 1.6, type I IFNs are among the first cytokines to be upregulated in virus-infected cells and play a key role in determining the outcome of infections by orchestration of the antiviral and inflammatory response. IFN signaling triggers the expression of over 300 antiviral proteins and chemokines, inducing an antiviral state in host cells [116]. Resilience towards IFN-mediated innate immunity seems to be associated with virulence and pathogenicity in many virus families [218]. As detailed in chapter 1.6, SARS-CoV is highly sensitive towards IFN treatment and evolved multiple mechanisms to counteract the induction of IFN and IFN signaling [122, 123]. Therefore, protein sequence divergence between described (and unknown) viral IFN antagonist may exhibit effects on the immune evasion phenotype of SARS-CoV-2 that might account for the distinct clinical presentation of SARS- and SARS-CoV-2.

In this part of the thesis, the IFN evasion phenotypes of SARS-CoV and SARS-CoV-2 were compared by focusing on differences in IFN induction and signaling. Evidence for a relatively lower IFN induction antagonism by SARS-CoV-2 could be functionally correlated to protein 6, as infection studies with mutant viruses, produced by reverse genetics, implicated that SARS-CoV-2 protein 6 is less efficient in antagonizing IFN signaling than SARS-CoV protein 6 [147].

2.2.2 – Results

2.2.2.1 Replication kinetics of SARS-CoV-2 and SARS-CoV in IFN competent and incompetent cell lines

In search for suitable cell culture systems to study the newly emerged and largely unknown SARS-CoV-2, the human bronchial cell line Calu-3 and the primate kidney cell line Vero E6 were tested for their capacity to support replication of both SARS-CoV and SARS-CoV-2.

Intriguingly, there was a striking cell line specificity in the ability to support replication of SARS-CoV and SARS-CoV-2. In Vero E6 cells that lack type I IFN genes [219], SARS-CoV grew to 36-fold higher titers than SARS-CoV-2 when inoculated with an MOI of 0.001. In Calu-3 cells that have a functional IFN response [220], SARS-CoV-2 infection yielded 5-fold higher titers compared to SARS-CoV at 24 hpi (**Figure 18A**). SARS-CoV and SARS-CoV-2 induced stronger cytopathic effect in Vero E6 and Calu-3 cells, respectively, which corresponded to the differential viral growth (**supplementary Figure 3**).

To shed light on these cell line-specific observations, the impact of a blunted type I IFN signaling was determined for both viruses. Treatment with the STAT1 phosphorylation inhibitor Ruxolitinib enhanced infection by both viruses in Calu-3 cells, as judged by quantification of double-stranded RNA replication intermediates and infectious particle production, suggesting that both viruses are sensitive to a naturally induced IFN-mediated antiviral response (**Figure 18B and C**).

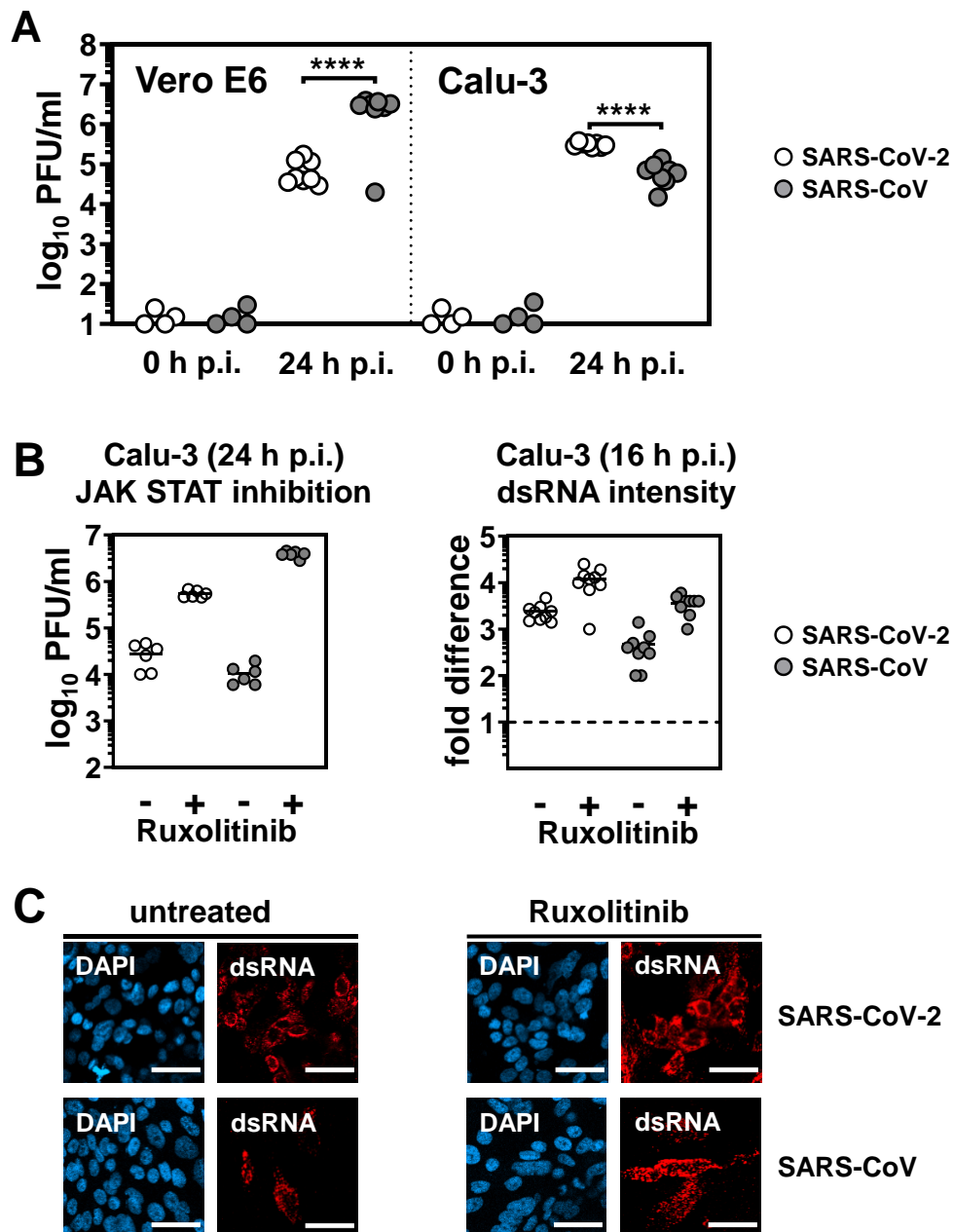


Figure 18. SARS-CoV-2 and SARS-CoV are sensitive to the IFN response. A) Multi-cycle infections (MOI = 0.001) of SARS-CoV-2 (strain Munich/2020/984; BetaCoV/Munich/BavPat1/2020 |EPI_ISL_406862) and SARS-CoV (strain Frankfurt (Fra); GenBank accession number AY310120) in the primate kidney cell line Vero E6 (left) and the human bronchial epithelial cell line Calu-3 (right). Viral titers in the culture supernatant were quantified by plaque titration on Vero E6 cells at 0, 24 and 48 hpi. Four experiments in duplicate infections were pooled. Statistical significance in difference of PFU/ml between SARS-CoV-2 and SARS-CoV PFU/ml was determined by two-tailed t-tests (p-value <0.0001;****). **B and C)** Virus replication under the influence of 100 nM of the JAK STAT inhibitor Ruxolitinib (Invivogen) as determined by plaque titration of SARS-CoV-2 and SARS-CoV in Calu-3 cells 24 hpi (MOI = 0.001). Immunofluorescent dsRNA staining was performed in Calu-3 cells at an MOI of 0.01 at 16 hpi. dsRNA signal intensity quantification was performed in ImageJ using six microscope picture frames per condition.

2.2.2.2 SARS-CoV-2 is more sensitive towards IFN treatment than SARS-CoV

For a quantitative assessment of IFN sensitivity, virus replication was compared in both cell lines after pre-infection or post-infection treatment with IFN-beta in increasing concentrations (Figure 18). To account for the cell line-specific differences in virus propagation capacity detailed in chapter 2.2.2.1, replication levels were normalized to untreated samples.

SARS-CoV-2 was more sensitive to IFN pre-treatment than SARS-CoV in particular in Vero E6 cells (**Figure 19A and B**). 1,000 IU/ml IFN reduced average SARS-CoV-2 replication to $1.31\% \pm 1.01\%$ of replication levels in untreated Vero E6 cells, while SARS-CoV replication remained unchanged. In Calu-3 cells, pretreatment with 1,000 IU/ml IFN reduced average SARS-CoV-2 replication to $0.68\% \pm 0.11\%$ and SARS-CoV replication to $6.02\% \pm 4.14\%$ of replication levels in untreated control cells.

Differences were generally less pronounced with IFN applied at 1 hpi (**Figure 18C and D**), pointing to IFN evasion by a virus-encoded antagonist that has to be available in the infected cell prior to the start of IFN signaling. 1,000 IU/ml IFN posttreatment reduced average SARS-CoV-2 replication to $58.26\% \pm 13.39\%$ and SARS-CoV replication to $17.08\% \pm 5.61\%$ in Calu-3 cells. In Vero E6 cells, average SARS-CoV-2 replication was reduced to $11.24\% \pm 8.49\%$ and SARS-CoV replication to $81.42\% \pm 52.74\%$.

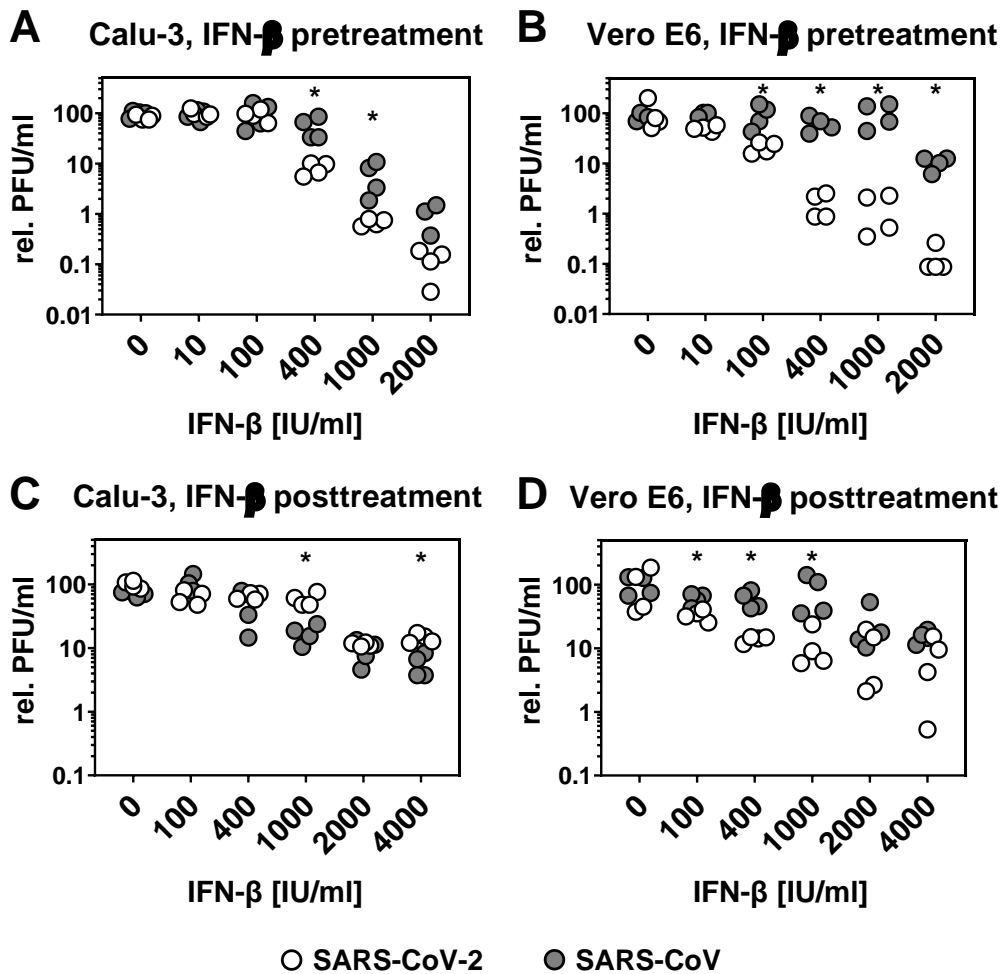


Figure 19. SARS-CoV-2 is more sensitive towards IFN treatment. A and B) IFN pretreatment. Calu-3 and Vero E6 cells were pretreated with 500 μ l of the indicated concentrations of recombinant human IFN- β 1 18 hours prior to infection with SARS-CoV-2 strain and SARS-CoV at an MOI of 0.001. **C and D)** IFN posttreatment. Calu-3 and Vero E6 cells were posttreated with 500 μ l of the indicated concentrations of recombinant human IFN- β 1 at 1 hpi with SARS-CoV-2 and SARS-CoV at an MOI of 0.001. Viral titers in the culture supernatant were quantified by plaque titration on Vero E6 cells at 24 hpi. Average of duplicate infections of four experiments are shown. PFU/ml were normalized to untreated samples and plotted as relative PFU/ml. Statistical significance in difference of PFU/ml between normalized SARS-CoV-2 and SARS-CoV PFU/ml was determined by Mann-Whitney tests test (p -value <0.0332 ;*, >0.1234 ; ns). Samples devoid of significance stars are statistically non-significant.

2.2.2.3 SARS-CoV-2 is less efficient in antagonizing cytokine and IFN-stimulated gene induction than SARS-CoV

The differences in IFN sensitivity described in chapter 2.2.2.2 encouraged an investigation towards differences in the capacity to antagonize the induction of cytokine expression between the two CoVs. SARS-CoV and other CoVs actively antagonize expression of antiviral cytokines [86, 144, 147, 221]. Therefore, the mRNA induction of type I IFN and other cytokines were investigated in Calu-3 cells infected with two distinct strains of SARS-CoV-2 at early time points after infection. The induction of the IRF3-regulated genes *IFNB1* and *IFNL1*, as well as of the IRF3- and NF- κ B-regulated gene *CCL5* was markedly higher following SARS-CoV-2-, as compared to SARS-CoV infection (**Figure 20A**), indicating a less efficient counteraction of infection-triggered cytokine induction by SARS-CoV-2.

In accordance with other reports, IRF3, an activator of IFN gene transcription, was retained in the cytoplasm of SARS-CoV-infected cells [120, 222] (**Figure 20B**). In contrast, upon SARS-CoV-2 infection, IRF3 readily translocated into the nucleus, suggesting that the mechanism of SARS-CoV-mediated retention of IRF3 is not conserved in SARS-CoV-2. Low IRF3 cytoplasmic retention may explain the higher induction of the IRF3-regulated genes *IFNB1* and *IFNL1* in SARS-CoV-2 infected cells.

To obtain more insight into the interference of SARS-CoV-2 with IFN-related signal transduction, the downstream activation of essential signaling pathways was tested by Western blot analysis of infected Calu-3 cells. In accordance with efficient IRF3 translocation, phosphorylated IRF3 was readily detected in lysates of SARS-CoV-2-, but not SARS-CoV, or uninfected cells (**Figure 20C**). Lower levels of the NF κ B inhibitor, I κ B α , were detectable in lysates of SARS-CoV-2 infected cells, which is in line with increased *CCL5* mRNA induction. Probing NF κ B in nuclear and cytosolic cell fractions showed more efficient NF κ B nuclear translocation in cells infected with SARS-CoV-2 than SARS-CoV (**Figure 19D**). In accordance with the increased mRNA induction of the ISGs *MX1* and *ISG56*, STAT1 was more efficiently translocated to the nucleus in cells infected with SARS-CoV-2 than SARS-CoV (**Figure 19B**). In line with this result, the IFN-sensitive genes *Mx1* and *ISG56* were induced more efficiently after infection with SARS-CoV-2 than SARS-CoV (**Figure 20E**).

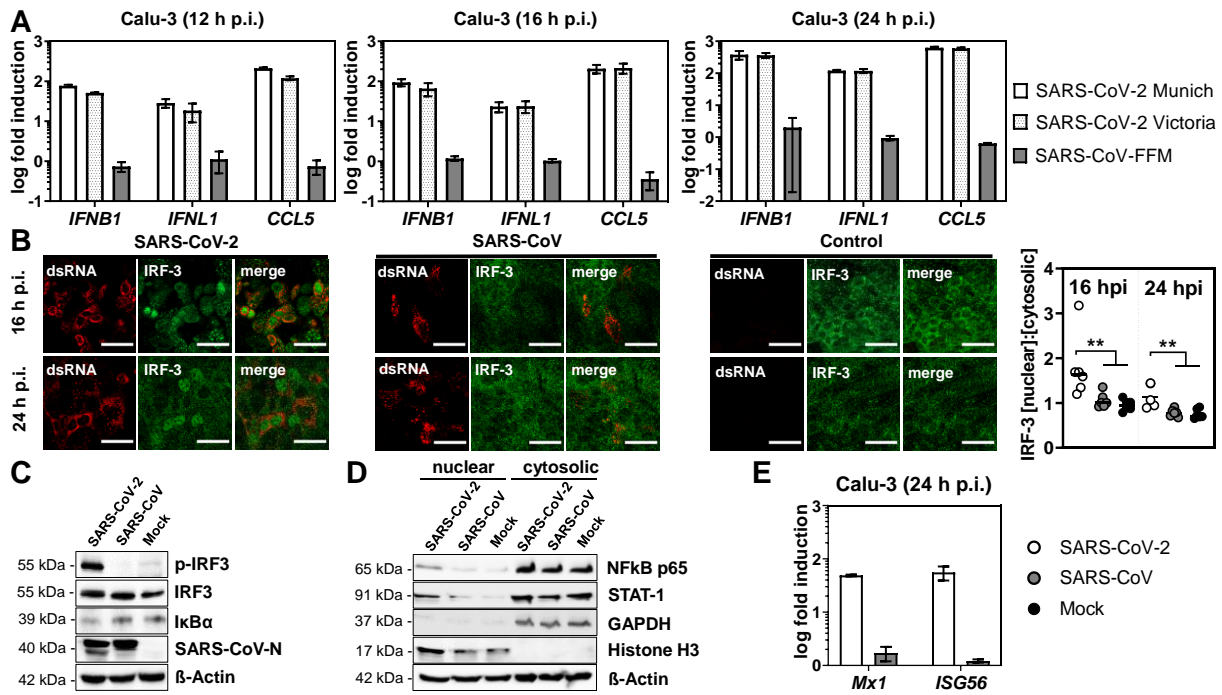


Figure 20. SARS-CoV-2 induces more strongly antiviral signaling pathways than SARS-CoV **A)** quantitative real-time RT-PCR analysis of cytokine mRNA induction in Calu-3 cells infected with two strains of SARS-CoV-2 (strain Munich and strain Victoria; BetaCoV/Australia/VIC01/2020; GenBank accession number MT007544) and SARS-CoV at MOI = 1. Target gene transcription levels were determined at 12 hpi, 16 hpi and 24 hpi and are expressed as fold induction over non-infected control cells, normalized to the housekeeping gene TATA-box-binding protein (TBP) using the $\Delta\Delta CT$ method. **B)** IRF3 translocation in SARS-CoV-2 and SARS-CoV infected Calu-3 cells. Cells were infected with SARS-CoV-2 and SARS-CoV at MOI = 1, fixed and stained for dsRNA and IRF3 at 16 and 24 hpi IRF3 signal intensity was measured in ImageJ inside (nuclear) and outside (cytosolic) of the cell nuclei in dsRNA positive cells and plotted as a ratio of nuclear to cytosolic signal intensity. **C** and **D)** Western blot analysis of protein of Calu-3 cells infected with a MOI of 0.5 with SARS-CoV-2 and SARS-CoV 16 hpi **C)** Calu-3 whole cell protein lysates were probed for IRF3, phosphorylated IRF3, I κ B α , cross-reactive SARS-CoV-N and beta actin. **D)** Calu-3 cell protein lysates were separated using the NE-PER kit (Thermo Scientific). Nuclear and cytosolic fractions were probed for NF κ B p65, STAT1, with GAPDH and Histone H3 as cytosolic and nuclear fraction controls, respectively, and beta actin as a loading control. **E)** q-RT-PCR analysis of *Mx1* and *ISG56* mRNA induction in Calu-3 cells infected with SARS-CoV-2 and SARS-CoV at an MOI = 1, 24 hpi.

2.2.2.4 Availability of the host protease TMPRSS2 is a major driver for SARS-CoV-2, but not SARS-CoV replication

The less efficient counteraction of SARS-CoV-2 against IFN induction does not correspond to the initial observation of more efficient growth of SARS-CoV-2 over SARS-CoV in fully IFN-competent Calu-3 cells. Recent research demonstrated that SARS-CoV-2 makes more efficient use of spike protein priming by the transmembrane protease TMPRSS2 than SARS-CoV [67]. Therefore, the contribution of TMPRSS2 to the replication of both viruses was investigated by employing its inhibitor Camostat mesylate in a multi-cycle infection experiment. Importantly, Calu-3, but not Vero E6 cells express TMPRSS2 [199]. Pharmacological inhibition of TMPRSS2 by Camostat mesylate [67] resulted in a more pronounced reduction of SARS-CoV-2 infection as compared to SARS-CoV, suggesting that the general growth advantage of SARS-CoV-2 in Calu-3 cells might be determined rather by its preferential utilization of TMPRSS2-dependent entry than by immune evasion (**Figure 21**).

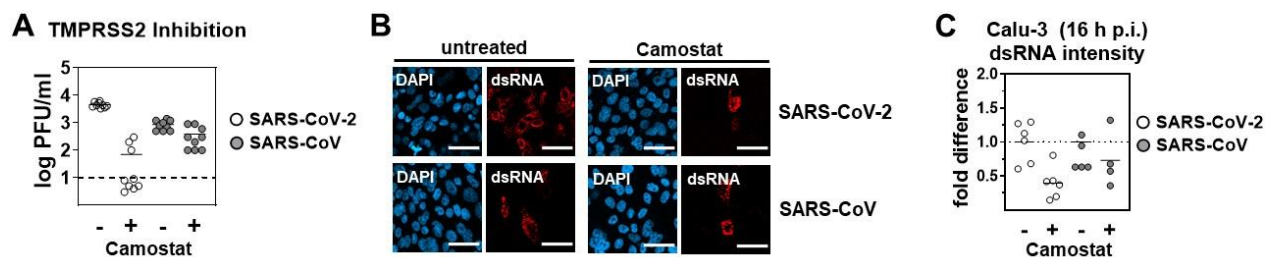


Figure 21. The TMPRSS2-mediated entry route accounts for higher replication of SARS-CoV-2 over SARS-CoV in IFN-competent Calu-3 cells. **A)** replication as determined by plaque titration in Vero E6 of SARS-CoV-2 and SARS-CoV in Calu-3 cells 24 hpi (MOI = 0.001) under the influence of 100 nM of the TMPRSS2 inhibitor Camostat mesylate. **B and C)** Replication as determined by dsRNA staining in fixed Calu-3 cells, 16 hpi with an MOI of 0.01. dsRNA signal intensity quantification was performed in ImageJ of six microscope picture frames per condition per virus.

2.2.2.4 SARS-CoV-2 protein 6 has reduced function in antagonizing IFN signaling

All results up to this point suggested that SARS-CoV-2 is less efficient than SARS-CoV in antagonizing the induction of cytokine genes as well as ISGs, despite the shared genome architecture and expression of homologous viral proteins. Among all previously described SARS-CoV IFN antagonists (nsp1, nsp3, nsp14, nsp15, nsp16, protein 6, protein 8, protein 9 and N), protein 6 (encoded by ORF6) shows the highest amino acid sequence divergence between SARS-CoV and SARS-CoV-2. SARS-CoV protein 6 binds importin alpha 1 and beta 1, which are required for STAT1 nuclear translocation, and thereby prevents ISG induction via ISRE (IFN-stimulated response elements) promoter elements [147]. To analyze the ISG-dependent antagonistic function of protein 6 in the context of SARS-CoV infection, recombinant SARS-CoV virus mutants in which SARS-CoV ORF6 was replaced with full-length ORF6 of SARS-CoV-2 (rSARS-CoV_{ORF6-SARS-2}) were constructed by reverse genetics. In brief, a SARS-CoV cDNA clone was subjected to mutagenesis via *en passant* Red-mediated recombination, as previously published [223, 224]. Further, ORF6 knockout mutants (rSARS-CoV_{ΔORF6}), in which the 4th and 5th codon of ORF6 were replaced with stop codons (**Figure 22A**), were included in the study. All rescued recombinant viruses were replication-competent. In multi-cycle infections in IFN-competent Calu-3 cells (MOI = 0.001), both rSARS-CoV_{ORF6-SARS-2} and rSARS-CoV_{ΔORF6} replicated more than 10-fold less than wt rSARS-CoV (**Figure 22B**). These data confirm that SARS-CoV protein 6 is not essential for replication but enhances replication in IFN-competent cells. To confirm that SARS-CoV-2 protein 6 has reduced function in antagonizing IFN signaling as compared to SARS-CoV ORF6, single-cycle infection experiments (MOI = 1) were performed in Vero E6 cells. Virus replication and viral protein expression was allowed for 16 hours, before exposition of cells with type I IFN for 30 minutes to mount JAK/STAT-mediated induction of ISGs. Induction of the ISG *MX1* whose induction is strictly dependent on IFN signaling [225] was tested after 8 hours (**Figure 22C**). Whereas the chimeric virus suppresses *MX1* induction to a lesser degree than wild type, induction is strongest in cells infected with rSARS-CoV_{ΔORF6}, suggesting that a residual antagonistic function is preserved in SARS-CoV-2 ORF6. Intriguingly, the induction phenotype of *ISG56* showed less pronounced differences between rSARS-CoV_{ORF6-SARS-2} and rSARS-CoV_{ΔORF6}. The induction of *ISG56* is mediated not only by JAK/STAT, but also by IRF3 signaling [226]. Therefore, subtle differences in *ISG56* induction by JAK/STAT signaling alone may be masked by IRF3-mediated *ISG56* induction, which is not impeded by the antagonistic functions of protein 6.

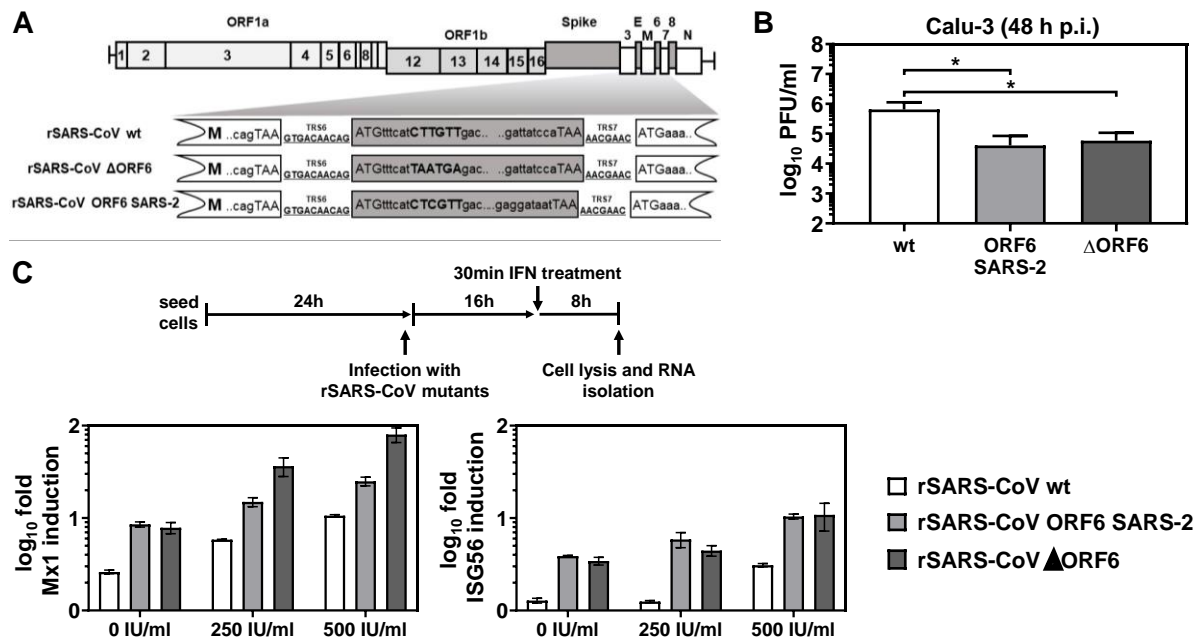


Figure 22. SARS-CoV and SARS-CoV-2 protein 6 are functional homologues with SARS-CoV-2 protein 6 displaying reduced capacity in antagonizing IFN signaling. **A)** left panel: cloning strategy of recombinant SARS-CoV ORF6 deletion (rSARS-CoV_{ΔORF6}) and SARS-CoV-2 ORF6 chimeric variant (rSARS-CoV_{ORF6 SARS-2}). **B)** multi-cycle infections (MOI = 0.001) of rSARS-CoV-wt, -ΔORF6 and -ORF6-SARS-CoV-2 recombinant viruses in Calu-3 cells. Virus titers were determined at 48 hpi by plaque titration on Vero E6 cells. The average of two experiments in duplicates is shown. Statistical significance in differences of PFU/ml between rSARS-CoV-wt and -ΔORF6 and -ORF6-SARS-CoV-2 recombinant viruses was determined by Mann-Whitney tests test (p-value <0.0332,*; >0.1234; ns). **C)** IFN pulse assay. The outline of the experiment is depicted in the top panel. Vero E6 cells were infected at MOI = 1. At 16 hpi, cells were treated with the indicated amounts of pan-species type I IFN for 30 minutes. 7.5 hours later (accounting for 24 hpi in total) cells were lysed and isolated total RNA subjected to quantitative real-time PCR for *Mx1* and *ISG56* mRNA induction.

2.2.3 – Discussion

The overall results of this study suggest SARS-CoV-2 suppresses cytokine induction as well as IFN signaling with lower efficiency than SARS-CoV. Studies employing a SARS-CoV reverse genetics clone that expresses SARS-CoV-2 ORF6 implicate that IFN signaling is antagonized to a lesser degree in SARS-CoV-2 infection, as function of reduced protein 6 activity.

As detailed in chapter 1.6, multiple viral proteins facilitate IFN antagonism in CoVs. Specifically for SARS-CoV, nsp3 and nsp1 prevent IRF3 phosphorylation, which is essential for nuclear translocation, thereby preventing IFN induction [135, 143, 227]. Nsp1 additionally prevents STAT1 phosphorylation upon IFN receptor binding. However, these genes are highly conserved between SARS-CoV and SARS-CoV-2. The less conserved protein 6 binds importin α 1 and β 1, thereby preventing STAT1 nuclear translocation and the activation of ISG promoter elements [147]. The data of this thesis demonstrate that SARS-CoV-2 protein 6 is less efficient in interfering with IFN signaling. A striking difference between SARS- and SARS-CoV-2 protein 6 is the loss of two charged residues (Q51E and Q56E) at the C-terminal domain, which has been shown to be essential for importin binding [147]. Loss of charge in SARS-CoV-2 protein 6 may reduce the capacity to interact with importins and warrants for further clarification by pulldown studies with tagged protein 6. These studies might help to address the question if SARS-CoV-2 protein 6 interacts with the same importins as SARS-CoV and if importin binding is conserved among different host species. As SARS-CoV-2 evolution is likely to take place in bats [46, 52], protein 6 might have undergone functional adaptation in binding to bat importins.

Under the impression of an ongoing SARS-CoV-2 pandemic, reduced antagonistic capacity of SARS-CoV-2 protein 6 in human cells conveys a warning to the course of the pandemic. As protein 6 of both SARS- and SARS-CoV-2 are structurally homologous and seem to evade IFN signaling via the same mechanism of action, the function of SARS-CoV-2 protein 6 may undergo adaptive evolution in humans. As the intense circulation of SARS-CoV-2 in the human population continues, potential increases of anti-IFN functions, as mediated by protein 6, may trigger increases of replication level that are ultimately selected for in virus evolution. As virus transmission continues, sequence-based surveillance combined with experimental assessment of phenotypic change should involve studies of ORF6 and other presumed IFN antagonists and monitor for possible changes in IFN signaling antagonism.

A recently published study compiled further evidence that both SARS- and SARS-CoV-2 protein 6 are IFN antagonists [146]. Intriguingly, the authors did not detect a reduced antagonistic capacity of SARS-CoV-2 protein 6. The authors further claim an additional antagonism of IRF3-mediated type I IFN induction by protein 6, which is not in line with data

obtained from wild-type SARS-CoV-2 infection (**Figure 20**) and could not be detected in rSARS-CoV_{ORF6 SARS-2} infection. However, there is a key difference in the applied methodology between the two studies. While Yuen et al. conducted promotor activation assays based on overexpression of protein 6, we investigated the effects of endogenous protein 6 in the context of virus replication. Unfortunately, the authors did not detail their exact methodology, e.g. which (and if the identical) expression vector backbones were used for each construct, or how much plasmid was transfected, which are key determinants for the outcome of promotor activation assays. Furthermore, results based on overexpression of single viral proteins suffer from systemic pitfalls, as they do not reflect endogenous protein levels in the context of virus infection and cannot account for interactions between several viral proteins.

A tempting extrapolation of the *in vitro* data presented here towards *in vivo* clinical presentation is that the less efficient innate immune evasion by SARS-CoV-2 correlates with the less severe clinical manifestation of COVID-19 over SARS. Increased cytokine and ISG induction by SARS-CoV-2 may enable quick virus clearance and halt disease progression in patients with a largely functional immune system. Intriguingly, a recently published study employed single cell sequencing on SARS-CoV-2 infected *ex vivo* lung explants and found SARS-CoV-2 to not induce significant amounts of IFNs, juxtaposed to increased NF- κ B-mediated genes, as observed here [228]. Contrasting to that, a single cell study performed by members of our institute observed a similar phenotype of SARS-CoV-2-mediated IFN mRNA upregulation, as observed here [229]. It should be added that the host response may vary as a function of applied MOI, of the timing of mRNA quantification, of the model system used for infection and possibly as a function of virus isolate used for infection. Consequently, extrapolations towards any clinical phenotype have to be confirmed by more data to clarify SARS-CoV-2 IFN evasion and antagonism, particularly in *ex vivo* systems.

Functional diversity in protein 6 and other accessory proteins may help to elucidate the zoonotic potential emanating from *Coronaviridae*. Previous studies have shed some light on the functional diversity of protein 8 [230] and nsp3 [227] in SARS-CoV, and protein 4b in MERS-CoV [176] and the data for protein 6 provided here add to that line of thought. Functional differences in the ability to counteract innate immunity seems to appear as a marker for pathogenicity of CoVs. The suppression of innate immunity, whose protein components are largely conserved among mammals, may help to explain why CoVs seem to be able to overcome species barriers so frequently. Considering SARS-CoV and SARS-CoV-2 as conspecific viruses with an overall homologous genome structure and receptor usage [52, 66, 67] the results presented here highlight that functional diversity may exist in members of closely related virus species, analogously to the results presented for MERS-CoV.

In sum, the results of both parts of the thesis at hand underline the urgency to intensify CoVs surveillance. Particularly in their animal reservoirs where diversity is largest, surveillance should be extended from purely sequence- and phylogeny-informed research towards phenotypical studies, as functional diversity seems to be present among closely related CoV species. The identification of causal networks between CoV genomic loci and their phenotypical traits might help to identify risk markers for CoV virulence and provide a better assessment of the pandemic potential of circulating CoVs.

3 – Methods

3.1 - General cell culture procedures

MERS-CoV plaque titrations (chapter 3.6) and virus stock production (chapter 3.2) were conducted using Vero B4 cells. For SARS-CoV and SARS-Cov-2 Vero E6 cells were used. In virus infection studies (chapter 3.4), Vero B4, Vero E6, Calu-3, Caco-2, Huh-7, T84 wild-type and T84 IFN alpha and lambda receptor double knockout cells were used. For the production of MERS-CoV spike protein-pseudotyped VSV particles, HEK-293T cells were used (chapter 3.17). All cells were maintained at 37°C, 5% CO₂ in Dulbecco's Modified Eagles Medium (DMEM), high glucose (4.5 g/L) supplemented with 5% Penicillin/Streptomycin, 5% non-essential amino acids, 5% sodium pyruvate, 5% L-glutamine and 10% FCS (lot number 2058470) (all Gibco). For freshly thawed Calu-3 cells, FCS supplement was increased to 20% for two passages. Culture vessels for T84 cells were coated with type I collagen for 1 hour prior to seeding. Passaging of cells was performed when cells reached a confluency of 80% or higher, in a 1:10 ratio for all cells, except for Calu-3 and T84 cells, which were passaged in a 1:3 ratio. For passaging, cells were washed with twice with PBS and exposed to 0.25% Trypsin solution until cell detachment was completed. Detached cells were counted in a Neubauer chamber and diluted to the appropriate concentration (chapter 3.4) prior to cell seeding.

3.2 - MERS-CoV isolate stock production

Generation of primary MERS-CoVs isolates from anonymous patient respiratory samples was performed by Doreen Muth in late 2015 [187]. In brief, qRT-PCR positive samples were diluted in OptiPro to reduce mucous viscosity and subsequently used to infect Caco-2 and Vero B4 cells, seeded in a 6-well format. Infections were performed as described in chapter 3.4. Cells were monitored daily and at the onset of CPE the culture supernatant was collected and stored at -80°C for working stock generation.

For MERS-CoV working stock production, Vero B4 cells seeded in a T162 flask format were infected with primary MERS-CoV isolates. To avoid carry-over of potential fungus contaminations, frequently observed in primary isolates from respiratory samples, inocula were passed through a 0.22 µm filter prior to inoculation. In addition, Amphotericin B was supplemented in the culture medium at a concentration of 1 µg/ml. Infected Vero B4 cells were incubated at 37°C, 5% CO₂ and monitored daily for CPE. Once complete CPE was observed after approximately 3-4 days, the culture supernatant was collected and centrifuged at 4,000 rpm for 30 minutes to remove cellular debris. Debris-free supernatants were collected and concentrated using Vivaspin 20 ml concentrator columns. In brief, supernatants were loaded

onto PBS equilibrated columns and centrifuged at 4,000 rpm at 4°C for 1 hour. The remaining volume was collected from the column filters by washing with 10 ml PBS. The resulting high titer virus solution was mixed in a 1:2 ratio with 0.5% gelatin-containing OptiPro medium and aliquots of 500 µl were stored at -80°C.

3.3 - IFN, Ruxolitinib and Camostat mesylate treatment

Prior to infection, Vero E6 (SARS and SARS-CoV-2) and Calu-3 cells (the former, plus MERS-CoV) were incubated with 500 µl of the indicated human IFN-β (Biochrom, Germany) or pan-species type I IFN (PBL Biomedical Laboratories) concentrations, diluted in culture medium, for 18 hours (chapter 2.1.2.12 and 2.2.2.2). For IFN posttreatment, culture medium was changed to full DMEM supplemented with the indicated concentrations of IFN-β one hour after infection. For IFN pulse experiments (chapter 2.2.2.4), pan-species type I IFN was diluted in culture medium at the indicated concentrations. At 16 hpi, the culture medium was replaced with IFN-supplemented culture medium for 30 minutes. Subsequently, IFN-containing medium was removed and composite DMEM without IFN was added to the cells.

Camostat mesylate (Sigma-Aldrich) and Ruxolitinib (Invivogen) treatment (chapter 2.1.2.8 and 2.2.2.4) was performed by supplementing complete DMEM with 100 µM Camostat mesylate or 100 nM Ruxolitinib, or DMSO (as a control for Ruxolitinib treated cells) and by pretreating Calu-3 cells 2 hours prior to infection. After infection, cells were maintained in Camostat Mesylate-, Ruxolitinib-, or DMSO-supplemented DMEM.

3.4 - MERS-, SARS- and SARS-CoV-2 infections

Detached cells were counted and seeded 16 hours prior to infection studies. Seeding densities were used as detailed below. 500 µl and 2,000 µl culture medium were used for 24-well and 6-well cultures, respectively.

Cell line:	Seeding density (cells/well):	
	24-well:	6-well:
Calu-3	3.0x10e5	1.2x10e6
Caco-2	1.5x10e5	Not applicable
T84 (wild-type and KO)	2.5x10e5	Not applicable
Vero (B4 and E6)	1.5x10e5	6.0x10e5

Virus stocks were thawed and diluted in OptiPro (Gibco) to the desired MOI (e.g. 500 PFU for 2.5e5 Calu-3 cells to reach an MOI of 0.002). Culture medium was removed and the cells were washed once with PBS, prior to inoculation with virus dilutions for 1 hour at 37°C. Following

incubation, cells were washed twice with PBS and 500 μ l (24-well format) or 2 ml (6-well format) culture medium was added to each well. Infected cells were further incubated at 37°C.

All experiments with MERS-CoV, SARS-CoV-2 and SARS-CoV were executed under BSL-3 conditions.

3.5 - Synchronized MERS-CoV infections

To investigate early steps in virus infections, virus attachment to host cells was performed at low temperatures, at which the energy barrier for efficient host cell fusion and cell entry is high [231]. After an particle attachment incubation period at 4°C, the temperature was rapidly shifted to 37°C to allow for synchronized virus entry into the cells (chapter 2.1.2.8 and 2.1.2.10).

Virus stocks were thawed and diluted in 4°C cold OptiPro to the desired MOI. Calu-3 and Vero B4 cells, seeded in 24-well format, were kept on ice, the culture medium was removed and the cells were washed once with cold PBS. After the addition of virus dilutions, the cells were incubated at 4°C for 1 hour and subsequently shifted to 37°C for 30 minutes. Cells were washed five times with PBS and 500 ml culture medium was added to each well. Further incubation was carried out at 37°C.

3.6 - Plaque titration assay

The amount of infectious particles in a virus containing dilution can be quantified by the plaque assay technique [232]. This technique applies the principle that virus progeny of a single infected cell can only infect immediately neighboring cells when the cell monolayer is overlaid with a viscous medium. Consequently, each infectious particle forms a so-called plaque, a hole, in the cell monolayer. The number of formed plaques positively reflects the amount of PFU present in the dilution used to infect the cell monolayer.

Samples with unknown virus concentration were 10-fold serially diluted and applied to Vero B4 or E6 cells (1.5e5 cells/well) in duplicates. After a 1-hour incubation period at 37°C, sample dilutions were removed and overlaid with a 1:2 solution of 2.4% Avicel (Sigma-Aldrich) and double-concentrated DMEM (Gibco). Four days post infection cells were washed once with PBS and fixed in 6% formaldehyde solution for 30 minutes. The cell monolayer was stained by adding a 6% formaldehyde solution containing crystal violet for 15 minutes. Stained and fixed plates were washed twice with water, dried at room temperature. Formed plaques were counted in duplicate wells to calculate the PFU/ml using the following equation:

$$\text{Virus titre } \left[\frac{\text{PFU}}{\text{ml}} \right] = \frac{\sum \text{plaques} \times \text{dilution factor}}{\sum \text{applied volume}}$$

3.7 - Primary human airway epithelium infection and culture procedures

Prof. Dr. Ronald Dijkman, Institute for Virology and Immunology, at the University of Bern, provided fully differentiated primary human airway epithelia (HAE). HAE cells were seeded on transwell inserts that allow cells to be supplied by medium from the apical (top) and basolateral (bottom) side. After reaching confluency and establishing a tight junction barrier (monitored by measuring the electrical resistance between apical and basolateral compartment), apical medium was removed to drive differentiation of HAEs by exposure to air on the apical site (creating an air-liquid-interface (ALI) culture). HAEs were fully differentiated in Bern and shipped to Berlin with an agarose overlay. Upon arrival, the agarose overlay was removed, and the inserts washed twice with HBSS (Gibco) to remove excess agarose. HAEs were further incubated for one week prior to infection, to allow the cells to recover from the shipment. ALI medium (produced in house by R. Dijkman) was exchanged from the basolateral site every second day [233].

For infection with MERS-CoV (chapter 2.1.2.14) HAEs were washed twice with HBSS to remove excess mucous and infected with 4,000 PFU diluted in HBSS for 1.5 hours. Subsequently, cells were washed three times with HBSS and further incubated. At 24, 48, 72 and 96 hpi supernatants were collected from the apical site. Viral loads were quantified by plaque titration on Vero B4 cells as described in chapter 3.6.

3.8 - Lung explants infection and culture procedures

Lung explant infections with selected MERS-CoV isolates were performed in cooperation with Christin Mache under Thorsten Wolff's supervision at the Robert Koch Institute, Unit 17, Influenza and other Respiratory Viruses, in Berlin, Germany.

Lung explants were obtained from patients undergoing lung resection. Written informed consent was obtained from all patients and the study was approved by the ethics committee at Charité- Universitätsmedizin Berlin (projects EA2/050/08 and EA2/023/07). For each experiment tumor-free, human lung tissue was cut into small pieces (weight approx. 0.1 - 0.2 mg per piece) and incubated in RPMI 1640 (Gibco) medium at 37°C with 5% CO₂. After overnight incubation, lung organ cultures were inoculated with 1x10⁵ PFU MERS-CoV for 1.5 hours, washed once with PBS and further incubated on a tissue culture shaker with 50 rpm (chapter 2.1.2.14). Lung tissue was incubated for up to 72 hpi in RPMI 1640 medium containing 10% FCS and 2 mM L-glutamine (both Gibco). Supernatants of infected lung tissue were collected at 0, 16, 24, 48 and 72 hpi and were titrated on Vero B4 cells by plaque titration assay as described in chapter 3.6.

3.9 - Plaque Reduction Neutralization Test (PRNT)

The plaque reduction neutralization test (PRNT) quantifies virus-specific neutralizing antibodies. The technique is based on the assumption that viruses do not form plaques when specific antibodies neutralize them. Serial dilutions of five serum samples (**Table 1** chapter 2.1.2.19), containing antibodies against MERS-CoV were incubated for 1 hour with 25 PFU prior to performing a plaque assay as described in chapter 3.6. After fixation and staining, as described in chapter 3.6, plaques were counted and the reduction of plaques in samples pre-incubated with serum dilutions was calculated. The standard measure for neutralization capacity is given as the PRNT₅₀, i.e. the serum dilution step at which half of the 25 input PFUs are neutralized.

3.10 - Virus competition assay

Calu-3 cells were infected in 24-well format with a mixture of two MERS-CoV strains, using two ratios (1:1 and 9:1) (chapter 2.1.2.6). The total infectious dose used to infect passage 0 cultures was set to 10,000 PFU, corresponding to an MOI = 0.04. All passaging infections were performed by sampling the supernatant of the previous passage at 24 hpi and inoculating a new Calu-3 culture with a 1:50 dilution of that sample. This process was repeated until the completion of five passages. Viral RNA was isolated from the initial inoculum (p0) and from the supernatant after five passages (p5) and subjected to Sanger sequencing of three different single nucleotide polymorphisms (SNP) sites that were each amplified from the virus population in separate RT-PCR reactions to control for PCR-based artifacts. The following PCR products were generated: amplicon 1 (300 bp): forward primer: 5'-TACCTGGTTGAGAGGCTCAT-3'; reverse primer 5'-CTTAAGCAGATTCTGGGCATATT-3'; amplicon 2 (541 bp): forward primer 5'-TGAGTGTGGAAGTTGTGGTAAT-3'; reverse primer 5'-ACCTTTGAGAAGCTGGCGTATT-3'; amplicon 3 (560 bp): forward primer 5'-TCGAGCCGCATAAGGTTTCAT-3'; reverse primer 5'-GCTGAGCTGCGTCCTGTTT-3'. For peak height analysis, the web based Chromat Quantator (Mullins lab, University of Washington, chapter 4.12) was used and obtained peak heights were averaged for all duplicates and calculated as a percent of the total height.

3.11 - Deep sequencing of MERS-CoV virus stocks

3 µg viral RNA, extracted from high titer MERS-CoV stocks (passage 2) as described in chapter 3.2 and 3.21, was subjected to cDNA synthesis using the SuperScript® One-Cycle cDNA Kit (Invitrogen) according to the manufacturer's protocol. 1 ng cDNA was fragmented and supplemented with adapter sequences using the Nextera® XT DNA Library Prep (Illumina), subsequently processed with the MiSeq Reagent Kit v3 (Illumina) and subjected to NGS on a MiSeq™ System (Illumina), all according to the manufacturer's protocol.

3.12 - Sequence assembly of NGS reads

Using the Geneious software, version 9.1.8, NGS reads were trimmed and mapped to the EMC MERS-CoV reference genome (accession number JX869059). Reads shorter than 50 bp were excluded from the mapping. Trimming of reads was set to 5%. The threshold for generation of the consensus sequence of all reads was initially set to 90%. Each obtained consensus sequence was manually screened for ambiguous nucleotides. If ambiguous nucleotides were identified, the consensus sequence threshold was lowered to 75%. Sequences that did not yield unambiguous consensus sequences at 75% reads were excluded from further studies (chapter 2.1.2.2).

3.13 - Phylogenetic analysis of MERS-CoV genome sequences

Phylogenetic analyses were estimated applying a Maximum-likelihood approach, implemented in RaxML, version 8.0.0, with a general time reversible (GTR) model of nucleotide substitution with 4 category gamma distributed rate variation and a proportion of invariant sites. 10,000 bootstrap replicates were set. No further changes to the default settings of RaxML were applied. Calculation were performed on the BIH server cluster, to allow for the replicates to be calculated in a reasonable time scale. Input alignments for all trees were created by ClustalW, implemented in the Geneious software, version 9.1.8. Calculated trees were edited for better graphical display, using FigTree v1.4.4 (chapter 2.1.2.4).

3.14 - In-depth recombination analysis

For detailed recombination analysis, we performed a BootScan analysis with 500 bootstraps in SimPlot, version 3.5.1., with a sliding window of 5,000 bp and 200 bp steps. An alignment of four sequences, comprising phylogenetic clade A (EMC-2012) and three clade B lineages, lineages 3, 4 and 5 (Riyadh-146 2014, Jeddah 2014 10306 and Riyadh 2015-1734) was used for the BootsScan analysis, with Riyadh 2015-1734, the suspected recombinant, set as query sequence (chapter 2.1.2.5).

3.15 - Cloning of MERS-CoV lineage-specific spike gene expression vector by mutagenesis PCR

For the generation of lineage-specific spike gene expression vectors, the previously cloned EMC-2012 isolate spike plasmid (pCG1-MERS-S) was used as a template for site-directed mutagenesis PCR. Lineage-specific nucleotide changes were introduced into the EMC spike plasmid by a set of specific primers, listed in chapter 4.8.3. Phosphorylated primers were used to allow for efficient ligation of the circular PCR product. The reaction as set up as a two-mix, hotstart PCR, using Phusion polymerase as described below:

Mix 1:

H2O	27.5 μ l
HF buffer (5x)	7.5 μ l
dNTPs	2 μ l
Primer Fwd	1 μ l
Primer Rev	1 μ l
Template (10 ng)	1 μ l
Total volume:	40 μl

Mix 2:

H2O	7 μ l
HF buffer (5x)	2.5 μ l
Phusion Polymerase	0.5 μ l
Total volume:	10 μl

The reaction was conducted in a PCR cycler with the following cycling conditions:

Add Mix 1	template denaturation	98°C	30 sec	1x
	template denaturation	80°C	1 min	
Add Mix 2	Denaturation	98°C	10 sec	35x
	Primer annealing	66°C	20 sec	
	Extension	72°C	200 sec	
	Final Extension	72°C	10 min	1x
	4°C	Storage	∞	

Amplification of DNA was verified by agarose gel electrophoresis. Successful amplicons were subjected to background template digestion employing 2 μ l Dpn1 restriction enzyme (NEB) in

50 µl total volume with 1x CutSmart buffer (NEB) at 37°C for 20 minutes. Subsequently, amplicons were column purified (Machery&Nagel) and 5 µl PCR product was ligated at room temperature using 1µl T4 Rapid enzyme (Thermo Scientific) in 1x RapidLigation buffer (Thermo Scientific) in a total volume of 10 µl for 30 minutes. Subsequently 3µl ligation product were used to transform *E. coli* One Shot Top10 bacteria (Thermo Scientific) as described in chapter 3.25.

Initially the mutation Q1020R was introduced into the EMC backbone and the obtained plasmid DNA was isolated from transformed bacteria using the Machery&Nagel Plasmid Purification Kit (chapter 3.16). The mutagenesis reaction was verified by Sanger sequencing, and the isolated plasmid subsequently used as a PCR template for the subsequent introduction of L411F and Q833R by a second round of mutagenesis PCR as described above. In total, three MERS-CoV spike gene plasmids were generated: L411F and Q1020R in combination, Q833R and Q1020R in combination, as well as Q1020R alone (chapter 4.9). All plasmids were isolated and purified as described in chapter 3.16.

3.16 - Isolation of plasmid DNA

For small scale DNA purification, the Machery&Nagel Plasmid purification kit was used. For large-scale DNA purification the Machery&Nagel Extra Midi EF kit was used, both according to the manufacturer's instructions. For small-scale DNA isolation, a single bacterial colony was inoculated in 5 ml LB broth supplemented with the required antibiotic. For large-scale DNA isolation, an overnight small-scale bacterial culture of a single bacterial colony was inoculated in 300 ml LB broth supplemented with the required antibiotic. Elution of purified plasmids was performed with 50 µl and 200 µl 50°C Tris-HCl buffer, pH 8, for small-scale and large-scale DNA purification, respectively.

3.17 - Generation of MERS-CoV spike protein-pseudotyped VSV particles (VSVpp) and virus transduction studies

Cell entry capacity of MERS-CoV-S proteins can be quantified by the VSVpp system [234, 235]. The system is based on a recombinant Vesicular Stomatitis Virus (rVSV) in which the gene mediating cell entry, VSV-G, was replaced by genes encoding for eGFP and firefly luciferase (fLuc). rVSV particles can be trans-supplemented with overexpressed viral glycoproteins, including MERS-CoV-S. These trans-supplemented MERS-CoV-S VSVpp can be used to infect MERS-CoV susceptible cell lines. MERS-CoV-S- VSVpp transduces infected cells with the eGFP and fLuc genes, than can subsequently be quantified.

In brief, 293T cells seeded in 6-well format were transfected with 6 µg pCG1 expression vectors (chapter 4.9) carrying MERS-CoV spike protein variants produced as by mutagenesis PCR as

described in chapter 3.15) [183], and VSV-G (positive control) or empty pCG1 expression vector (negative control). 16 hours post transfection, the 293T cells were inoculated with 1 ml VSV* Δ G-fLuc diluted in OptiPro at an MOI = 3 at 37°C for 1 hour, washed twice with 1 ml cold PBS and further incubated at 37°C with 2 ml culture medium, supplemented with 1:1,000 anti-VSV-G antibody (except for cells expressing VSV-G). After 16-18 hours incubation, 2 ml of the VSVpp containing culture supernatant was collected and the cell debris removed by centrifugation (4,000 rpm, 4°C, 10 min). Aliquots of 250 μ l were stored at -80°C.

For transduction of target cells, Calu-3, Caco-2 and Huh-7 cells were seeded into 96-well cell culture plates for 16 hours, the culture medium was removed and cells were inoculated with 100 μ l MERS-CoV-S VSVpp. At 18 hours postinoculation cells were lysed for 15 minutes at room temperature in 50 μ l Luciferase Cell Culture Lysis Reagent (Promega). Lysates were diluted 1:10 in water and 20 μ l were transferred into white, opaque-walled 96-well plates and activity of virus-encoded fluc was measured using 50 μ l of the Luciferase Assay System substrate (Promega) and a Hidex Sense plate reader (Hidex).

3.18 - Quantification of MERS-S binding to DPP4 by flow cytometry

Analysis of spike protein binding to the host receptor DPP4 was analyzed by flow cytometry employing a previously published protocol and was performed by Hannah Kleine-Weber at the German Primate Center (DPZ) in Göttingen [183]. In brief, 293T cells were transfected with the overexpression vector pCG1 carrying the MERS-CoV Spike protein of clade A (EMC, accession number JX869059), lineage 3 (L411F/Q1020R), lineage 4 (Q833R/Q1020R), or lineage 5 (Q1020R), as well as empty vector for negative control. At 48 hours post transfection, cells were resuspended in PBS, centrifuged (5 minutes at 600x g at 4 °C) and resuspended in PBS containing 1% bovine serum albumin (1% BSA/PBS) for washing. The cells were centrifuged again and incubated in 1% BSA/PBS containing soluble DPP4 equipped with a C-terminal human Fc-tag (solDPP4-Fc, 1:50, 1:200 and 1:1,000; ACROBiosystems) at 4 °C in an overhead shaker for 1 hour. Afterwards, the cells were pelleted and incubated in 1% BSA/PBS containing an AlexaFluor488-conjugated anti-human antibody (1:500), for 1 hour at 4 °C in an overhead shaker. Subsequently the cells were pelleted, washed with 1% BSA/PBS and fixed in 4% paraformaldehyde (PFA) solution for 20 minutes at room temperature. Prior to analysis via flow cytometry, the cells were pelleted again and washed with 1% BSA/PBS. Flow cytometry was conducted on an LSR II Flow Cytometer (BD Bioscience). Data was further processed in the FCS Express 4 Flow research software (De Novo software). Assessment of entry and DPP4-binding capacity of pseudotyped VSV particles was performed in collaboration with Hannah Kleine-Weber, a member of Stefan Pöhlmann's group at the DPZ in Göttingen.

3.19 - IRF3 translocation assays

1.5e5 Calu-3 cells were seeded in 8-well μ -slides (80826, ibidi) and infected with SARS-CoV FFM-1 or SARS-CoV-2 Munich 984 at the indicated MOI. 16 or 24 hpi, cells were fixed in 6% PFA, permeabilized in 0.1% Triton-X and blocked with 2% BSA in PBS. Antibody-staining was performed with a 50 μ l dilution of mouse anti-dsRNA (J2, English and Scientific Consulting, Hungary, 1:200) and rabbit anti-IRF3 (FL-425, sc-9028, Santa Cruz Biotechnology, 1:200) in PBS, 2% BSA for 2 hours. For secondary staining, 50 μ l of a goat anti-mouse Alexa Fluor-647 (A-21235, Thermo Fisher Scientific, 1:300 with 1:1000 Dapi solution (Thermo)) dilution and a goat anti-rabbit Alexa Fluor-488 (A-11008, Thermo Fisher Scientific, 1:300) dilution were applied for 1 hour. Cells were washed three times in PBS following blocking, as well as primary and secondary antibody incubation. Imaging was performed using the Zeiss LSM800 Airyscan confocal microscope. Signal intensities were analyzed using ImageJ 2.

3.20 - Western blot analysis

Calu-3 cells were lysed in Pierce RIPA lysis buffer (Thermo Scientific) supplemented with PhosStop (Roche) and complete Protease Inhibitor mix (Roche) at 16 hpi. For nuclear and cytosolic fraction analysis, protein lysates were separated using the NE-PER kit, according to the manufacturer's instructions (Thermo Scientific). Cell lysates were resolved on 14% SDS-PAGE gels and blotted onto nitrocellulose membranes using a Trans-Blot Turbo system (BioRad). Subsequently, membranes were blocked with 5% milk powder in TBS with 0.05% Tween-20 (TBST) for 1 hour, prior to overnight incubation at 4°C with the respective primary antibodies, diluted 1:1,000 in TBST, 5% milk powder as follows: p-IRF3 (cs#4947s); IRF3 (cs#4302s); I κ B α (cs#4812s); SARS-CoV-N (GTX632269); β -Actin (Sigma A5316); NF κ B p65 (cs#6956s); STAT-1 (cs#9172); GAPDH (cs#5174s) and Histone H3 Sigma (H0164). After overnight incubation, membranes were washed with TBST and probed with secondary HRP-conjugated antibodies (Thermo Scientific), diluted 1:20,000 in TBST, 5% milk powder, for 1 hour at room temperature. Protein band visualization by autoradiography was performed by addition of SuperSignal West Pico Plus (Thermo Scientific) chemiluminescence substrate.

3.21 - Manual isolation of viral RNA

Viral RNA was isolated from culture supernatants of infected cells using the Machery&Nagel viral RNA kit according to the manufacturer's instructions. 50 μ l of cell culture supernatant were added to 300 μ l RAV1 lysis buffer, supplemented with carrier RNA. Samples were either stored at -80°C or processed immediately. Virus containing RAV1 samples were heat-inactivated for 10 minutes at 70°C, before being exported from the BSL-3. RNA was eluted in 50 μ l H₂O and stored at -80°C.

3.20 - Manual isolation of total cellular RNA

At the respective time point post infection, cell culture supernatant was removed and the cells were lysed in 350 µl RA1 buffer, supplemented with 2-mercaptoethanol. Samples were either stored at -80°C or processed immediately. Virus-containing RAV1 samples were incubated for 10 minutes at 70°C before being exported from the BSL-3. RNA was isolated using the Machery&Nagel total RNA kit according to the manufacturer's instructions. RNA was eluted in 50 µl H₂O and stored at -80°C.

3.21 - Automated isolation of viral RNA

Large-scale cellular RNA isolations were performed on an automated nucleic acid isolation extraction platform (MagNAPure (Roche)). In brief, cells were lysed in 350 µl MagNA Pure cell lysis buffer, transferred to Eppendorf tubes and either stored at -80°C or processed immediately. Lysed samples were incubated for 10 minutes at 70°C, before being exported from the BSL-3. After BSL-3 export, 300 µl of each samples were transferred to 96 deep-well plates and the nucleic acid isolation was performed using the small volume nucleic acid kit (Roche), and following the manufacturer's preset protocol for blood samples. Elution was done in 100 µl H₂O and the eluate was stored at -80°C.

3.22 - Purification of PCR products

PCR products intended for cloning or sequencing were UV visualized after electrophoresis on 1% agarose gels to check for the presence of unspecific PCR byproducts. PCR products that displayed no unspecific PCR products were purified using the Machery&Nagel NucleoSpin Gel and PCR clean-up system, according to the manufacturer's protocol. PCR products with unspecific products and PCR products obtained from plasmid templates were separated from unspecific products by low voltage (70V) 1% agarose TAE gel electrophoresis, excised with a disposable scalpel and subsequently subjected to purification using the Machery&Nagel NucleoSpin Gel and PCR clean-up system, according to the manufacturer's protocol. Excised agarose gel pieces were incubated with 400 µl NTI buffer at 50°C and 1,000 rpm for 10 minutes.

3.23 - Photometric quantification of nucleic acid concentration

A NanoDrop 1000 (Thermo Fisher Scientific) spectrophotometer was used for nucleic acid concentration measurements, blanked with the same solvent that nucleic acids were resuspended in, usually H₂O or Tris-HCl buffer.

3.24 - Bacterial transformation, colony PCR and glycerol stock production

Ligation reactions were transformed into 50 µl chemically competent TOP10 (Invitrogen) or NEB 10-beta *E. coli* (NEB) according to manufacturer's protocol. In brief, 50 µl of TOP10 or NEB 10-beta *E. coli* cells were thawed on ice. 5 µl ligation reaction was incubated on ice for 20 minutes, subjected to a heat shock at 42°C for 30 seconds, placed on ice for another 2 minutes before recovery in 250 µl SOC medium (NEB) at 37°C 300 rpm for 1 hour. 300 µl transformed bacterial cells were in SOC medium were spread out in on LB agar plates containing the respective selection antibiotic (30 µg/ml Kanamycin, 50 µg/ml Carbenicillin, or 10 µg/ml Chloramphenicol, all from Thermo Scientific) and incubated overnight at 37°C or for two days at 32°C.

Single bacterial colonies resuspended in 15 µl H₂O were used as a template for colony PCR using Taq Polymerase (Thermo Scientific) according to manufacturer's protocol. For mutagenesis PCR control, a set of primers was used that generates a 500 bp PCR amplicon, which comprises the respective area of mutagenesis. For each mutated region (L411F, Q833R and Q1020R), four PCR reactions with four individual colonies were sent for Sanger sequencing to distinguish mutagenesis and background template constructs. Confirmed positive colonies were inoculated in 200 ml LB medium, supplemented with the respective selection antibiotic, and incubated at 37°C, 300 rpm for 14-16 hours. Saturated LB medium cultures were subjected to plasmid preparation as described in chapter 3.16. In addition, 500 µl of the bacterial culture was mixed with 500 µl of 50% glycerol in water and stored at -80°C for long-term storage.

3.25 - Sanger Sequencing

Sanger sequencing of purified PCR products was outsourced to MicroSynth Seqab in Göttingen. Sequencing primers (500 nM final concentration) and PCR products were provided according to the company's recommendations, with 40-100 ng/µl final plasmid concentration and 4-30 ng/µl final PCR product concentration in 12 µl total volume. Ab1 files with obtained sequencing reads were mapped to their respective template in Geneious v9.1.8.

3.26 - Quantitative real-time PCR (q-RT-PCR)

Quantitative real time RT-PCR analysis was to quantify viral RNA in the cell culture supernatants of infected cells, or to quantify transcriptional regulation of cellular mRNAs. For quantification of viral RNA, 50 µl cell culture supernatant were isolated using the Machery&Nagel viral RNA kit (chapter 3.21). For quantification of cellular mRNAs, total RNA

of virus-infected cells was isolated using either Machery&Nagel total RNA kit, or by using the automated MagNAPure platform (chapter 3.21).

For host mRNA quantification, a two-step PCR protocol was used. First, cDNA was prepared from 5 µl of a 100 ng/µl viral RNA dilution using the iScript™ cDNA synthesis kit (Bio-Rad), according to the manufacturer's protocol. Second, cDNA was amplified and quantified using Taq-polymerase (Invitrogen) and a set of real time primer and probes for each transcript under investigation (chapter 4.8.4). For quantification of sgRNA N and genomic ORF1a transcripts, cells were lysed at 0, 2, 4, 6, 8, 10, 12 and 24 hpi. Total RNA was isolated and subjected to quantitative real-time PCR using the one-step SuperScript III kit (Invitrogen) according to the manufacturer's protocol. PCR cyclers conditions were set as follows: a single cycle of 20 minutes at 55°C and 3 minutes at 98°C, followed by 40 cycles of 15 seconds at 98°C and 30 seconds at 58°C.

3.27 - Cloning of recombinant rSARS-CoV_{ORF6-SARS-CoV-2} and rSARS-CoV_{ΔORF6} cDNA constructs by red-mediated recombination

SARS-CoV carrying SARS-CoV-2 ORF6 (rSARS-CoV_{ORF6-SARS-CoV-2}) and the ORF6 deletion virus (rSARS-CoV_{ΔORF6}) were constructed from a rSARS-CoV cDNA clone [224] by red-mediated recombination [223, 236]. The transfer constructs required for recombination and selection were generated as follows: For the generation of the ORF6 deletion transfer cassette, the I-Scel-*aphAI* transfer cassette was amplified, containing 5' and 3' 37 bp homologous hooks to the SARS-CoV genome with the forward primer 5'-GCTTTGCTAGTACAGTAAGTGACAACAGATGTTTCATT**AA**TAGGGATAACAGGGTAATC GATTT-3' and the reverse primer 5'-TGATAATCAATATCTCTGCTATTGTAACCTGGAAGTCT**CA**GCCAGTGTTACAACCAATTA ACC-3'. Bold sequences indicate the mutagenesis to stop codons. Sequences in italics indicate the I-Scel-*aphAI* transfer cassette primer binding part. For the generation of the SARS-CoV-2 ORF6 chimeric virus, we ordered a synthetic dsDNA construct (IDT), designed as a 1349bp transfer cassette for red-recombination with the following build-up: the first 5' 65 bp provide the 5' homologous hook to our rSARS-CoV cDNA clone upstream of ORF6 (i.e. the last 55 bp of the M gene and the following 10 bp constituting TRS6), followed by the first 141 bp of SARS-CoV-2 ORF6 sequence (Severe acute respiratory syndrome coronavirus 2 isolate Wuhan-Hu-1; accession number MN908947), followed by the the I-Scel-*aphAI* transfer cassette, followed by a 50 bp repeat of the ORF6 sequence (bp 92-142; required for the second recombination step) and the last 44 bp of SARS-CoV-2 ORF6, followed by a 65 bp 3' homologous hook to our rSARS-CoV cDNA clone, comprising the sequence immediately downstream of ORF6. Electroporation of the transfer constructs, and both recombination steps were performed as described in Muth et al., 2017. Bacterial clones carrying the correct insert

size after first and second recombination, were identified by PCR using the primers SARS-F-26918 5` GATCACTGTGGCTACATCACGAAC-3` and SARS-R-28182 5` GGGTCCACCAAATGTAATGCGG-3`.

Virus rescue from purified full-length SARS-CoV cDNA clones was performed as described in Muth et. 2017 and in chapter 3.28-30. In brief, 5-10 µg extracted cDNA plasmids were linearized by 5 µl NotI digestion in 200 µl for 30 minutes. 1 µg of phenol chloroform extracted, linearized cDNA was *in-vitro* transcribed and capped using the mMMESSAGE mMACHINE T7 Transcription Kit (Invitrogen), detailed in chapter 3.28. 1-10 µg *in vitro* transcripts were electroporated into 4x10⁶ BHK-J cells (chapter 3.29). 24 hours post electroporation, the supernatant was transferred to susceptible Vero E6 cells and virus replication monitored by quantitative real-time PCR [237]. Recombinant viruses were harvested three days post infection and subjected to virus purification, as described for MERS-CoV.

3.28 - Linearization and phenol-chloroform extraction of rSARS-CoV cDNA

Prior to *in vitro* transcription, the 5-10 µg of clones pBelo vectors carrying full SARS cDNA genomes were linearized by digestion with 5 µl NotI in 200 µl volume for 1 hour at 37°C. Completeness of linearization was confirmed by agarose gel electrophoresis. Linearized plasmid was purified by phenol-chloroform and ethanol extraction. In brief, 200 µl Phenol/Chloroform/Isoamyl (25:24:1) was added to 200 µl diluted, linearized pBelo vector, mixed by inversion and centrifuged for 5 minutes at 11,000x g to allow for phase separation. The upper aqueous phase was transferred to a fresh tube and mixed with 200 µl Chloroform/Isoamyl (24:1), mixed by inversion and centrifuged for 5 minutes at 11,000x g. The upper aqueous phase was transferred to a fresh tube, mixed with 20 µl 3M NaOAc and 400 µl ethanol and incubated at -20°C for 30 minutes or overnight. Subsequently, plasmid DNA was centrifuged for 30 minutes at 14,000x g, washed and precipitated with 70% ethanol and dried for one minute. Linearized plasmids were resuspended in 15 µl RNase-free H₂O.

3.29 - Generation of infectious rSARS-CoV *in vitro* transcripts

In vitro transcription (IVT) and capping of purified, linearized pBelo BAC vectors was done by using the mMESSAGING mMACHINE T7 Transcription Kit (Invitrogen) using the following reaction.

2x NTP/CAP	10 μ l
10x T7 Buffer	2 μ l
30mM GTP	2 μ l
T7 enzyme mix	2 μ l
Template (concentration 250 ng/ μ l)	4 μ l
Total volume:	20 μl

The IVT reaction was incubated at 37°C for 4 hours. Residual input DNA template was digested by the addition of 1 μ l DNase for 15 minutes. IVT RNA was precipitated by the addition of 30 μ l 7,5M LiCl and 30 μ l H₂O, followed by a 60 minutes incubation at -20°C, centrifugation at 14,000x g, 4°C for 30 minutes and subsequent ethanol precipitation. Dried viral RNA transcripts were resuspended in 12 μ l nuclease free H₂O and RNA concentration was quantified on a NanoDrop spectrometer (Chapter 3.23). Aliquots of 10 μ g were stored at -80°C.

3.30 - Generation of recombinant virus from *in vitro* transcripts

Recombinant viruses are produced by a two-step protocol. 10 μ g capped *in vitro* transcribed full genome rSARS-CoV RNA and 2 μ g SARS-CoV N transcript were electroporated into a 100 μ l dilution of 4x10⁶ BHK-J cells in OptiPro. Pre-cooled 2 mm gaps cuvettes (VWR) were used for electroporation. SARS-CoV nucleocapsid transcript is co-electroporated in order to improve translation efficiency of viral proteins [238]. The suspension was carefully resuspended on ice and electroporated on a Gene Pulser Xcell (Bio-Rad) using a single 140 V pulse for 25 milliseconds. After electroporation, BHK-J cells were resuspended in 5 ml culture medium and transferred to a T25 flask. Hamster kidney derived BHK-J cells can efficiently be electroporated and serve as an initial host cell for virus particle production, but hamster cells are not susceptible for SARS-CoV infection. For virus stock production, the supernatant of the electroporated BHK-J cells was transferred to SARS-CoV susceptible Vero E6 cells 24 hours post electroporation. Vero E6 cells were grown to 90% confluency and passaged 1:2 into a T162 flask with DMEM culture medium containing 2% FCS, 1 prior to infection. At 0 and 72 hpi 50 μ l supernatant were subjected to isolation of viral RNA (chapter 3.21). Virus replication, as a function in increase in viral RNA, was monitored by quantitative real-time PCR (chapter 3.26). Upon confirmation of virus replication, the whole culture medium was subjected to virus stock production (chapter 3.2).

4 – Materials

4.1 - Cell Lines

Name:	Species and tissue:	Source:
293T (ATCC-CRL-3216)	Human fetal liver cell line	Bernhard Nocht Institute, Hamburg
BHK-J (derived from ATCC-CCL-10)	Baby hamster kidney cell line	Bernhard Nocht Institute, Hamburg
Caco-2 (ATCC-HTB-37)	Human colon epithelium	ATCC
Calu-3 (ATCC-HTB-55)	Human bronchial epithelium	ATCC
Huh-7 (ATCC-CCL-185)	Human liver epithelium	ATCC
T84 wild-type (CCL-248)	Human colon cell line	Steeve Boulant, University of Heidelberg
T84 IFNA/LR KO (derived from CCL-248)	CRISPR knockout of IFN alpha and IFN lambda receptor	Steeve Boulant, University of Heidelberg
Vero (B4 and E6) (derived from CCL-248)	African green monkey kidney cell line	ATCC

4.2 - MERS-CoV viruses isolates

Name	Collection date	Phylogenetic clade and lineage	GenBank accession number
EMC-2012	2012	A	JX869059
Riyadh_58_2014	2014	B, lineage 3	MN481964
Riyadh_150_2014	2014	B, lineage 3	MN481965
Riyadh_146_2014	2014	B, lineage 3	MN481966
Riyadh_1734_2015	2015	B, lineage 5	MN481979
Riyadh_1147_2014	2014	B, lineage 3	MN481967
Riyadh_586_2014	2014	B, lineage 3	MN481968
Riyadh_1735_2015	2015	B, lineage 5	MN481980
Riyadh_1737_2015	2015	B, lineage 5	MN481981
Riyadh_1340_2014	2014	B, lineage 3	MN481969
Riyadh_1760_2015	2015	B, lineage 5	MN481982
Riyadh_1758_2015	2015	B, lineage 5	MN481983
Riyadh_1757_2015	2015	B, lineage 5	MN481984
Riyadh_1769_2015	2015	B, lineage 5	MN481985
Jeddah_9042_2014	2014	B, lineage 4	MN481970
Jeddah_9055_2014	2014	B, lineage 4	MN481971
Jeddah_9278_2014	2014	B, lineage 4	MN481972
Jeddah_8965_2014	2014	B, lineage 4	MN481973
Jeddah_9313_2014	2014	B, lineage 4	MN481974
Riyadh_1764_2015	2014	B, lineage 5	MN481986
Jeddah_9289_2014	2014	B, lineage 4	MN481975
Riyadh_167_2014	2014	B, lineage 3	MN481976
Jeddah_9355_2014	2014	B, lineage 4	MN481977
Jeddah_10306_2014	2014	B, lineage 4	MN481978

All virus sequences were uploaded to GenBank and are publically available under the provided accession numbers. All viruses were generated from anonymous respiratory swabs of Saudi Arabian MERS patient. The collection date refers to the time point of sample taking.

4.3 - SARS- and SARS-CoV-2 isolates

SARS-CoV-2 strain Munich/2020/984 (BetaCoV/Munich/BavPat1/2020|EPI_ISL_406862) was isolated from a respiratory swab obtained from the early 2020 Munich patient cohort [214], SARS-CoV-2 strain Victoria (BetaCoV/Australia/VIC01/2020; accession number MT007544). SARS-CoV strain Frankfurt (accession number AY310120) was isolated in 2003 from a respiratory swab of a SARS patient in Germany 2003 [6]. Recombinant SARS-CoV strain Frankfurt (NC_004718), was cloned and rescued by Susanne Pfefferle at the Institute of Virology, University of Bonn Medical Center [224]. rSARS-CoV_{ΔORF6} was cloned by Dr. Doreen Muth at the Institute of Virology, University of Bonn Medical Center, in 2016.

4.4 - Bacteria strains

Name	Source
<i>E. coli</i> GS1783	Klaus Osterrieder, FU Berlin
<i>E. coli</i> One Shot Top10	Life Technologies/ made in-house
<i>E. coli</i> NEB-10 beta	NEB

4.5 - Bacteria medium and supplements

Name	Source
Carbenicillin (50 µg/ml)	Sigma Aldrich-Aldrich
Kanamycin (30 µg/ml)	Sigma Aldrich-Aldrich
Chloramphenicol (10 µg/ml)	Sigma Aldrich-Aldrich
Lysogeny Broth (LB) broth	Carl Roth, Karlsruhe
Lysogeny Broth (LB) agar	Carl Roth, Karlsruhe
S.O.C Medium	NEB
Stable Outgrow Medium	NEB

4.6 - Enzymes

Name	Application	Source
Antarctic Phosphatase	cloning	New England Biolabs
Dpn1 FastDigest	cloning	Thermo Fisher Scientific
NotI FastDigest	BAC linearization	Fermentas
Phusion High-Fidelity DNA polymerase	PCR	Thermo Fisher Scientific
RNAseH	PCR	Thermo Fisher Scientific
Superscript III Reverse Transcriptase	q-RT-PCR	Thermo Fisher Scientific
TaqPolymerase	Colony PCR	Thermo Fisher Scientific
T4 DNA Ligase	Cloning	Thermo Fisher Scientific

4.7 - DNA markers for agarose gel electrophoresis

Name	Source
1 kb Plus DNA Ladder	Invitrogen
1 kb DNA Ladder	Promega

4.8 - Oligonucleotides (Primers)

This section contains all primers that were not explicitly mentioned in the methods section. Many of these primers were designed by former members of the institute, including Dr. Doreen Muth and Dr. Benjamin Meyer. Primer sequences that were obtained from published research articles by other research groups are referenced. Primers were either manually designed in using the Geneious software, or designed using the primer design tool (Geneious), or using the IDT primer design web tool (PrimerQuest Tool). All sequences are provided in the 5' to 3' direction.

4.8.1 - Forward primers for MERS-CoV Sanger sequencing

Name	Sequence
47 Fwd	CAGAACTTTGATTTTAACGAACTTA
428 Fwd	GGATGGCGAAAATGCCTATGAA
1286 Fwd	TGAGTGTGGAAGTTGTGGTAAT
2640 Fwd	GTATCCAGTAACATGGTTGAAACT
3609 Fwd	TTGTCCAATTTTGAACATAAGGTTAT
4593 Fwd	CTCCTGCATTGGTCTGATCAAA
5669 Fwd	GGTATTCTTTGGACGGTAATTTCA
6092 Fwd	CAATAGAGCTAGTTTGCGTCAAAT
6710 Fwd	CGTTGTGACAGGTAATGTTGTAA
7652 Fwd	TTATGTGGATTCCGTTACAGTTAA
8210 Fwd	CAATAATTATGTACCCTCATATGTTAA
9020 Fwd	ATACTGCCATGATCCTACTGTTT
9827 Fwd	AACTAATGATGCCTATTCACGATTT
10599 Fwd	CACCAAGTTCAGTTAACAGACAAA
11332 Fwd	GATTGTACAACCCATCACTTTCTAA
12558 Fwd	GAAATTGTTAAGTCTTCAGATGTTGTA
13862 Fwd	TGCTGTGATGTTACCTACTTTGAA
15198 Fwd	GTGGCTGGGATTTTCATGCTTAAA
16581 Fwd	CTACAACAGAACCACTCAAACCTT
17477 Fwd	TGTCCTAGATTGATGTGTAACCTTA
18254 Fwd	AGCTGGATAGGCTTCGATGTT
19197 Fwd	CACGTGTGCATTCTGAGTTCAAT
20021 Fwd	GGTCCTGATTATGCTTACTTCAAT

21015 Fwd	ATGTAACAGGTAGTAATGAGTCAAA
21826 Fwd	CCAATTCCACTGGCACTGTTA
22208 Fwd	AGAGTGGTTTGGCATTACACAAA
22588 Fwd	CTGAAGGTGTTGAATGTGATTTT
23455 Fwd	CTAAAACCCACGCTACTCTATT
24329 Fwd	TGGCTGGACTGCTGGCTTAT
24817 Fwd	CACATATAGTGTCCCTTTGTTGTAA
25489 Fwd	TCGAGCCGCATAAGGTTTCAT
26767 Fwd	GTCTTCCAATCAGGGTAATAAACAA
28176 Fwd	TGGTCATTCAATCCTGAGACTAA
29503 Fwd	AACTTACCCATCAGAACAATGAT

4.8.2 - Reverse primers for MERS-CoV Sanger sequencing

Name	Sequence
842 Rev	CTTAAGCAGATTCTGGGCATATT
1826 Rev	ACCTTTGAGAAGCTGGCGTATT
2841 Rev	GTGCACCTCCCTTAAGTCTAAA
3278 Rev	AGTCTCATGAGAAACGTCAACTT
3745 Rev	ATACCACCGCCATGCTTAAGA
4074 Rev	CTTGGGAATTAACGACGACTAAA
4719 Rev	GTGTCGTGCGTGAATCCAAT
5856 Rev	CAGACGATACAAGGCAGCTATT
6839 Rev	CAATACCATAGTTGTGCATAACATAA
8327 Rev	ACCATTAGAATTACGCAAGACAATT
9169 Rev	GACAGAGTTCTAGTAATCCTAAGT
9963 Rev	CAGTCTCGCTGTATGTTTGTAA
10707 Rev	CACTAGTGCGATTAGGTTTTACAA
11489 Rev	AGTAACAAAGACTGTAATCGTATAA
12261 Rev	CCTGATCAGCCATACGTTCTAA
13595 Rev	CATCTAATTCTACAAACCTACAAGTAT
14837 Rev	CAACTTCCATGCAGAACAACATT
15780 Rev	TTCTGATAATACAGCGTTTCCTTAA
16821 Rev	TACTCACCGAGCTGCACTTT
17662 Rev	GCTAGCATCATGCGTCACATT
18375 Rev	ACAACACCAACTGGCTGAACAA
19351 Rev	CACTTCACATGGTGTAGTAGAATA
20138 Rev	ACTCAGTAGGATCAATAAACTCATT
21550 Rev	TCAATACAAGCAGACTTAACAGAAT
22360 Rev	GAACGAATACTGTGAGGAATGATA
23196 Rev	GTCTGTACCATATTGAACTGTAAT

24057 Rev	CACCTCCAAAACCTGGTATGATA
24917 Rev	ACCATAAGCAGAAACAACCTCAAT
25679 Rev	CAGCTTGGGCAGTTTTAATAACAA
26480 Rev	AGGCGAACTCATGTAGCTCAAAT
27587 Rev	GACATTATGAAGGAGTTCGTTAAA
28679 Rev	CAGTGTACCAAGAGACAGTGTTA
29142 Rev	CTGATCTTGAACCTTGTGAACTA
29621 Rev	CTCAAGAAGCTCCAACCACTTA

4.8.3 - MERS-CoV Spike mutagenesis primer

Name	Mutation	Direction	Sequence
MERS S QS L411F Fwd	L411F	Forward	CCAATTGCAATTATAATTTTACCAAATTGCTTTCA CTTTTTTCTGT
MERS S QS L411F Rev	L411F	Reverse	TAAAACCAAACGCTTGAAATTATAAACCTGAGG AGGT
MERS S QS Q833R Fwd	Q833R	Forward	TTCCAAAATAAACCGGGCTCTCCATGGTGC
MERS S QS Q833R Rev	Q833R	Reverse	CAAAACTGGCCATACTCGCGCAGTAATTGC
MERS S QS Q1020R Fwd	Q1020R	Forward	TAATGAAGCTTTTCGGAAGGTTTCAGGATGC
MERS S QS Q1020R Rev	Q1020R	Reverse	GTTGTAGTGAAGCCTGTTTGCATAGCTCCC

4.8.4 - Quantitative real-time PCR primers and probes

Name	Direction	Sequence
TBP fwd	Forward	CTGCGGTAATCATGAGGATAAG
TBP prb	Probe	TGTGCACAGGAGCCAAGAGTGAAG
TBP rev	Reverse	TTCTTGCTGCCAGTCTGGAC
IFNb1 fwd	Forward	AGGATTCTGGATTACCTGAAGG
IFNb1 prb	Probe	TCCACTCTGACTATGGTCCAGGCA
IFNb1 rev	Reverse	GGCTAGGAGATCTTCAGTTTCG
IFNL1 fwd	Forward	CTCTGTCACCTTCAACCTCTTC

IFNL1 prb	Probe	CACGCGAGACCTGAATTGTGTTGC
IFNL1 rev	Reverse	ATCTCAGGTTGCATGACTGG
CCL5 fwd	Forward	TGCCCACATCAAGGAGTATTTTC
CCL5 prb	Probe	TCACCCGAAAGAACCGCCAAGT
CCL5 rev	Reverse	CCATCCTAGCTCATCTCCAAAG
Mx1 fwd	Forward	TTCAGCACCTGATGGCCTATC
Mx1 prb	Probe	CAGGAGGCCAGCAAGCGCCATC
Mx1 rev	Reverse	TGG ATG ATC AAA GGG ATG TGG
ISG56 fwd	Forward	CCTGGAGTACTATGAGCGGGC
ISG56 prb	Probe	ACAGAGTTCTCAAAGTCAGCAGCCAGTCTCAGT
ISG56 rev	Reverse	TGGGTGCCTAAGGACCTTGTC
TNFa fwd	Forward	TGGCCCAGGCAGTCAGA
TNFa prb	Probe	CATCTTCTCGAACCCCGAGTGACAAGC
TNFa rev	Reverse	TGTAGCCCATGTTGTAGCAAACC
sgN RNA fwd [239]	Forward	CTCGTTCTCTTGCAGAACTTTG
sgN RNA prb [239]	Probe	CACGAGCTGCACCAAATAAACTGTCTC
sgN RNA rev [239]	Reverse	GTAAGAGGGACTTTCCCGTGTTG
MERS ORF1a fwd [190]	Forward	CCACTACTCCCATTTTCGTCAG
MERS ORF1a prb [190]	Probe	CAGTATGTGTAGTGCGCATATAAGCA
MERS ORF1a rev [190]	Reverse	TTGCAAATTGGCTTGCCCCACT
E_Sarbeco_F [237]	Forward	ACAGGTACGTTAATAGTTAATAGCGT
E_Sarbeco_P1 [237]	Probe	AACTAGCCATCCTTACTGCGCTTCG
E_Sarbeco_R [237]	Reverse	ATATTGCAGCAGTACGCACACA

4.9 - Plasmids

Name	Source	Application
pCG1 (empty)	M. Hoffman; DPZ Göttingen	VSVpp
pCG1-VSV-G	M. Hoffman; DPZ Göttingen	VSVpp
pCG1-MERS-S	Cloned by B. Meyer	VSVpp
pCG1-MERS-S-Q1020R	This thesis	VSVpp
pCG1-MERS-S-Q1020R-L411F	This thesis	VSVpp
pCG1-MERS-S-Q1020R-Q833R	This thesis	VSVpp
pBelo-rSARS-wt	Cloned by S. Pfefferle [224]	rSARS-CoV cloning
pBelo-rSARS-ORF6-SARS-2	This thesis	rSARS-CoV cloning
pBelo-rSARS-delORF6	Cloned D. Muth and A. Siemens	rSARS-CoV cloning

4.10 - Commercial Kits

Name	Application	Source
Nextera® XT DNA Library Prep	Library preparation for NGS	Illumina
MagNA Pure 96 DNA and Viral NA SV	RNA extraction	Roche Diagnostics
MiSeq Reagent Kit v3	NGS	Illumina
mMessage mMachine T7	<i>In vitro</i> RNA transcription	Thermo Fisher Scientific
NE-PER	Nucleus cytosol fractionation	Thermo Fisher Scientific
NucleoBond Xtra Midi EF	DNA extraction	Macherey&Nagel
NucleoSpin Gel and PCR clean-up	PCR clean-up, gel extraction	Macherey&Nagel
Renilla Luciferase Assay System	VSVpp quantification	Promega
Superscript III/TaqPol OS kit	Real-time PCR	Thermo Fisher Scientific
SuperScript® One-Cycle cDNA Kit	cDNA synthesis for NGS	Invitrogen

4.11 - Antibodies

Antibody	Source	Application*
Anti VSV-G, from CRL-2700	ATCC	VSVpp
AlexaFlour488-conjugated anti-human	Thermo Fisher Scientific	VSVpp
Soluble DPP4 C-terminal human Fc-tag	ACROBiosystems	VSVpp
p-IRF3 cs#4947s	Cell Signaling Technology	Western blot
IRF3 cs#4302s	Cell Signaling Technology	Western blot
IκBα cs#4812s	Cell Signaling Technology	Western blot
SARS-CoV-N GTX632269	Genetex	Western blot
β-Actin A5316	Sigma Aldrich	Western blot
NFκB p65 cs#6956s	Cell Signaling Technology	Western blot
STAT-1 cs#9172	Cell Signaling Technology	Western blot
GAPDH cs#5174s	Cell Signaling Technology	Western blot
Histone H3 H0164	Sigma Aldrich	Western blot
Goat anti-Rabbit IgG, HRP, 65-6120	Thermo Scientific	Western blot
Goat anti-Mouse IgG, HRP, 62-6520	Thermo Scientific	Western blot

*Applied dilutions are provided in chapter 3.17-20

4.12 - Software

Name:	Application	Source
BioRender	Figure 4A preparation	Biorender.com
Chromat Quantitator	Sanger Sequencing peak high quantification	Mullins lab, open access; https://indra.mullins.microbiol.washington.edu/cgi-bin/chromatquant.cgi
FigTree v1.4.4	Display and editing of phylogenetic trees	Andrew Rambaut; open access tree.bio.ed.ac.uk
Geneious v9.1.8 with MrBayes and RaxML plugins	Planning of cloning strategy; primer design; alignment calculations; phylogenetic trees (RaxML and MrBayes); NGS read assembly and editing; Sanger sequencing evaluation	Geneious

GraphPad Prism v8.2.1	Plotting of all data; statistical analysis of all data	GraphPad
PrimerQuest Tool	Primer design	IDT, open access; https://www.idtdna.com/pages/tools/primerquest
Promega Image Lab	Gel electrophoresis imaging and extraction	Promega
NetNGlyc and NetOGlyc	Glycolysation prediction	Open access; [240] http://www.cbs.dtu.dk/services/NetOGlyc/ and [241] http://www.cbs.dtu.dk/services/NetNGlyc/
SimPlot 3.5.1	Bootstrap analysis for recombination detection	[242], open access https://omictools.com/simplot-tool

4.13 - Technical Equipment

Equipment	Model	Source
Autoclave S2	VS-100	Systec
Autoclave S3	Custom made	Matachana
BSL3 respirator	OptimAir 3000	MSA
Blotting system	TransBlotTurbo	BioRad
Balance	Kern 572	Kern
Centrifuge	Eppendorf 5424	Eppendorf
Centrifuge	Eppendorf 5430R	Eppendorf
Centrifuge	Eppendorf 5810R	Eppendorf
Electroporation System	Gene Pulser Xcell	Bio-Rad
Freezer	-20er	Liebherr
Freezer	-80er, Model U725	New Brunswick
Gel electrophoresis System	41-1325	Peqlab
Gel documentation	Universal Hood II	Bio-Rad
Heating block	TS pro	CellMedia
Hood (Sterile bench)	Safe2020	Thermo Fisher Scientific
Incubator	C170	Binder
Microscope cell culture	CK30	Olympus
Microscope BSL3	Axio Observer	Zeiss
Microscope (confocal)	LSM800 Airyscan	Zeiss
Multistep Pipette	HandyStep	Brand
Multichannel Pipette	Xplorer	Eppendorf

NGS sequencing platform	MiSeq System	Illumina
PCR cycler	Nexus Gradient	Eppendorf
Photometer	Nanodrop 1000	Thermo Fisher Scientific
Pipettes	Research Plus, 100-1000 µl, 10-100 µl, 0.5-10 µl, 0.1-2 µl	Eppendorf
Power supply	Standard Power Pack P25	Biometra
Real-time PCR Cycler	LightCycler 480 II	Roche Diagnostics
Vortexer	VV2	VWR

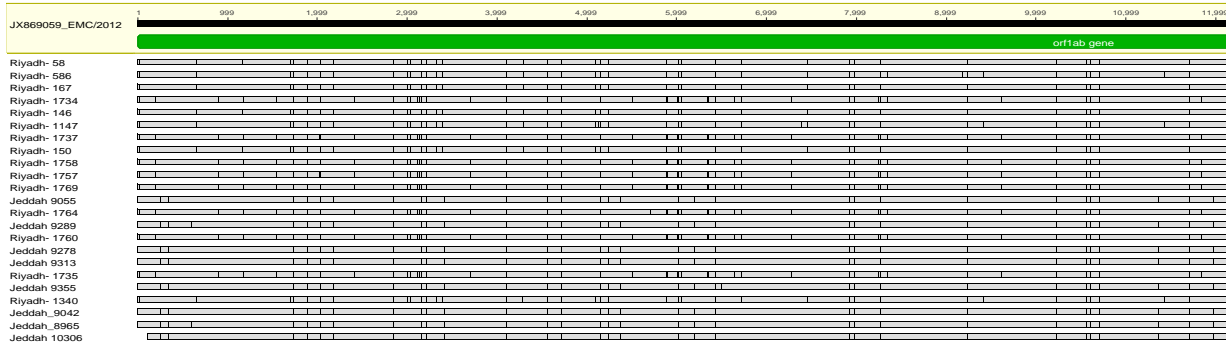
5 - Abbreviations

Abbreviation	Full name
3CLpro	chymotrypsin-like protease 3
ACE2	Angiotensin-converting enzyme 2
ALI	Air liquid interface
bp	basepairs
CoV	Coronavirus
CoVs	Coronaviruses
CPE	Cytoplasmic effect
CT	Cycle treshold
CTD	C-terminal domain
DPP4	Dipeptidylpeptidase 4
DMEM	Dulbecco's Modified Eagle's Medium
dsRNA	Double-stranded RNA
E	Envelope protein
EndoU	uridylylate-specific endoribonuclease
ExoN	Exonuclease
GTR	general time reversible
HAE	Human airway epithelium
hpi	hours post infection
IFIT	Interferon-induced protein with tetratricopeptide repeats
IFITM	Interferon-induced transmembrane proteins
IFN	Interferon
ISG	Interferon stimulated gene
ISRE	Interferon stimulated response element
IVT	<i>in vitro</i> transcription
JAK	Januskinase
KO	Knock out
kbp	kilobasepairs
LB	Lysogeny broth
M	Membrane protein
MAVS	Mitochondrial antiviral-signaling protein
MERS	Middle East respiratory syndrome
MOI	Multiplicity of infection
N	Nucleocapsid protein
NF-kB	nuclear factor 'kappa-light-chain-enhancer' of activated B-cells
nsp	Non-structural protein
NTD	N-terminal domain
ORF	Open reading frame
p.	Passage

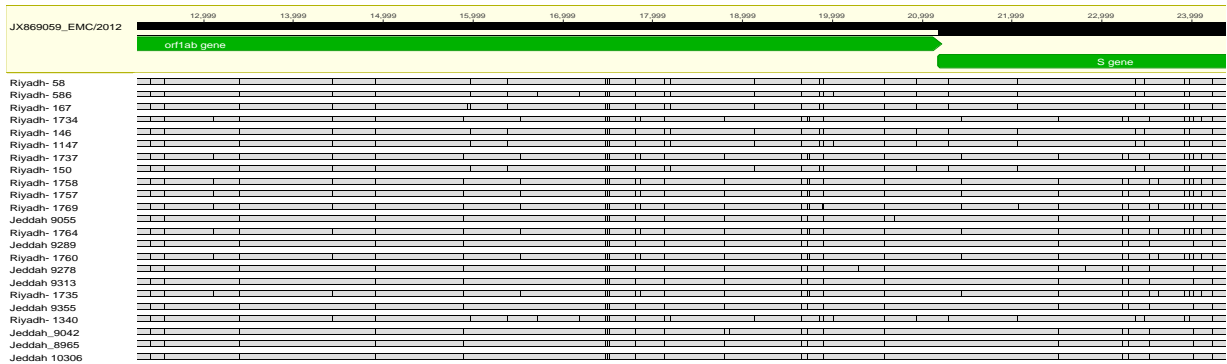
p	Protein
PBS	Phosphate buffered saline
pp	polyprotein
PACT	Protein activator of the interferon-induced protein kinase
PAMP	Pathogen associated molecular patten
PCR	Polymerase chain reaction
PFU	Plaque forming unit
PLpro	Papain-like protease
PRNT	Plaque reduction neutralization test
PRR	Pattern recognition receptor
q-RT-PCR	Quantitative real-time PCR
RBD	Receptor-binding domain
RdRp	RNA dependent RNA polymerase
rSARS-CoV	Recombinant SARS-CoV
S	Spike protein
SARS	Severe acute respiratory syndrome
sg	subgenomic
sgmRNA	Subgenomic messenger RNA
TMPRSS2	transmembrane protease serine subtype 2
TRS	Transcription regulatory sequence
UTR	Untranslated region

6 - Supplements

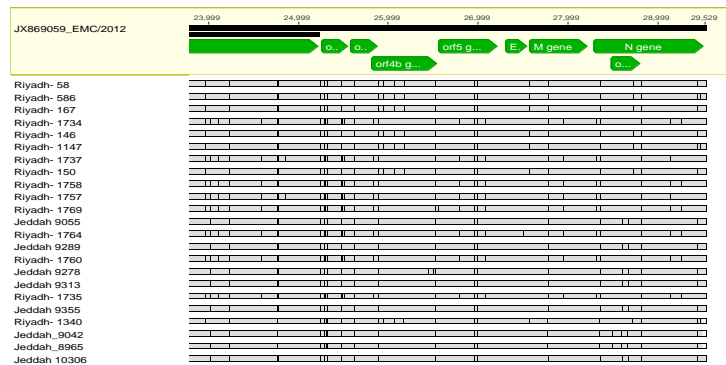
Genome position 1-12,000 bp



Genome position 12,000-24,000 bp



Genome position 24,000- 30,000 bp



Supplementary Figure 1: Overview of SNPs in coding regions of MERS-CoV isolates generated in this thesis (relative to the reference strain EMC). Green arrows indicate the gene in which the SNP is located. Each black dash indicates a SNP in comparison to the reference strain (EMC). SNPs that encode for amino acid exchanges between the MERS-CoV lineages are listed in supplementary Table 1.

Supplementary Table 1: Amino acid divergence of generated MERS-CoV isolates reflecting changes found in all isolates of the respective phylogenetic lineage. AA = amino acid; the AA positions for nsp1-15 are provided relative to the start of ORF1ab. An overview of amino acid divergence in the spike protein is provided in supplementary figure 2.

	nsp1	
AA position	8	158
lineage 3	I	F
lineage 4	T	F
lineage 5	I	V

	nsp2	
AA position	219	519
lineage 3	E	L
lineage 4	K	L
lineage 5	K	I

	nsp3					
AA position	1000	1040	1045	1072	1110	1236
lineage 3	V	A	A	Q	L	A
lineage 4	I	A	A	Q	P	A
lineage 5	V	V	V	R	P	T

	nsp3							
AA position	1700	1794	1835	1964	2003	2119	2215	2426
lineage 3	C	P	E	A	A	M	K	T
lineage 4	R	S	E	E	A	M	K	T
lineage 5	R	P	A	A	V	I	E	I

	nsp4
AA position	2747
lineage 3	A
lineage 4	A
lineage 5	V

	nsp6
AA position	3785
lineage 3	L
lineage 4	F
lineage 5	L

	nsp8
AA position	3947
lineage 3	Q
lineage 4	Q
lineage 5	R

Supplementary Table 1 (continued):

	nsp10
AA position	4373
lineage 3	A
lineage 4	A
lineage 5	V

	nsp13
AA position	5574
lineage 3	N
lineage 4	S
lineage 5	S

	nsp14		
AA position	5957	6368	6381
lineage 3	V	I	T
lineage 4	V	I	A
lineage 5	I	V	A

	nsp15
AA position	6580
lineage 3	M
lineage 4	M
lineage 5	I

	protein 3	
AA position	17	85
lineage 3	L	G
lineage 4	L	G
lineage 5	F	L

	protein 4b		
AA position	6	47	85
lineage 3	M	F	F
lineage 4	M	L	L
lineage 5	T	L	L

	M
AA position	123
lineage 3	F
lineage 4	F
lineage 5	I

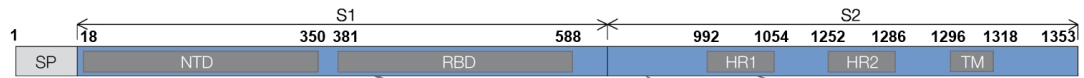
	N			
AA position	11	126	144	283
lineage 3	S	D	L	L
lineage 4	S	H	S	L
lineage 5	F	D	S	F

Supplementary Table 2: Summary of MERS-CoV isolates that were used in each experiment and their respective phylogenetic lineage (accession numbers are provided in chapter 4.2).

Figure	MERS-CoV isolate	lineage
8A	Riyadh-146 2014	3
	Riyadh-1147 2014	3
	Jeddah-9278 2014	4
	Jeddah-10306 2014	4
	Riyadh-1734 2015	5
	Riyadh-1764 2015	5
8B	Riyadh-58 2014	3
	Riyadh-146 2014	3
	Riyadh-150 2014	5
	Riyadh-167 2014	5
	Riyadh-586 2014	3
	Riyadh-1147 2014	3
	Riyadh-1340 2014	3
	Jeddah-8965 2014	4
	Jeddah-9042 2014	4
	Jeddah-9055 2014	4
	Jeddah-9278 2014	4
	Jeddah-9313 2014	4
	Jeddah-9355 2014	4
	Jeddah-9355 2014	4
	Jeddah-10306 2014	4
	Riyadh-1734 2015	5
	Riyadh-1735 2015	5
	Riyadh-1737 2015	5
	Riyadh-1757 2015	5
	Riyadh-1758 2015	5
Riyadh-1760 2015	5	
Riyadh-1764 2015	5	
Riyadh-1769 2015	5	
8C	Riyadh-146 2014	3
	Riyadh-1147 2014	3
	Jeddah-9278 2014	4
	Jeddah-10306 2014	4
	Riyadh-1734 2015	5
	Riyadh-1764 2015	5
8D	Riyadh-1147 2014	3
	Jeddah-10306 2014	4
	Riyadh-1764 2015	5

Supplementary Table 2 (continued):

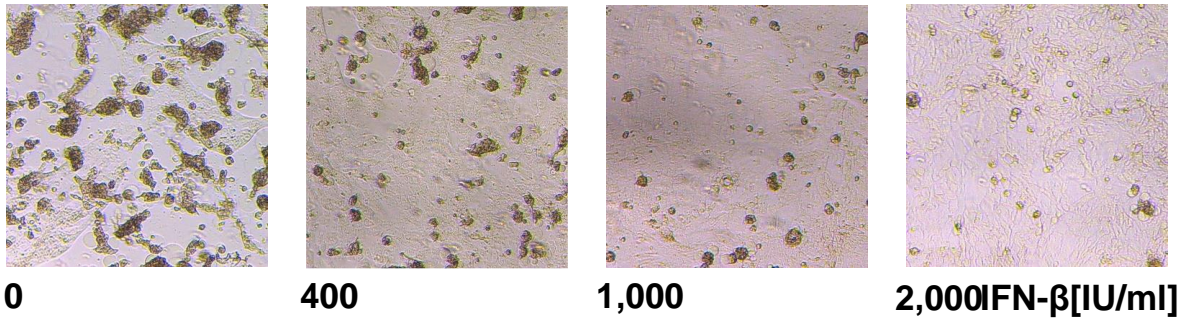
Figure	MERS-CoV isolate	Lineage
9	Riyadh-1147 2014	3
	Riyadh-1764 2015	5
10	VSVpp	3
	VSVpp	4
	VSVpp	5
11	Riyadh-1147 2014	3
	Jeddah-10306 2014	4
	Riyadh-1764 2015	5
12	Riyadh-1147 2014	3
	Jeddah-10306 2014	4
	Riyadh-1734 2015	5
13	Riyadh-146 2014	3
	Riyadh-1147 2014	3
	Jeddah-9289 2014	4
	Jeddah-10306 2014	4
	Riyadh-1734 2015	5
	Riyadh-1737 2015	5
14	Riyadh-146 2014	3
	Riyadh-167 2014	3
	Jeddah-9278 2014	4
	Jeddah-9289 2014	4
	Riyadh-1734 2015	5
	Riyadh-1737 2015	5
15	Riyadh-1147 2014	3
	Riyadh-146 2014	3
	Jeddah-8965 2014	4
	Jeddah-9278 2014	4
	Riyadh-1764 2015	5
	Riyadh-1734 2015	5
16A	Riyadh-1147 2014	3
	Riyadh-146 2014	3
	Jeddah-10306 2014	4
	Jeddah-9278 2014	4
	Riyadh-1764 2015	5
	Riyadh-1734 2015	5
16B	Riyadh-1147 2014	3
	Jeddah-10306 2014	4
	Riyadh-1764 2015	5



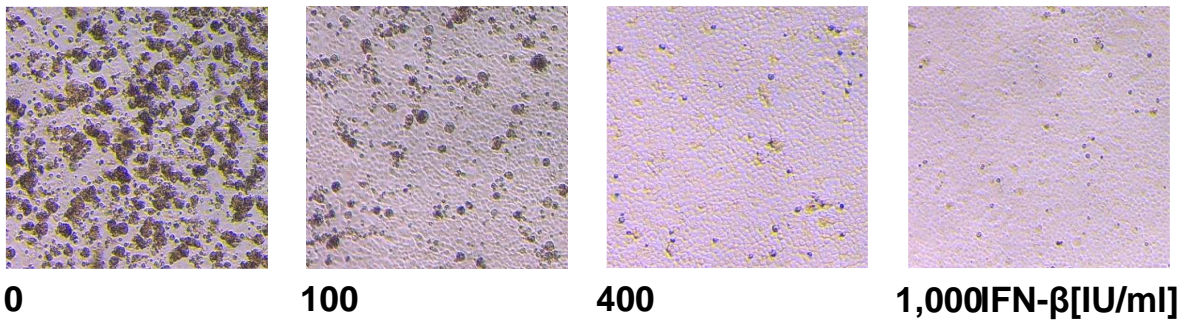
Phylogenetic lineage	strain	411	833	1020
	EMC	L	Q	Q
lineage 3	Riyadh-58 2014	F	.	R
lineage 3	Riyadh-146 2014	F	.	R
lineage 3	Riyadh-150 2014	F	.	R
lineage 3	Riyadh-167 2014	F	.	R
lineage 3	Riyadh-586 2014	F	.	R
lineage 3	Riyadh-1147 2014	F	.	R
lineage 3	Riyadh-1340 2014	F	.	R
lineage 5	Riyadh-1734 2015	.	.	R
lineage 5	Riyadh-1735 2015	.	.	R
lineage 5	Riyadh-1737 2015	.	.	R
lineage 5	Riyadh-1757 2015	.	.	R
lineage 5	Riyadh-1758 2015	.	.	R
lineage 5	Riyadh-1760 2015	.	.	R
lineage 5	Riyadh-1764 2015	.	.	R
lineage 5	Riyadh-1769 2015	.	.	R
lineage 4	Jeddah-8965 2014	.	R	R
lineage 4	Jeddah-9042 2014	.	R	R
lineage 4	Jeddah-9055 2014	.	R	R
lineage 4	Jeddah-9278 2014	.	R	R
lineage 4	Jeddah-9289 2014	.	R	R
lineage 4	Jeddah-9313 2014	.	R	R
lineage 4	Jeddah-9355 2014	.	R	R
lineage 4	Jeddah-10306 2014	.	R	R

Supplementary Figure 2: Differences in the spike protein amino acid sequence of the MERS-CoV isolates investigated in this study. The EMC reference spike protein sequence was used as a reference for the alignment. Numbers indicate the respective amino acid position. S1/2 = subunit 1/2; SP = signal peptide; NTD = N-terminal domain; RBD = receptor-binding domain; HR1/2 = Heptad repeat 1/2; TM = transmembrane domain

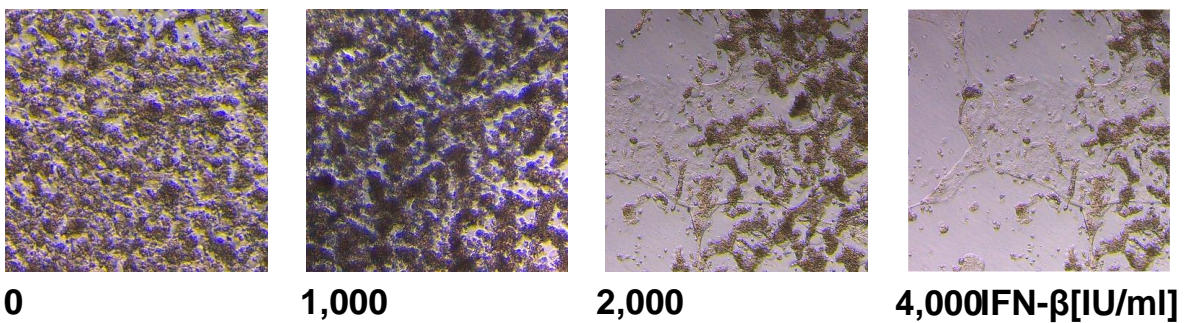
A Calu-3 IFN- β pretreatment (SARS-CoV-2 moi = 0.001)



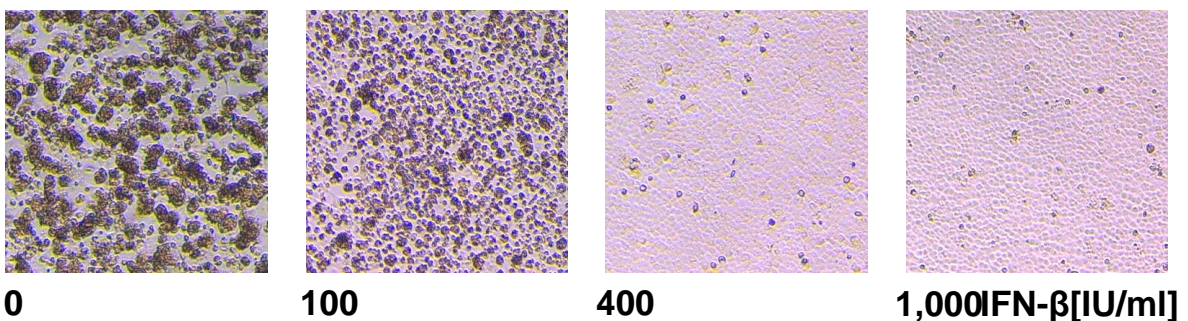
B Vero E6 IFN- β pretreatment (SARS-CoV-2 moi = 0.001)



C Calu-3 IFN- β posttreatment (SARS-CoV-2 moi = 0.001)



D Vero E6 IFN- β posttreatment (SARS-CoV-2 moi = 0.001)



Supplementary Figure 3: CPE induction by SARS- and SARS-CoV-2 in Calu-3 and Vero E6 cells, with IFN treatment as indicated. Images were taken on a Zeiss Axio Observer with 20x magnification

7 - References

1. Nga, P.T., et al., *Discovery of the first insect nidovirus, a missing evolutionary link in the emergence of the largest RNA virus genomes*. PLoS Pathog, 2011. **7**(9): p. e1002215.
2. Gorbalenya, A.E., et al., *Nidovirales: Evolving the largest RNA virus genome*. Virus Research, 2006. **117**(1): p. 17-37.
3. Forni, D., et al., *Molecular Evolution of Human Coronavirus Genomes*. Trends Microbiol, 2017. **25**(1): p. 35-48.
4. Almeida, J.D. and D.A.J. Tyrrell, *The Morphology of Three Previously Uncharacterized Human Respiratory Viruses that Grow in Organ Culture*. Journal of General Virology, 1967. **1**(2): p. 175-178.
5. Kapikian, A.Z., et al., *Isolation from man of "avian infectious bronchitis virus-like" viruses (coronaviruses) similar to 229E virus, with some epidemiological observations*. J Infect Dis, 1969. **119**(3): p. 282-90.
6. Drosten, C., et al., *Identification of a novel coronavirus in patients with severe acute respiratory syndrome*. N Engl J Med, 2003. **348**(20): p. 1967-76.
7. Zaki, A.M., et al., *Isolation of a novel coronavirus from a man with pneumonia in Saudi Arabia*. N Engl J Med, 2012. **367**(19): p. 1814-20.
8. Zhu, N., et al., *A Novel Coronavirus from Patients with Pneumonia in China, 2019*. N Engl J Med, 2020. **382**(8): p. 727-733.
9. Beaudette, F.a.H., CB, *Cultivation of the virus of infectious bronchitis*. J. Am. Vet. Med. Assoc., 1937. **90**: p. 51–58.
10. van der Hoek, L., et al., *Identification of a new human coronavirus*. Nature Medicine, 2004. **10**(4): p. 368-373.
11. Woo, P.C.Y., et al., *Characterization and complete genome sequence of a novel coronavirus, coronavirus HKU1, from patients with pneumonia*. Journal of virology, 2005. **79**(2): p. 884-895.
12. van Elden, L.J., et al., *Frequent detection of human coronaviruses in clinical specimens from patients with respiratory tract infection by use of a novel real-time reverse-transcriptase polymerase chain reaction*. J Infect Dis, 2004. **189**(4): p. 652-7.
13. Mackay, I.M., et al., *Co-circulation of four human coronaviruses (HCoVs) in Queensland children with acute respiratory tract illnesses in 2004*. Viruses, 2012. **4**(4): p. 637-53.
14. Friedman, N., et al., *Human Coronavirus Infections in Israel: Epidemiology, Clinical Symptoms and Summer Seasonality of HCoV-HKU1*. Viruses, 2018. **10**(10).
15. Saberi, A., et al., *A planarian nidovirus expands the limits of RNA genome size*. PLOS Pathogens, 2018. **14**(11): p. e1007314.
16. Eigen, M., *Selforganization of matter and the evolution of biological macromolecules*. Naturwissenschaften, 1971. **58**(10): p. 465-523.
17. Drake, J.W. and J.J. Holland, *Mutation rates among RNA viruses*. Proceedings of the National Academy of Sciences, 1999. **96**(24): p. 13910.
18. Jenkins, G.M., et al., *Rates of Molecular Evolution in RNA Viruses: A Quantitative Phylogenetic Analysis*. Journal of Molecular Evolution, 2002. **54**(2): p. 156-165.
19. Sanjuán, R., et al., *Viral Mutation Rates*. Journal of Virology, 2010. **84**(19): p. 9733.
20. Drake, J.W., *Rates of spontaneous mutation among RNA viruses*. Proc Natl Acad Sci U S A, 1993. **90**(9): p. 4171-5.
21. Steinhauer, D.A., E. Domingo, and J.J. Holland, *Lack of evidence for proofreading mechanisms associated with an RNA virus polymerase*. Gene, 1992. **122**(2): p. 281-288.
22. Eigen, M., *Error catastrophe and antiviral strategy*. Proceedings of the National Academy of Sciences, 2002. **99**(21): p. 13374.
23. Pfeiffer, J.K. and K. Kirkegaard, *Increased Fidelity Reduces Poliovirus Fitness and Virulence under Selective Pressure in Mice*. PLOS Pathogens, 2005. **1**(2): p. e11.

24. Domingo, E., *Chapter 3 - Darwinian Principles Acting on Highly Mutable Viruses*, in *Virus as Populations*, E. Domingo, Editor. 2016, Academic Press: Boston. p. 73-122.
25. Domingo, E., *Chapter 5 - Viral Fitness as a Measure of Adaptation*, in *Virus as Populations*, E. Domingo, Editor. 2016, Academic Press: Boston. p. 169-195.
26. Graci, J.D., et al., *Mutational robustness of an RNA virus influences sensitivity to lethal mutagenesis*. *J Virol*, 2012. **86**(5): p. 2869-73.
27. Poirier, E.Z., et al., *Low-Fidelity Polymerases of Alphaviruses Recombine at Higher Rates To Overproduce Defective Interfering Particles*. *J Virol*, 2015. **90**(5): p. 2446-54.
28. Gnädig, N.F., et al., *Coxsackievirus B3 mutator strains are attenuated in vivo*. *Proc Natl Acad Sci U S A*, 2012. **109**(34): p. E2294-303.
29. Rozen-Gagnon, K., et al., *Alphavirus mutator variants present host-specific defects and attenuation in mammalian and insect models*. *PLoS Pathog*, 2014. **10**(1): p. e1003877.
30. Snijder, E.J., et al., *Unique and conserved features of genome and proteome of SARS-coronavirus, an early split-off from the coronavirus group 2 lineage*. *J Mol Biol*, 2003. **331**(5): p. 991-1004.
31. Subissi, L., et al., *One severe acute respiratory syndrome coronavirus protein complex integrates processive RNA polymerase and exonuclease activities*. *Proceedings of the National Academy of Sciences*, 2014. **111**(37): p. E3900.
32. Eckerle, L.D., et al., *High Fidelity of Murine Hepatitis Virus Replication Is Decreased in nsp14 Exoribonuclease Mutants*. *Journal of Virology*, 2007. **81**(22): p. 12135.
33. Denison, M.R., et al., *Coronaviruses: an RNA proofreading machine regulates replication fidelity and diversity*. *RNA Biol*, 2011. **8**(2): p. 270-9.
34. Bouvet, M., et al., *RNA 3'-end mismatch excision by the severe acute respiratory syndrome coronavirus nonstructural protein nsp10/nsp14 exoribonuclease complex*. *Proceedings of the National Academy of Sciences*, 2012. **109**(24): p. 9372.
35. Walker, P.J., et al., *Changes to virus taxonomy and the International Code of Virus Classification and Nomenclature ratified by the International Committee on Taxonomy of Viruses (2019)*. *Archives of Virology*, 2019. **164**(9): p. 2417-2429.
36. Woo, P.C.Y., et al., *Discovery of seven novel Mammalian and avian coronaviruses in the genus deltacoronavirus supports bat coronaviruses as the gene source of alphacoronavirus and betacoronavirus and avian coronaviruses as the gene source of gammacoronavirus and deltacoronavirus*. *Journal of virology*, 2012. **86**(7): p. 3995-4008.
37. Cui, J., F. Li, and Z.-L. Shi, *Origin and evolution of pathogenic coronaviruses*. *Nature Reviews Microbiology*, 2019. **17**(3): p. 181-192.
38. Drexler, J.F., V.M. Corman, and C. Drosten, *Ecology, evolution and classification of bat coronaviruses in the aftermath of SARS*. *Antiviral Res*, 2014. **101**: p. 45-56.
39. Lau, S.K., et al., *Severe acute respiratory syndrome coronavirus-like virus in Chinese horseshoe bats*. *Proc Natl Acad Sci U S A*, 2005. **102**(39): p. 14040-5.
40. Li, W., et al., *Bats are natural reservoirs of SARS-like coronaviruses*. *Science*, 2005. **310**(5748): p. 676-9.
41. Woo, P.C., et al., *Molecular diversity of coronaviruses in bats*. *Virology*, 2006. **351**(1): p. 180-7.
42. Corman, V.M., et al., *Rooting the phylogenetic tree of middle East respiratory syndrome coronavirus by characterization of a conspecific virus from an African bat*. *J Virol*, 2014. **88**(19): p. 11297-303.
43. Corman, V.M., et al., *Evidence for an Ancestral Association of Human Coronavirus 229E with Bats*. *Journal of Virology*, 2015. **89**(23): p. 11858-11870.
44. Tao, Y., et al., *Surveillance of Bat Coronaviruses in Kenya Identifies Relatives of Human Coronaviruses NL63 and 229E and Their Recombination History*. *J Virol*, 2017. **91**(5).
45. Hu, B., et al., *Discovery of a rich gene pool of bat SARS-related coronaviruses provides new insights into the origin of SARS coronavirus*. *PLOS Pathogens*, 2017. **13**(11): p. e1006698.

46. Zhou, P., et al., *A pneumonia outbreak associated with a new coronavirus of probable bat origin*. Nature, 2020. **579**(7798): p. 270-273.
47. Zhou, P., et al., *Fatal swine acute diarrhoea syndrome caused by an HKU2-related coronavirus of bat origin*. Nature, 2018. **556**(7700): p. 255-258.
48. Corman, V.M., et al., *Link of a ubiquitous human coronavirus to dromedary camels*. Proc Natl Acad Sci U S A, 2016. **113**(35): p. 9864-9.
49. Huynh, J., et al., *Evidence supporting a zoonotic origin of human coronavirus strain NL63*. J Virol, 2012. **86**(23): p. 12816-25.
50. Woo, P.C., et al., *Phylogenetic and recombination analysis of coronavirus HKU1, a novel coronavirus from patients with pneumonia*. Arch Virol, 2005. **150**(11): p. 2299-311.
51. Vijgen, L., et al., *Complete Genomic Sequence of Human Coronavirus OC43: Molecular Clock Analysis Suggests a Relatively Recent Zoonotic Coronavirus Transmission Event*. Journal of Virology, 2005. **79**(3): p. 1595.
52. Gorbalenya, A.E., et al., *The species Severe acute respiratory syndrome-related coronavirus: classifying 2019-nCoV and naming it SARS-CoV-2*. Nature Microbiology, 2020.
53. Reusken, C.B., et al., *Middle East respiratory syndrome coronavirus neutralising serum antibodies in dromedary camels: a comparative serological study*. Lancet Infect Dis, 2013. **13**(10): p. 859-66.
54. Corman, V.M., et al., *Antibodies against MERS coronavirus in dromedary camels, Kenya, 1992-2013*. Emerg Infect Dis, 2014. **20**(8): p. 1319-22.
55. Haagmans, B.L., et al., *Middle East respiratory syndrome coronavirus in dromedary camels: an outbreak investigation*. Lancet Infect Dis, 2014. **14**(2): p. 140-5.
56. Memish, Z.A., et al., *Human infection with MERS coronavirus after exposure to infected camels, Saudi Arabia, 2013*. Emerg Infect Dis, 2014. **20**(6): p. 1012-5.
57. van Boheemen, S., et al., *Genomic Characterization of a Newly Discovered Coronavirus Associated with Acute Respiratory Distress Syndrome in Humans*. mBio, 2012. **3**(6): p. e00473-12.
58. Drosten, C., et al., *Transmission of MERS-coronavirus in household contacts*. N Engl J Med, 2014. **371**(9): p. 828-35.
59. Memish, Z.A., et al., *Family cluster of Middle East respiratory syndrome coronavirus infections*. N Engl J Med, 2013. **368**(26): p. 2487-94.
60. Badawi, A. and S.G. Ryoo, *Prevalence of Diabetes in the 2009 Influenza A (H1N1) and the Middle East Respiratory Syndrome Coronavirus: A Systematic Review and Meta-Analysis*. J Public Health Res, 2016. **5**(3): p. 733.
61. Cho, S.Y., et al., *MERS-CoV outbreak following a single patient exposure in an emergency room in South Korea: an epidemiological outbreak study*. Lancet, 2016. **388**(10048): p. 994-1001.
62. Park, J.W., et al., *Hospital Outbreaks of Middle East Respiratory Syndrome, Daejeon, South Korea, 2015*. Emerg Infect Dis, 2017. **23**(6): p. 898-905.
63. Oboho, I.K., et al., *2014 MERS-CoV Outbreak in Jeddah — A Link to Health Care Facilities*. New England Journal of Medicine, 2015. **372**(9): p. 846-854.
64. Peiris, J.S.M., et al., *The Severe Acute Respiratory Syndrome*. New England Journal of Medicine, 2003. **349**(25): p. 2431-2441.
65. Guan, Y., et al., *Isolation and characterization of viruses related to the SARS coronavirus from animals in southern China*. Science, 2003. **302**(5643): p. 276-8.
66. Wu, A., et al., *Genome Composition and Divergence of the Novel Coronavirus (2019-nCoV) Originating in China*. Cell Host & Microbe, 2020. **27**(3): p. 325-328.
67. Hoffmann, M., et al., *SARS-CoV-2 Cell Entry Depends on ACE2 and TMPRSS2 and Is Blocked by a Clinically Proven Protease Inhibitor*. Cell, 2020.
68. Rothe, C., et al., *Transmission of 2019-nCoV Infection from an Asymptomatic Contact in Germany*. New England Journal of Medicine, 2020. **382**(10): p. 970-971.

69. Sola, I., et al., *RNA-RNA and RNA-protein interactions in coronavirus replication and transcription*. RNA biology, 2011. **8**(2): p. 237-248.
70. Madhugiri, R., et al., *Structural and functional conservation of cis-acting RNA elements in coronavirus 5'-terminal genome regions*. Virology, 2018. **517**: p. 44-55.
71. Brierley, I., P. Digard, and S.C. Inglis, *Characterization of an efficient coronavirus ribosomal frameshifting signal: requirement for an RNA pseudoknot*. Cell, 1989. **57**(4): p. 537-47.
72. Perlman, S. and J. Netland, *Coronaviruses post-SARS: update on replication and pathogenesis*. Nat Rev Microbiol, 2009. **7**(6): p. 439-50.
73. Ziebuhr, J., E.J. Snijder, and A.E. Gorbalenya, *Virus-encoded proteinases and proteolytic processing in the Nidovirales*. J Gen Virol, 2000. **81**(Pt 4): p. 853-79.
74. Angelini, M.M., et al., *Severe acute respiratory syndrome coronavirus nonstructural proteins 3, 4, and 6 induce double-membrane vesicles*. mBio, 2013. **4**(4): p. e00524-13.
75. Becares, M., et al., *Mutagenesis of Coronavirus nsp14 Reveals Its Potential Role in Modulation of the Innate Immune Response*. J Virol, 2016. **90**(11): p. 5399-5414.
76. Ahn, D.G., et al., *Biochemical characterization of a recombinant SARS coronavirus nsp12 RNA-dependent RNA polymerase capable of copying viral RNA templates*. Arch Virol, 2012. **157**(11): p. 2095-104.
77. Adedeji, A.O., et al., *Mechanism of nucleic acid unwinding by SARS-CoV helicase*. PLoS One, 2012. **7**(5): p. e36521.
78. Bouvet, M., et al., *In vitro reconstitution of SARS-coronavirus mRNA cap methylation*. PLoS Pathog, 2010. **6**(4): p. e1000863.
79. Bouvet, M., et al., *Coronavirus Nsp10, a critical co-factor for activation of multiple replicative enzymes*. J Biol Chem, 2014. **289**(37): p. 25783-96.
80. Daffis, S., et al., *2'-O methylation of the viral mRNA cap evades host restriction by IFIT family members*. Nature, 2010. **468**(7322): p. 452-6.
81. Raj, V.S., et al., *Dipeptidyl peptidase 4 is a functional receptor for the emerging human coronavirus-EMC*. Nature, 2013. **495**(7440): p. 251-4.
82. Molenkamp, R. and W.J. Spaan, *Identification of a specific interaction between the coronavirus mouse hepatitis virus A59 nucleocapsid protein and packaging signal*. Virology, 1997. **239**(1): p. 78-86.
83. Pewe, L., et al., *A severe acute respiratory syndrome-associated coronavirus-specific protein enhances virulence of an attenuated murine coronavirus*. Journal of virology, 2005. **79**(17): p. 11335-11342.
84. Tangudu, C., et al., *Severe Acute Respiratory Syndrome Coronavirus Protein 6 Accelerates Murine Coronavirus Infections*. Journal of Virology, 2007. **81**(3): p. 1220.
85. Canton, J., et al., *MERS-CoV 4b protein interferes with the NF-kappaB-dependent innate immune response during infection*. PLoS Pathog, 2018. **14**(1): p. e1006838.
86. Niemeyer, D., et al., *Middle East respiratory syndrome coronavirus accessory protein 4a is a type I interferon antagonist*. J Virol, 2013. **87**(22): p. 12489-95.
87. Sola, I., et al., *Continuous and Discontinuous RNA Synthesis in Coronaviruses*. Annual Review of Virology, 2015. **2**(1): p. 265-288.
88. Li, W., et al., *Angiotensin-converting enzyme 2 is a functional receptor for the SARS coronavirus*. Nature, 2003. **426**(6965): p. 450-4.
89. Li, W., et al., *Identification of sialic acid-binding function for the Middle East respiratory syndrome coronavirus spike glycoprotein*. Proc Natl Acad Sci U S A, 2017. **114**(40): p. E8508-e8517.
90. Marzi, A., et al., *DC-SIGN and DC-SIGNR Interact with the Glycoprotein of Marburg Virus and the S Protein of Severe Acute Respiratory Syndrome Coronavirus*. Journal of Virology, 2004. **78**(21): p. 12090.
91. Hofmann, H. and S. Pöhlmann, *Cellular entry of the SARS coronavirus*. Trends in Microbiology, 2004. **12**(10): p. 466-472.

92. Wang, H., et al., *SARS coronavirus entry into host cells through a novel clathrin- and caveolae-independent endocytic pathway*. Cell research, 2008. **18**(2): p. 290-301.
93. Hoffmann, M., H. Kleine-Weber, and S. Pöhlmann, *A Multibasic Cleavage Site in the Spike Protein of SARS-CoV-2 Is Essential for Infection of Human Lung Cells*. Molecular Cell, 2020. **78**(4): p. 779-784.e5.
94. Heurich, A., et al., *TMPRSS2 and ADAM17 cleave ACE2 differentially and only proteolysis by TMPRSS2 augments entry driven by the severe acute respiratory syndrome coronavirus spike protein*. Journal of virology, 2014. **88**(2): p. 1293-1307.
95. Shirato, K., M. Kawase, and S. Matsuyama, *Wild-type human coronaviruses prefer cell-surface TMPRSS2 to endosomal cathepsins for cell entry*. Virology, 2018. **517**: p. 9-15.
96. Kleine-Weber, H., et al., *Functional analysis of potential cleavage sites in the MERS-coronavirus spike protein*. Sci Rep, 2018. **8**(1): p. 16597.
97. Matsuyama, S., et al., *Enhanced isolation of SARS-CoV-2 by TMPRSS2-expressing cells*. Proceedings of the National Academy of Sciences, 2020. **117**(13): p. 7001.
98. Belouzard, S., V.C. Chu, and G.R. Whittaker, *Activation of the SARS coronavirus spike protein via sequential proteolytic cleavage at two distinct sites*. Proceedings of the National Academy of Sciences, 2009. **106**(14): p. 5871.
99. Park, J.-E., et al., *Proteolytic processing of Middle East respiratory syndrome coronavirus spikes expands virus tropism*. Proceedings of the National Academy of Sciences, 2016. **113**(43): p. 12262.
100. Millet, J.K. and G.R. Whittaker, *Host cell entry of Middle East respiratory syndrome coronavirus after two-step, furin-mediated activation of the spike protein*. Proceedings of the National Academy of Sciences, 2014. **111**(42): p. 15214.
101. Knoops, K., et al., *SARS-Coronavirus Replication Is Supported by a Reticulovesicular Network of Modified Endoplasmic Reticulum*. PLOS Biology, 2008. **6**(9): p. e226.
102. van Hemert, M.J., et al., *SARS-coronavirus replication/transcription complexes are membrane-protected and need a host factor for activity in vitro*. PLoS Pathog, 2008. **4**(5): p. e1000054.
103. Kuo, L. and P.S. Masters, *Functional analysis of the murine coronavirus genomic RNA packaging signal*. J Virol, 2013. **87**(9): p. 5182-92.
104. Sturman, L.S., K.V. Holmes, and J. Behnke, *Isolation of coronavirus envelope glycoproteins and interaction with the viral nucleocapsid*. Journal of virology, 1980. **33**(1): p. 449-462.
105. Mortola, E. and P. Roy, *Efficient assembly and release of SARS coronavirus-like particles by a heterologous expression system*. FEBS Lett, 2004. **576**(1-2): p. 174-8.
106. de Haan, C.A.M. and P.J.M. Rottier, *Molecular interactions in the assembly of coronaviruses*. Advances in virus research, 2005. **64**: p. 165-230.
107. Sawicki, S.G., D.L. Sawicki, and S.G. Siddell, *A contemporary view of coronavirus transcription*. J Virol, 2007. **81**(1): p. 20-9.
108. Enard, D., et al., *Viruses are a dominant driver of protein adaptation in mammals*. Elife, 2016. **5**.
109. Meyerson, N.R. and S.L. Sawyer, *Two-stepping through time: mammals and viruses*. Trends Microbiol, 2011. **19**(6): p. 286-94.
110. Elde, N.C., et al., *Protein kinase R reveals an evolutionary model for defeating viral mimicry*. Nature, 2009. **457**(7228): p. 485-9.
111. Shin, J. and T. MacCarthy, *Potential for evolution of complex defense strategies in a multi-scale model of virus-host coevolution*. BMC Evolutionary Biology, 2016. **16**(1): p. 233.
112. Boehm, T. and J.B. Swann, *Origin and Evolution of Adaptive Immunity*. Annual Review of Animal Biosciences, 2014. **2**(1): p. 259-283.
113. Boehm, T., *Design principles of adaptive immune systems*. Nature Reviews Immunology, 2011. **11**(5): p. 307-317.
114. Janeway, C.A. and R. Medzhitov, *Innate Immune Recognition*. Annual Review of Immunology, 2002. **20**(1): p. 197-216.

115. Zalinger, Z.B., et al., *MDA5 Is Critical to Host Defense during Infection with Murine Coronavirus*. Journal of Virology, 2015. **89**(24): p. 12330.
116. Takaoka, A. and H. Yanai, *Interferon signalling network in innate defence*. Cell Microbiol, 2006. **8**(6): p. 907-22.
117. Schoggins, J.W., et al., *A diverse range of gene products are effectors of the type I interferon antiviral response*. Nature, 2011. **472**(7344): p. 481-485.
118. Hubel, P., et al., *A protein-interaction network of interferon-stimulated genes extends the innate immune system landscape*. Nature Immunology, 2019. **20**(4): p. 493-502.
119. Cinatl, J., et al., *Treatment of SARS with human interferons*. Lancet, 2003. **362**(9380): p. 293-4.
120. Zielecki, F., et al., *Human cell tropism and innate immune system interactions of human respiratory coronavirus EMC compared to those of severe acute respiratory syndrome coronavirus*. J Virol, 2013. **87**(9): p. 5300-4.
121. Kindler, E., et al., *Efficient Replication of the Novel Human Betacoronavirus EMC on Primary Human Epithelium Highlights Its Zoonotic Potential*. mBio, 2013. **4**(1): p. e00611-12.
122. Kindler, E. and V. Thiel, *To sense or not to sense viral RNA--essentials of coronavirus innate immune evasion*. Curr Opin Microbiol, 2014. **20**: p. 69-75.
123. Haagmans, B.L., et al., *Pegylated interferon-alpha protects type 1 pneumocytes against SARS coronavirus infection in macaques*. Nat Med, 2004. **10**(3): p. 290-3.
124. Falzarano, D., et al., *Inhibition of novel β coronavirus replication by a combination of interferon- α 2b and ribavirin*. Scientific Reports, 2013. **3**(1): p. 1686.
125. Falzarano, D., et al., *Treatment with interferon- α 2b and ribavirin improves outcome in MERS-CoV-infected rhesus macaques*. Nature medicine, 2013. **19**(10): p. 1313-1317.
126. Frieman, M.B., et al., *SARS-CoV pathogenesis is regulated by a STAT1 dependent but a type I, II and III interferon receptor independent mechanism*. PLoS Pathog, 2010. **6**(4): p. e1000849.
127. Menachery, V.D., et al., *Middle East Respiratory Syndrome Coronavirus Nonstructural Protein 16 Is Necessary for Interferon Resistance and Viral Pathogenesis*. mSphere, 2017. **2**(6).
128. Chen, Y., et al., *Functional screen reveals SARS coronavirus nonstructural protein nsp14 as a novel cap N7 methyltransferase*. Proceedings of the National Academy of Sciences, 2009. **106**(9): p. 3484.
129. Chen, Y., et al., *Biochemical and Structural Insights into the Mechanisms of SARS Coronavirus RNA Ribose 2'-O-Methylation by nsp16/nsp10 Protein Complex*. PLOS Pathogens, 2011. **7**(10): p. e1002294.
130. Züst, R., et al., *Ribose 2'-O-methylation provides a molecular signature for the distinction of self and non-self mRNA dependent on the RNA sensor Mda5*. Nature Immunology, 2011. **12**(2): p. 137-143.
131. Hackbart, M., X. Deng, and S.C. Baker, *Coronavirus endoribonuclease targets viral polyuridine sequences to evade activating host sensors*. Proceedings of the National Academy of Sciences, 2020. **117**(14): p. 8094.
132. Kindler, E., et al., *Early endonuclease-mediated evasion of RNA sensing ensures efficient coronavirus replication*. PLOS Pathogens, 2017. **13**(2): p. e1006195.
133. Case, J.B., et al., *Murine Hepatitis Virus nsp14 Exoribonuclease Activity Is Required for Resistance to Innate Immunity*. J Virol, 2018. **92**(1).
134. Chan, R.W., et al., *Tropism of and innate immune responses to the novel human betacoronavirus lineage C virus in human ex vivo respiratory organ cultures*. J Virol, 2013. **87**(12): p. 6604-14.
135. Narayanan, K., et al., *Severe Acute Respiratory Syndrome Coronavirus nsp1 Suppresses Host Gene Expression, Including That of Type I Interferon, in Infected Cells*. Journal of Virology, 2008. **82**(9): p. 4471.
136. Tanaka, T., et al., *Severe acute respiratory syndrome coronavirus nsp1 facilitates efficient propagation in cells through a specific translational shutdown of host mRNA*. J Virol, 2012. **86**(20): p. 11128-37.

137. Huang, C., et al., *SARS coronavirus nsp1 protein induces template-dependent endonucleolytic cleavage of mRNAs: viral mRNAs are resistant to nsp1-induced RNA cleavage*. PLoS Pathog, 2011. **7**(12): p. e1002433.
138. Lokugamage, K.G., et al., *Middle East Respiratory Syndrome Coronavirus nsp1 Inhibits Host Gene Expression by Selectively Targeting mRNAs Transcribed in the Nucleus while Sparing mRNAs of Cytoplasmic Origin*. J Virol, 2015. **89**(21): p. 10970-81.
139. Fehr, A.R., et al., *The Conserved Coronavirus Macrodome Promotes Virulence and Suppresses the Innate Immune Response during Severe Acute Respiratory Syndrome Coronavirus Infection*. mBio, 2016. **7**(6).
140. Clementz, M.A., et al., *Deubiquitinating and Interferon Antagonism Activities of Coronavirus Papain-Like Proteases*. Journal of Virology, 2010. **84**(9): p. 4619.
141. Matthews, K., et al., *The SARS coronavirus papain like protease can inhibit IRF3 at a post activation step that requires deubiquitination activity*. Virology journal, 2014. **11**: p. 209-209.
142. Mielech, A.M., et al., *MERS-CoV papain-like protease has deISGylating and deubiquitinating activities*. Virology, 2014. **450-451**: p. 64-70.
143. Devaraj, S.G., et al., *Regulation of IRF-3-dependent innate immunity by the papain-like protease domain of the severe acute respiratory syndrome coronavirus*. J Biol Chem, 2007. **282**(44): p. 32208-21.
144. Kopecky-Bromberg, S.A., et al., *Severe acute respiratory syndrome coronavirus open reading frame (ORF) 3b, ORF 6, and nucleocapsid proteins function as interferon antagonists*. J Virol, 2007. **81**(2): p. 548-57.
145. Shi, C.S., et al., *SARS-coronavirus open reading frame-9b suppresses innate immunity by targeting mitochondria and the MAVS/TRAF3/TRAF6 signalosome*. J Immunol, 2014. **193**(6): p. 3080-9.
146. Yuen, C.-K., et al., *SARS-CoV-2 nsp13, nsp14, nsp15 and orf6 function as potent interferon antagonists*. Emerging Microbes & Infections, 2020. **9**(1): p. 1418-1428.
147. Frieman, M., et al., *Severe acute respiratory syndrome coronavirus ORF6 antagonizes STAT1 function by sequestering nuclear import factors on the rough endoplasmic reticulum/Golgi membrane*. J Virol, 2007. **81**(18): p. 9812-24.
148. Siu, K.L., et al., *Middle east respiratory syndrome coronavirus 4a protein is a double-stranded RNA-binding protein that suppresses PACT-induced activation of RIG-I and MDA5 in the innate antiviral response*. J Virol, 2014. **88**(9): p. 4866-76.
149. Menachery, V.D., et al., *MERS-CoV Accessory ORFs Play Key Role for Infection and Pathogenesis*. mBio, 2017. **8**(4): p. e00665-17.
150. Comar, C.E., et al., *Antagonism of dsRNA-Induced Innate Immune Pathways by NS4a and NS4b Accessory Proteins during MERS Coronavirus Infection*. mBio, 2019. **10**(2): p. e00319-19.
151. Dolan, P.T., Z.J. Whitfield, and R. Andino, *Mechanisms and Concepts in RNA Virus Population Dynamics and Evolution*. Annual Review of Virology, 2018. **5**(1): p. 69-92.
152. Sanjuán, R., A. Moya, and S.F. Elena, *The distribution of fitness effects caused by single-nucleotide substitutions in an RNA virus*. Proceedings of the National Academy of Sciences of the United States of America, 2004. **101**(22): p. 8396.
153. Domingo-Calap, P., J.M. Cuevas, and R. Sanjuán, *The Fitness Effects of Random Mutations in Single-Stranded DNA and RNA Bacteriophages*. PLOS Genetics, 2009. **5**(11): p. e1000742.
154. Vale, P., et al., *The Distribution Of Mutational Fitness Effects Of Phage ΦX174 On Different Hosts*. Evolution; international journal of organic evolution, 2012. **66**: p. 3495-507.
155. Lanfear, R., H. Kokko, and A. Eyre-Walker, *Population size and the rate of evolution*. Trends in Ecology & Evolution, 2014. **29**(1): p. 33-41.
156. Chao, L., *Fitness of RNA virus decreased by Muller's ratchet*. Nature, 1990. **348**(6300): p. 454-455.
157. Muller, H.J., *The relation of recombination to mutational advance*. Mutation Research/Fundamental and Molecular Mechanisms of Mutagenesis, 1964. **1**(1): p. 2-9.

158. Duarte, E., et al., *Rapid fitness losses in mammalian RNA virus clones due to Muller's ratchet*. Proc Natl Acad Sci U S A, 1992. **89**(13): p. 6015-9.
159. Froissart, R., et al., *Recombination every day: abundant recombination in a virus during a single multi-cellular host infection*. PLoS biology, 2005. **3**(3): p. e89-e89.
160. Oberste, M.S., K. Maher, and M.A. Pallansch, *Evidence for frequent recombination within species human enterovirus B based on complete genomic sequences of all thirty-seven serotypes*. J Virol, 2004. **78**(2): p. 855-67.
161. Schlub, T.E., et al., *Accurately Measuring Recombination between Closely Related HIV-1 Genomes*. PLOS Computational Biology, 2010. **6**(4): p. e1000766.
162. Charpentier, C., et al., *Extensive Recombination among Human Immunodeficiency Virus Type 1 Quasispecies Makes an Important Contribution to Viral Diversity in Individual Patients*. Journal of Virology, 2006. **80**(5): p. 2472.
163. Kempf, B.J., et al., *Picornavirus RNA Recombination Counteracts Error Catastrophe*. J Virol, 2019. **93**(14).
164. Xiao, Y., et al., *RNA Recombination Enhances Adaptability and Is Required for Virus Spread and Virulence*. Cell Host Microbe, 2016. **19**(4): p. 493-503.
165. Lai, M.M., et al., *Recombination between nonsegmented RNA genomes of murine coronaviruses*. J Virol, 1985. **56**(2): p. 449-56.
166. Makino, S., et al., *High-frequency RNA recombination of murine coronaviruses*. J Virol, 1986. **57**(3): p. 729-37.
167. Keck, J.G., et al., *In vivo RNA-RNA recombination of coronavirus in mouse brain*. J Virol, 1988. **62**(5): p. 1810-3.
168. Kottier, S.A., D. Cavanagh, and P. Britton, *Experimental evidence of recombination in coronavirus infectious bronchitis virus*. Virology, 1995. **213**(2): p. 569-80.
169. Herrewegh, A.A., et al., *Feline coronavirus type II strains 79-1683 and 79-1146 originate from a double recombination between feline coronavirus type I and canine coronavirus*. J Virol, 1998. **72**(5): p. 4508-14.
170. Terada, Y., et al., *Emergence of pathogenic coronaviruses in cats by homologous recombination between feline and canine coronaviruses*. PLoS One, 2014. **9**(9): p. e106534.
171. Tian, P.F., et al., *Evidence of recombinant strains of porcine epidemic diarrhea virus, United States, 2013*. Emerg Infect Dis, 2014. **20**(10): p. 1735-8.
172. Wang, Y., et al., *Origin and Possible Genetic Recombination of the Middle East Respiratory Syndrome Coronavirus from the First Imported Case in China: Phylogenetics and Coalescence Analysis*. MBio, 2015. **6**(5): p. e01280-15.
173. Sabir, J.S., et al., *Co-circulation of three camel coronavirus species and recombination of MERS-CoVs in Saudi Arabia*. Science, 2016. **351**(6268): p. 81-4.
174. Zhang, Z., L. Shen, and X. Gu, *Evolutionary Dynamics of MERS-CoV: Potential Recombination, Positive Selection and Transmission*. Sci Rep, 2016. **6**: p. 25049.
175. Lamers, M.M., et al., *Naturally occurring recombination in ferret coronaviruses revealed by complete genome characterization*. J Gen Virol, 2016. **97**(9): p. 2180-2186.
176. Chu, D.K.W., et al., *MERS coronaviruses from camels in Africa exhibit region-dependent genetic diversity*. Proc Natl Acad Sci U S A, 2018. **115**(12): p. 3144-3149.
177. Yusof, M.F., et al., *Diversity of Middle East respiratory syndrome coronaviruses in 109 dromedary camels based on full-genome sequencing, Abu Dhabi, United Arab Emirates*. Emerg Microbes Infect, 2017. **6**(11): p. e101.
178. Assiri, A.M., et al., *Epidemiology of a Novel Recombinant Middle East Respiratory Syndrome Coronavirus in Humans in Saudi Arabia*. J Infect Dis, 2016. **214**(5): p. 712-21.
179. Cauchemez, S., et al., *Middle East respiratory syndrome coronavirus: quantification of the extent of the epidemic, surveillance biases, and transmissibility*. Lancet Infect Dis, 2014. **14**(1): p. 50-56.
180. Dudas, G., et al., *MERS-CoV spillover at the camel-human interface*. Elife, 2018. **7**.

181. Donnelly, C.A., et al., *Worldwide Reduction in MERS Cases and Deaths since 2016*. Emerg Infect Dis, 2019. **25**(9): p. 1758-1760.
182. El-Kafrawy, S.A., et al., *Enzootic patterns of Middle East respiratory syndrome coronavirus in imported African and local Arabian dromedary camels: a prospective genomic study*. The Lancet Planetary Health.
183. Kleine-Weber, H., et al., *Mutations in the Spike Protein of Middle East Respiratory Syndrome Coronavirus Transmitted in Korea Increase Resistance to Antibody-Mediated Neutralization*. J Virol, 2019. **93**(2).
184. Seong, M.W., et al., *Microevolution of Outbreak-Associated Middle East Respiratory Syndrome Coronavirus, South Korea, 2015*. Emerg Infect Dis, 2016. **22**(2): p. 327-30.
185. Selinger, C., et al., *Cytokine systems approach demonstrates differences in innate and pro-inflammatory host responses between genetically distinct MERS-CoV isolates*. BMC Genomics, 2014. **15**(1): p. 1161.
186. Drosten, C., et al., *An observational, laboratory-based study of outbreaks of middle East respiratory syndrome coronavirus in Jeddah and Riyadh, kingdom of Saudi Arabia, 2014*. Clin Infect Dis, 2015. **60**(3): p. 369-77.
187. Muth, D., et al., *Infectious Middle East Respiratory Syndrome Coronavirus Excretion and Serotype Variability Based on Live Virus Isolates from Patients in Saudi Arabia*. J Clin Microbiol, 2015. **53**(9): p. 2951-5.
188. van Doremalen, N. and V.J. Munster, *Animal models of Middle East respiratory syndrome coronavirus infection*. Antiviral Res, 2015. **122**: p. 28-38.
189. Thornbrough, J.M., et al., *Middle East Respiratory Syndrome Coronavirus NS4b Protein Inhibits Host RNase L Activation*. MBio, 2016. **7**(2): p. e00258.
190. Corman, V.M., et al., *Detection of a novel human coronavirus by real-time reverse-transcription polymerase chain reaction*. Euro Surveill, 2012. **17**(39).
191. Song, W., et al., *Identification of residues on human receptor DPP4 critical for MERS-CoV binding and entry*. Virology, 2014. **471-473**: p. 49-53.
192. Fagbo, S.F., et al., *Molecular Epidemiology of Hospital Outbreak of Middle East Respiratory Syndrome, Riyadh, Saudi Arabia, 2014*. Emerg Infect Dis, 2015. **21**(11): p. 1981-8.
193. Lulla, V., et al., *An upstream protein-coding region in enteroviruses modulates virus infection in gut epithelial cells*. Nat Microbiol, 2019. **4**(2): p. 280-292.
194. Lulla, V. and A.E. Firth, *Enterovirus Competition Assay to Assess Replication Fitness*. Bio-protocol, 2019. **9**(10): p. e3233.
195. Gierer, S., et al., *The Spike Protein of the Emerging Betacoronavirus EMC Uses a Novel Coronavirus Receptor for Entry, Can Be Activated by TMPRSS2, and Is Targeted by Neutralizing Antibodies*. Journal of Virology, 2013. **87**(10): p. 5502.
196. Drosten, C., et al., *Clinical features and virological analysis of a case of Middle East respiratory syndrome coronavirus infection*. The Lancet Infectious Diseases, 2013. **13**(9): p. 745-751.
197. Meyer, B., et al., *Antibodies against MERS coronavirus in dromedary camels, United Arab Emirates, 2003 and 2013*. Emerg Infect Dis, 2014. **20**(4): p. 552-9.
198. Saqib, M., et al., *Serologic Evidence for MERS-CoV Infection in Dromedary Camels, Punjab, Pakistan, 2012-2015*. Emerg Infect Dis, 2017. **23**(3): p. 550-551.
199. Shirato, K., M. Kawase, and S. Matsuyama, *Middle East Respiratory Syndrome Coronavirus Infection Mediated by the Transmembrane Serine Protease TMPRSS2*. Journal of Virology, 2013. **87**(23): p. 12552.
200. Assiri, A., et al., *Hospital outbreak of Middle East respiratory syndrome coronavirus*. N Engl J Med, 2013. **369**(5): p. 407-16.
201. Domingo, E., *Chapter 7 - Long-Term Virus Evolution in Nature*, in *Virus as Populations*, E. Domingo, Editor. 2016, Academic Press: Boston. p. 227-262.

202. Domingo, E., *Chapter 6 - Virus Population Dynamics Examined with Experimental Model Systems*, in *Virus as Populations*, E. Domingo, Editor. 2016, Academic Press: Boston. p. 197-225.
203. Bean, A.G.D., et al., *Studying immunity to zoonotic diseases in the natural host — keeping it real*. *Nature Reviews Immunology*, 2013. **13**(12): p. 851-861.
204. Chan, R.W.Y., et al., *Tropism and replication of Middle East respiratory syndrome coronavirus from dromedary camels in the human respiratory tract: an in-vitro and ex-vivo study*. *The Lancet Respiratory Medicine*, 2014. **2**(10): p. 813-822.
205. Thi Nhu Thao, T., et al., *Rapid reconstruction of SARS-CoV-2 using a synthetic genomics platform*. *Nature*, 2020. **582**(7813): p. 561-565.
206. Cooper, M.D. and M.N. Alder, *The Evolution of Adaptive Immune Systems*. *Cell*, 2006. **124**(4): p. 815-822.
207. Kimbrell, D.A. and B. Beutler, *The evolution and genetics of innate immunity*. *Nat Rev Genet*, 2001. **2**(4): p. 256-67.
208. Bordería, A.V., et al., *Group Selection and Contribution of Minority Variants during Virus Adaptation Determines Virus Fitness and Phenotype*. *PLoS Pathog*, 2015. **11**(5): p. e1004838.
209. Tejero, H., F. Montero, and J.C. Nuño, *Theories of Lethal Mutagenesis: From Error Catastrophe to Lethal Defection*. *Curr Top Microbiol Immunol*, 2016. **392**: p. 161-79.
210. Vignuzzi, M., et al., *Quasispecies diversity determines pathogenesis through cooperative interactions in a viral population*. *Nature*, 2006. **439**(7074): p. 344-8.
211. Acevedo, A. and R. Andino, *Library preparation for highly accurate population sequencing of RNA viruses*. *Nat Protoc*, 2014. **9**(7): p. 1760-9.
212. Whitfield, Z.J. and R. Andino, *Characterization of Viral Populations by Using Circular Sequencing*. *Journal of Virology*, 2016. **90**(20): p. 8950.
213. Zhou, S., et al., *Primer ID Validates Template Sampling Depth and Greatly Reduces the Error Rate of Next-Generation Sequencing of HIV-1 Genomic RNA Populations*. *J Virol*, 2015. **89**(16): p. 8540-55.
214. Wölfel, R., et al., *Virological assessment of hospitalized patients with COVID-2019*. *Nature*, 2020.
215. Wrapp, D., et al., *Cryo-EM structure of the 2019-nCoV spike in the prefusion conformation*. *Science*, 2020. **367**(6483): p. 1260-1263.
216. Bertram, S., et al., *Influenza and SARS-Coronavirus Activating Proteases TMPRSS2 and HAT Are Expressed at Multiple Sites in Human Respiratory and Gastrointestinal Tracts*. *PLOS ONE*, 2012. **7**(4): p. e35876.
217. Meyerholz, D.K., A.M. Lambertz, and P.B. McCray, Jr., *Dipeptidyl Peptidase 4 Distribution in the Human Respiratory Tract: Implications for the Middle East Respiratory Syndrome*. *The American journal of pathology*, 2016. **186**(1): p. 78-86.
218. Kikkert, M., *Innate Immune Evasion by Human Respiratory RNA Viruses*. *Journal of Innate Immunity*, 2020. **12**(1): p. 4-20.
219. Emeny, J.M. and M.J. Morgan, *Regulation of the interferon system: evidence that Vero cells have a genetic defect in interferon production*. *J Gen Virol*, 1979. **43**(1): p. 247-52.
220. Yoshikawa, T., et al., *Dynamic innate immune responses of human bronchial epithelial cells to severe acute respiratory syndrome-associated coronavirus infection*. *PLoS one*, 2010. **5**(1): p. e8729-e8729.
221. Thiel, V. and F. Weber, *Interferon and cytokine responses to SARS-coronavirus infection*. *Cytokine Growth Factor Rev*, 2008. **19**(2): p. 121-32.
222. Spiegel, M., et al., *Inhibition of Beta Interferon Induction by Severe Acute Respiratory Syndrome Coronavirus Suggests a Two-Step Model for Activation of Interferon Regulatory Factor 3*. *Journal of Virology*, 2005. **79**(4): p. 2079.
223. Muth, D., et al., *Transgene expression in the genome of Middle East respiratory syndrome coronavirus based on a novel reverse genetics system utilizing Red-mediated recombination cloning*. *Journal of General Virology*, 2017. **98**(10): p. 2461-2469.

224. Pfefferle, S., et al., *Reverse genetic characterization of the natural genomic deletion in SARS-Coronavirus strain Frankfurt-1 open reading frame 7b reveals an attenuating function of the 7b protein in-vitro and in-vivo*. Virology Journal, 2009. **6**(1): p. 131.
225. Holzinger, D., et al., *Induction of MxA Gene Expression by Influenza A Virus Requires Type I or Type III Interferon Signaling*. Journal of Virology, 2007. **81**(14): p. 7776.
226. Daffis, S., et al., *Cell-Specific IRF-3 Responses Protect against West Nile Virus Infection by Interferon-Dependent and -Independent Mechanisms*. PLOS Pathogens, 2007. **3**(7): p. e106.
227. Niemeyer, D., et al., *The papain-like protease determines a virulence trait that varies among members of the SARS-coronavirus species*. PLOS Pathogens, 2018. **14**(9): p. e1007296.
228. Blanco-Melo, D., et al., *Imbalanced Host Response to SARS-CoV-2 Drives Development of COVID-19*. Cell, 2020. **181**(5): p. 1036-1045.e9.
229. Emanuel, W., et al., *Bulk and single-cell gene expression profiling of SARS-CoV-2 infected human cell lines identifies molecular targets for therapeutic intervention*. bioRxiv, 2020: p. 2020.05.05.079194.
230. Muth, D., et al., *Attenuation of replication by a 29 nucleotide deletion in SARS-coronavirus acquired during the early stages of human-to-human transmission*. Scientific Reports, 2018. **8**(1): p. 15177.
231. Da Silva Santos, C., K. Tartour, and A. Cimarelli, *A Novel Entry/Uncoating Assay Reveals the Presence of at Least Two Species of Viral Capsids During Synchronized HIV-1 Infection*. PLOS Pathogens, 2016. **12**(9): p. e1005897.
232. Herzog, P., C. Drosten, and M.A. Müller, *Plaque assay for human coronavirus NL63 using human colon carcinoma cells*. Virol J, 2008. **5**: p. 138.
233. Dijkman, R., et al., *Isolation and characterization of current human coronavirus strains in primary human epithelial cell cultures reveal differences in target cell tropism*. J Virol, 2013. **87**(11): p. 6081-90.
234. Berger Rentsch, M. and G. Zimmer, *A vesicular stomatitis virus replicon-based bioassay for the rapid and sensitive determination of multi-species type I interferon*. PloS one, 2011. **6**(10): p. e25858.
235. Zimmer, G., et al., *Pseudotyping of vesicular stomatitis virus with the envelope glycoproteins of highly pathogenic avian influenza viruses*. J Gen Virol, 2014. **95**(Pt 8): p. 1634-1639.
236. Karstentischer, B., et al., *Two-step Red-mediated recombination for versatile high-efficiency markerless DNA manipulation in Escherichia coli*. BioTechniques, 2006. **40**(2): p. 191-197.
237. Corman, V.M., et al., *Detection of 2019 novel coronavirus (2019-nCoV) by real-time RT-PCR*. Euro surveillance : bulletin Europeen sur les maladies transmissibles = European communicable disease bulletin, 2020. **25**(3): p. 2000045.
238. Yount, B., et al., *Systematic assembly of a full-length infectious cDNA of mouse hepatitis virus strain A59*. J Virol, 2002. **76**(21): p. 11065-78.
239. Zhou, J., et al., *Human intestinal tract serves as an alternative infection route for Middle East respiratory syndrome coronavirus*. Science Advances, 2017. **3**(11): p. eaao4966.
240. Steentoft, C., et al., *Precision mapping of the human O-GalNAc glycoproteome through SimpleCell technology*. Embo j, 2013. **32**(10): p. 1478-88.
241. Gupta, R., E. Jung, and S. Brunak, *Prediction of N-glycosylation sites in human proteins*. 2004. **46**: p. 203-206.
242. Lole, K.S., et al., *Full-length human immunodeficiency virus type 1 genomes from subtype C-infected seroconverters in India, with evidence of intersubtype recombination*. Journal of virology, 1999. **73**(1): p. 152-160.

Publications

Publications accepted for review:

Schroeder S, Mache C, Kleine-Weber H, Muth D, Corman VM, Fatykhova D, Memish ZA, Stanifer M, Boulant S, Dijkman R, Richter A, Eggeling S, Hocke A, Hippenstiel S, Thiel V, Pöhlmann S, Wolff T, Müller MA, Drosten C. Functional comparison of MERS-coronavirus lineages reveals increased zoonotic potential of the recombinant lineage 5. **Submitted to Nat. Comm., 2020**

Schroeder S, Pott F, Niemeyer D, Veith T., Richter A, Muth D, Goffinet C, Müller MA, Drosten C. Interferon antagonism by SARS-CoV-2: a functional study using reverse genetics. **Submitted to Lancet Microbe, 2020**

Accepted publications:

Hoffmann M, Kleine-Weber H, **Schroeder S**, et al. *SARS-CoV-2 Cell Entry Depends on ACE2 and TMPRSS2 and Is Blocked by a Clinically Proven Protease Inhibitor.* **Cell.** **2020**;181(2):271-280.e8. doi:10.1016/j.cell.2020.02.052

Hoffmann M, **Schroeder S**, Kleine-Weber H, Müller MA, Drosten C, Pöhlmann S. *Nafamostat Mesylate Blocks Activation of SARS-CoV-2: New Treatment Option for COVID-19.* **Antimicrob Agents Chemother.** **2020**;64(6):e00754-20. Published 2020 May 21. doi:10.1128/AAC.00754-20

Thi Nhu Thao T, Labrousseau F, Ebert N, V'kovski P, Stalder H, Portmann J, Kelly J, Steiner S, Holwerda M, Kratzel A, Gultom M, Schmied K, Laloli L, Hüsler L, Wider M, Pfaender S, Hirt D, Cippà V, Crespo-Pomar S, **Schroeder S**, Muth D, Niemeyer D, Corman VM, Müller MA, Drosten C, Dijkman R, Jores J, Thiel V. *Rapid reconstruction of SARS-CoV-2 using a synthetic genomics platform.* **Nature** 582, 561–565 (2020). <https://doi.org/10.1038/s41586-020-2294-9>

Kleine-Weber H, **Schroeder S**, Krüger N, et al. *Polymorphisms in dipeptidyl peptidase 4 reduce host cell entry of Middle East respiratory syndrome coronavirus.* **Emerg Microbes Infect.** **2020**;9(1):155-168. Published 2020 Jan 21. doi:10.1080/22221751.2020.1713705

Paraskevopoulou S, Pirzer F, Goldmann N, Schmid J, Corman VM, Gottula LT, **Schroeder S**, Rasche A, Muth D, Drexler JF, Heni AC, Eibner GJ, Page RA, Jones TC, Müller MA, Sommer S, Glebe D, Drosten C. *Mammalian deltavirus without hepadnavirus coinfection in the neotropical rodent Proechimys semispinosus.* **Proc Natl Acad Sci U S A.** **2020**;202006750. doi:10.1073/pnas.2006750117

Kiambi S, Corman VM, Sitawa R, Githinji J, Ngoci J, Ozomata AS, Gardner E, von Dobschuetz S, Morzaria S, Kimutai J, **Schroeder S**, Njagi O, Simpkin P, Rugalema G, Tadesse Z, Lubroth J, Makonnen Y, Drosten C, Müller MA, Fasina FO.. *Detection of distinct MERS-Coronavirus strains in dromedary camels from Kenya, 2017.* **Emerg Microbes Infect.** **2018**;7(1):195. Published 2018 Nov 28. doi:10.1038/s41426-018-0193-z

Muth D, Meyer B, Niemeyer D, **Schroeder S**, Osterrieder N, Müller MA, Drosten C. *Transgene expression in the genome of Middle East respiratory syndrome coronavirus based on a novel reverse genetics system utilizing Red-mediated recombination cloning.* **J Gen Virol.** **2017**;98(10):2461-2469. doi:10.1099/jgv.0.000919

Oral presentations and posters:

March 2020, Berlin: 30th Annual Meeting of the Society for Virology
– oral presentation (cancelled due to the SARS-CoV-2 pandemic)

October 2019, Berlin: Zoonoses 2019 - International Symposium on Zoonoses Research
– oral presentation

June 2019, Killarney, IR: Keystone Symposia conference on positive-strand RNA viruses
– poster presentation

For reasons of data protection, the curriculum vitae is not published in the electronic version.